

Nonlinear Hierarchical Adaptive Control of a  
Quad Tilt-Wing UAV

by

Ahmet Eren Demirel

Submitted to the Graduate School of Sabanci University  
in partial fulfillment of the requirements for the degree of  
Master of Science

Sabanci University

August, 2015

Nonlinear Hierarchical Adaptive Control of a  
Quad Tilt-Wing UAV

APPROVED BY:

Prof. Dr. Mustafa Ünel  
(Thesis Advisor)

*Mustafa Ünel*

Prof. Dr. Asif Şabanović

*Asif Şabanović*

Assist. Prof. Dr. Hüseyin Üvet

*Hüseyin Üvet*

DATE OF APPROVAL:

*5 / 8 / 2015*

© Ahmet Eren Demirel 2015  
All Rights Reserved

# Nonlinear Hierarchical Adaptive Control of a Quad-Tilt-Wing UAV

Ahmet Eren Demirel

ME, Master's Thesis, 2015

Thesis Supervisor: Prof. Dr. Mustafa Ünel

Keywords: Quad-tilt wing UAV, Nonlinear Control, Feedback  
Linearization, Model Reference Adaptive Control

## **Abstract**

Unmanned aerial vehicles (UAVs) have become an indispensable part of many military and civilian applications. The popularity of these vehicles have led to a demand for novel mechanical configurations and controllers which are adaptable for the requirements of the desired tasks.

In this thesis, a nonlinear hierarchical adaptive controller is proposed for the control of a quad tilt-wing unmanned aerial vehicle (SUAVI: Sabanci University Unmanned Aerial Vehicle). SUAVI can take-off vertically as a helicopter and flies like a fixed-wing airplane during the long duration flights for power efficiency. In order to compensate for the uncertainties such as moment of inertia changes during the transition from vertical mode to horizontal mode and aerodynamic disturbances an adaptive controller framework is proposed.

In the outer loop of the hierarchical control, a model reference adaptive controller with robustifying terms creates required forces to track the reference trajectory and in the inner loop a nonlinear adaptive controller tracks the desired attitude angles to achieve these forces. The proposed controller is applied to a high fidelity UAV model in the presence of uncertainties, wind disturbances and measurement noise. A structural failure is introduced which results in sudden actuator power drops, mass, inertia and center of gravity changes. Performance of the proposed controller is compared with the feedback linearized fixed controller used in earlier studies.

# Dört Rotorlu Döner-Kanat bir İnsansız Hava Aracının Doğrusal Olmayan Hiyerarşik Uyarlanır Denetimi

Ahmet Eren Demirel

ME, Master Tezi, 2015

Tez Danışmanı: Prof. Dr. Mustafa Ünel

Anahtar Kelimeler: Dört Rotorlu Dört-Kanat İnsansız Hava Aracı,  
Doğrusal Olmayan Denetim, Geribeslemeli Doğrusallaştırma, Model  
Tabanlı Uyarlanır Denetim

## Özet

İnsansız hava araçları (İHA'lar) birçok askeri ve sivil uygulamanın vazgeçilmez bir parçası olmuştur. Bu araçların popüleritesi tanımlanan görevin gerekliliklerine göre uyabilen yeni mekanik yapılar ve denetleyiciler için talep oluşmasına neden olmuştur.

Bu tezde, dört rotorlu döner-kanat bir İHA'nın (SUAVI: Sabancı Üniversitesi İnsansız Hava Aracı) denetlenmesi için hiyerarşik uyarlanır bir denetleyici sunulmuştur. SUAVI, helikopter gibi dikey kalkış yapabilir ve uzun süreli uçuşlarda güç verimliliği için sabit-kanat bir uçak gibi uçabilir. Dikey durumdan yatay duruma geçerken oluşan atalet momentleri değişiklikleri ve aerodinamik dış bozucular gibi belirsizlikleri telafi etmek için uyarlanır bir denetleyici sunulmuştur.

Kontrolcü hiyerarşisinin dış döngüsünde güçlendirmiş terimli model tabanlı uyarlanır bir denetleyici referans yörüngeyi takip etmek için gereken kuvvetleri oluşturur ve iç döngüsünde doğrusal olmayan uyarlanır bir denetleyici bu kuvvetleri oluşturmak için istenilen durum açılarını takip eder. Sunulan denetleyici belirsizlikleri, rüzgar bozucuları ve ölçüm gürültüleri yüksek doğruluk derecesine sahip bir İHA modeline uygulanmıştır. Ani eyleyici güç düşümlerine, kütle, atalet ve ağırlık merkezi değişimlerine sebep olan yapısal bir bozukluk uygulanmıştır. Sunulan denetleyicinin performansı önceki çalışmalarda kullanılan sabit geribeslemeli denetleyicinin performansı ile karşılaştırılmıştır.

## Acknowledgements

I would like to express my sincere gratitude to my thesis advisor Prof. Dr. Mustafa Ünel for his inspirational guidance, precious support and constant encouragement. I am greatly indebted to him for his invaluable academic and personal advises. His perspective on research and sharp insights on almost any issue have been my guide in academy and in my personal life.

I would like to thank Prof. Dr. Asif Şabanovic and Assist. Prof. Dr. Hüseyin Üvet for their precious feedbacks and spending their valuable time as my jurors.

I would like to thank Assoc. Prof. Dr. Şeref Naci Engin and Assist. Prof. Dr. Yıldray Yıldız for their invaluable academic and personal guidance and kind support.

I would like to acknowledge the financial support provided by Yousef Abdul Latif Jameel.

I am gratefully thanking my fellow colleagues Ines Karmous, Gökhan Alcan, Orhan Ayit, Sanem Evren, Talha Boz, Fırat Yavuz, Ebru Uysal and all remaining CVR Research group members for their friendship and collaboration.

Finally, I would like to thank my sisters Ozge, Banu Demirel, my dear parents and my soulmate Tumay Teoman for all their love and endless support throughout my life. I would not be able to accomplish anything without each and every single one of them.

# Contents

<b>1</b>	<b>Introduction</b>	<b>1</b>
1.1	Thesis Contributions and Organization . . . . .	4
1.2	Publications . . . . .	5
<b>2</b>	<b>Related Work</b>	<b>7</b>
2.1	Hybrid-Wing UAVs . . . . .	7
2.2	UAV Flight Control Systems . . . . .	9
2.2.1	Linear Flight Control Systems . . . . .	10
2.2.2	Model-based Nonlinear Controllers . . . . .	12
2.2.3	Learning-based Flight Controllers . . . . .	14
<b>3</b>	<b>Mathematical Model of SUAVI</b>	<b>16</b>
3.1	System Model . . . . .	17
3.2	Example Flight Scenario . . . . .	29
3.2.1	Trajectory Generation for Pitch Angle Minimization . . . . .	29
3.2.2	Moment of Inertia and Mass Variations During Transition Mode and Component Failure . . . . .	32
3.2.3	Center of Gravity Variation Due to the Failure . . . . .	37
<b>4</b>	<b>Nonlinear Hierarchical Adaptive Control</b>	<b>38</b>
4.1	Feedback Linearization Approach . . . . .	38
4.1.1	PID Based Controllers via Dynamic Inversion . . . . .	38
4.1.2	Feedback Linearization Based Attitude Controllers . . . . .	40
4.2	Nonlinear Adaptive Control Approach . . . . .	42
4.2.1	MRAC Design . . . . .	43
4.2.2	Attitude Reference Calculation . . . . .	48

4.2.3	Nonlinear Adaptive Control Design . . . . .	50
<b>5</b>	<b>Simulation Results</b>	<b>52</b>
5.1	Normal Flight Scenario . . . . .	54
5.2	Failure Scenario . . . . .	63
5.3	Wind Disturbance Added Failure Scenario . . . . .	74
5.4	Full Flight Scenario . . . . .	85
<b>6</b>	<b>Conclusion and Future Works</b>	<b>97</b>
<b>7</b>	<b>Appendix</b>	<b>111</b>

## List of Figures

1.1	(a) Ultra Stick 25e fixed-wing UAV [18], (b) A rotary-wing UAV platform with VICON markers [19], (c) First-insect scale flapping wing UAV [20]. . . . .	3
2.1	(a) Flight test of small scaled tilt-rotor UAV [25], (b) Dual tilt wing UAV HARVee [26]. . . . .	8
2.2	CAD models showing (a) vertical and (b) transition modes and prototype aircraft in (c) horizontal mode. . . . .	8
2.3	Examples of QTW UAVs . . . . .	9
3.1	SUAVI in different wing configurations; (Left) Horizontal, (Middle) Transition, (Right) Vertical [75]. . . . .	16
3.2	Coordinate frames, forces and momets on SUAVI. . . . .	17
3.3	Effective angle of attack, $\alpha_i$ . . . . .	21
3.4	Cubic polynomial curve fitting to the lift and drag coefficients' wind tunnel data. . . . .	22
3.5	Implemented flight scenario. . . . .	30
3.6	(a) CAD model of SUAVI (b) Model after failure (Fallen components' places are indicated for front right wing). . . . .	33
3.7	Evolution of principal moment of inertias due to wing movement, before the failure. . . . .	34
3.8	Evolution of principal moment of inertias due to wing movement, after the failure. . . . .	35
4.1	Closed loop control system block diagram. . . . .	43
5.1	Evolution of wing angles. . . . .	53
5.2	Changes in principal moment of inertias. . . . .	53
5.3	X tracking (top), tracking error (bottom). . . . .	54

5.4	Y tracking (top), tracking error (bottom).	55
5.5	Z tracking (top), tracking error (bottom).	55
5.6	Trajectory tracking of the UAV.	56
5.7	$\phi$ tracking (top), tracking error (bottom).	57
5.8	$\theta$ tracking (top), tracking error (bottom).	57
5.9	$\psi$ tracking (top), tracking error (bottom).	58
5.10	Control inputs.	58
5.11	X tracking (top), tracking error (bottom).	59
5.12	Y tracking (top), tracking error (bottom).	60
5.13	Z tracking (top), tracking error (bottom).	60
5.14	Trajectory tracking of the UAV.	61
5.15	$\phi$ tracking (top), tracking error (bottom).	61
5.16	$\theta$ tracking (top), tracking error (bottom).	62
5.17	$\psi$ tracking (top), tracking error (bottom).	62
5.18	Control inputs.	63
5.19	X tracking (top), tracking error (bottom).	64
5.20	Y tracking (top), tracking error (bottom).	64
5.21	Z tracking (top), tracking error (bottom).	65
5.22	Trajectory tracking of the UAV.	66
5.23	$\phi$ tracking (top), tracking error (bottom).	66
5.24	$\theta$ tracking (top), tracking error (bottom).	67
5.25	$\psi$ tracking (top), tracking error (bottom).	67
5.26	Control inputs.	68
5.27	X tracking (top), tracking error (bottom).	69
5.28	Y tracking (top), tracking error (bottom).	69
5.29	Z tracking (top), tracking error (bottom).	70

5.30	Trajectory tracking of the UAV. . . . .	71
5.31	$\phi$ tracking (top), tracking error (bottom). . . . .	72
5.32	$\theta$ tracking (top), tracking error (bottom). . . . .	72
5.33	$\psi$ tracking (top), tracking error (bottom). . . . .	73
5.34	Control inputs. . . . .	73
5.35	Wind Disturbances. . . . .	75
5.36	X tracking (top), tracking error (bottom). . . . .	75
5.37	Y tracking (top), tracking error (bottom). . . . .	76
5.38	Z tracking (top), tracking error (bottom). . . . .	76
5.39	Trajectory tracking of the UAV. . . . .	77
5.40	$\phi$ tracking (top), tracking error (bottom). . . . .	77
5.41	$\theta$ tracking (top), tracking error (bottom). . . . .	78
5.42	$\psi$ tracking (top), tracking error (bottom). . . . .	78
5.43	Control inputs. . . . .	79
5.44	Wind Disturbances. . . . .	80
5.45	X tracking (top), tracking error (bottom). . . . .	81
5.46	Y tracking (top), tracking error (bottom). . . . .	81
5.47	Z tracking (top), tracking error (bottom). . . . .	82
5.48	Trajectory tracking of the UAV. . . . .	82
5.49	$\phi$ tracking (top), tracking error (bottom). . . . .	83
5.50	$\theta$ tracking (top), tracking error (bottom). . . . .	83
5.51	$\psi$ tracking (top), tracking error (bottom). . . . .	84
5.52	Control inputs. . . . .	84
5.53	Additive measurement noises. . . . .	86
5.54	X tracking (top), tracking error (bottom). . . . .	86
5.55	Y tracking (top), tracking error (bottom). . . . .	87

5.56	Z tracking (top), tracking error (bottom).	87
5.57	Trajectory tracking of the UAV.	88
5.58	$\phi$ tracking (top), tracking error (bottom).	89
5.59	$\theta$ tracking (top), tracking error (bottom).	89
5.60	$\psi$ tracking (top), tracking error (bottom).	90
5.61	Control inputs.	90
5.62	X tracking (top), tracking error (bottom).	91
5.63	Y tracking (top), tracking error (bottom).	92
5.64	Z tracking (top), tracking error (bottom).	92
5.65	Trajectory tracking of the UAV.	93
5.66	$\phi$ tracking (top), tracking error (bottom).	93
5.67	$\theta$ tracking (top), tracking error (bottom).	94
5.68	$\psi$ tracking (top), tracking error (bottom).	94
5.69	Control inputs.	95
5.70	Wing Forces.	95

## List of Tables

3.1	Minimum, maximum values and percent changes of the principal moments of inertias due to wing movement (Before failure).	33
3.2	Minimum, maximum values and percent changes of the principal moments of inertias due to wing movement (After failure).	35
3.3	Norm of the residuals for the inertia curve fitting results. . . .	36
3.4	Mass of the UAV and missing components. . . . .	36
3.5	Percent changes of principal moment of inertias due to wing movement and failure. . . . .	37
7.1	Evolution of principal moments of inertia from horizontal to vertical mode, before the failure. . . . .	111
7.2	Evolution of principal moments of inertia from horizontal to vertical mode. after the failure. . . . .	112

# Chapter I

## 1 Introduction

Robot arms, or manipulators, are the key parts of the industrial manufacturing since they can perform repetitive tasks such as painting, grinding and spot welding with great speed and accuracy. They are bolted to a specific position in the assembly line and work in an engineered environment. Their lack of mobility represents a disadvantage for some of the robotic applications.

Mobile robots overcome this incompetency with their different kinds of locomotion capabilities such as flying, walking, running and swimming. They can be classified by the environment in which they move. For instance, land robots or usually referred as Unmanned Ground Vehicles (UGVs) use wheeled, legged or tracked locomotion. Google's self-driving car [1], Big Dog [2], which is a four-legged robot or a quadruped, and Black Knight [3], which is a combat UGV, are the examples of wheeled, legged and tracked robots, respectively. Additionally, Autonomous Underwater Vehicles (AUVs) operates under water such as Seaglider [4] which is an autonomous underwater vehicle for oceanographic vehicle.

Aerial exploration is crucial for most of the military, reconnaissance and rescue applications. Therefore aerial mobile robots, which are usually referred as Unmanned Aerial Vehicles (UAVs), have become an indispensable part of many military and civilian applications. UAVs usually perform tasks that are dangerous and expensive for a manned airplane. Additionally they do not require a cockpit, thus they are usually lighter with respect to traditional aerial vehicles. This leads to a decrease of manufacturing and opera-

tional costs. Moreover, they can endure large amount of g-forces caused by sudden manoeuvres.

UAVs can be utilized in a variety of military and civilian applications such as

- Tactical reconnaissance, surveillance and operational support [5].
- Border patrols, law enforcement, monitoring trafficking [6].
- Observation of power lines, bridges and domes [7].
- Inspection of oil and gas pipelines [8].
- Landmine detection, operation in disaster zones [9].
- Search and rescue operations [10].
- Monitoring and control of transportation lines [11].
- Crop yield prediction, drought monitoring, spraying of pesticides [12].
- Forest monitoring, fire detection and firefighting [13].
- Archaeological prospecting [14].
- Environmental and climate research [15].
- Unmanned airshipping, postal delivery [16].

Due to their extensive application areas various types of UAVs have been produced. They can be categorized based on weight, endurance, operational altitude and mechanical configurations. Fixed, rotary, flapping wing and hybrid designs [17] can be referred as main categories based on mechanical configurations (see Fig. 1.1 for some examples). Fixed wing UAVs require

a runway to take-off and landing, or catapult launching. Generally they have long endurance and can fly at high cruising speeds. Rotary-wing UAVs, which are also called rotorcraft UAVs, have the capability of hovering and high maneuverability. Flapping-wing UAVs have flexible and morphing wings which are inspired by birds and insects such as hummingbird and hawkmoth. There are also hybrid configurations which will be discussed with more details in Chapter 2.

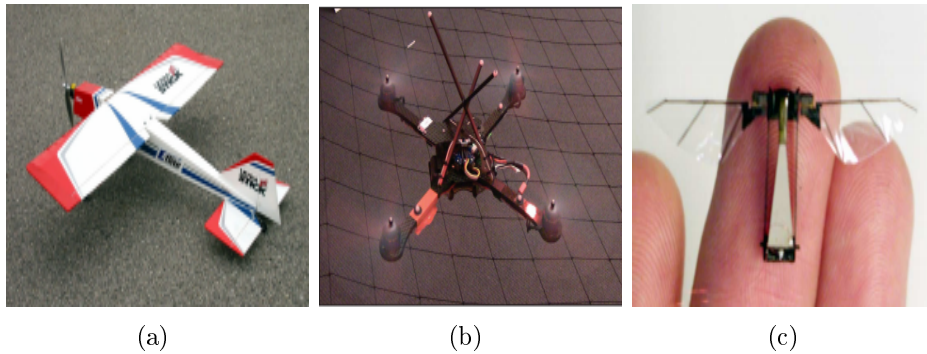


Figure 1.1: (a) Ultra Stick 25e fixed-wing UAV [18], (b) A rotary-wing UAV platform with VICON markers [19], (c) First-insect scale flapping wing UAV [20].

Another comprehensive categorization is suggested by Unmanned Vehicle System (UVS) International [21]. According to this classification tactical, strategic and special task UAVs constitute main categories. Tactical UAVs cover a range from Micro Aerial Vehicles (MAVs), which weighs less than 5 kg, to Medium Altitude Long Endurance (MALE) UAVs, that usually weighs around 1000 to 1500 kg. Strategic UAVs are bigger than the tactical ones and they weigh more than 2500 kg. Last category is solely formed by military UAVs such as combat and decoy UAVs.

## 1.1 Thesis Contributions and Organization

The contributions of the thesis can be summarized as follows:

- A high fidelity model of a novel quad-tilt wing UAV, which is called SUAVI (Sabanci University Unmanned Aerial Vehicle), is developed where
  - Uncertainties which result from a combination of wing asymmetry, component failure and unexpected damages are quantified,
  - The effect of wing angle evolution during the transition phase on plant dynamics is modeled,
  - A unique reference trajectory is generated to test the proposed model.
- A nonlinear hierarchical adaptive controller is proposed where each controller is computationally cheap, both the overall hierarchical framework and individual controllers are easy to implement and no linearization is needed in plant dynamics.
- Simulation results that compare performance of the proposed adaptive controllers with the feedback linearization controller that was also used in [22] with the presence of component failure, wind disturbance and sensor noise.

Organization of the paper is as follows:

In Chapter II a literature survey is provided regarding hybrid wing UAVs and variety of flight controller approaches that are applied to control UAVs.

Chapter III develops the full nonlinear dynamic model of SUAVI including uncertainties such as principal moments of inertias and mass changes emanating from unexpected failures and evolution of wing angles during transition. A flight reference trajectory is generated to test the proposed controllers.

In Chapter IV a hierarchical nonlinear controller approach, which can adapt its parameters online, is developed. In the proposed controller approach a Model Reference Adaptive Controller provides the reference attitude angles for the lower level nonlinear adaptive controller.

Simulation results are provided in Chapter V which includes a comparison between the feedback linearization approach and the proposed nonlinear adaptive controller approach for three different flight scenarios. First scenario includes a component failure and actuator uncertainties; in the second scenario a wind disturbance is added to the first scenario, and in the third scenario sensor measurement noises are also added to the second scenario.

Chapter VI concludes the thesis with several remarks and indicates possible future directions.

## 1.2 Publications

The following papers are produced during my MS thesis work.

- Adaptive Nonlinear Hierarchical Control of a Quad Tilt-Wing UAV, Y. Yildiz, M. Unel, A. E. Demirel, ECC' 15: European Control Conference, Linz, Austria, July 15-17, 2015.
- Nonlinear Hierarchical Control of a Quad-Tilt-Wing UAV: An Adaptive Control Approach, Y. Yildiz, M. Unel, A. E. Demirel, IEEE Transactions On Control Systems Technology, 2015. (Submitted)

- Modeling, Control and Simulation of a Prototype Ornithopter, A. E. Demirel, M. Unel, TOK' 14: Turkish Automatic Control Conference, Kocaeli, Turkey, 2014.

# Chapter II

## 2 Related Work

An extensive literature survey about hybrid wing UAVs and flight control systems of autonomous unmanned aerial systems will be presented in Section 2.1 and 2.2, respectively.

### 2.1 Hybrid-Wing UAVs

Hybrid-wing UAVs combine the advantages of rotary and fixed wing UAVs. They have the rotary wing UAVs' ability of vertical take-off and landing (VTOL); therefore, they do not need a runway. Additionally, after their take-off they can change their wing configuration and fly for extended period of time with high speeds. Tilt-rotor UAVs are a subclass under the hybrid-wing UAVs which constitute the characteristic of efficient energy use [23, 24]. Dual-tilt rotor and dual-tilt wing UAVs can be found in this sub-class (Fig. 2.1). However, they are sensitive to rotor malfunctions and for longitudinal motion they need the complex rotor pitch mechanism such as a swash plate.

The GL-10 prototype tilt-wing UAV [27] was developed at NASA Langley Research Center (See Fig. 2.2). It weighs 60 lbs with a 10.5 ft wingspan and since it has 10 rotors, it is more reliable for rotor malfunctions with respect to the dual-tilt wing counterparts. It is still an ongoing project which aims to develop a long endurance (approximately 24 hours of cruise flight) and fully autonomous UAV.

Quad-Tilt Wing (QTW) UAVs form another category which have a tandem wing configuration with four propellers, each mounted on middle of the



Figure 2.1: (a) Flight test of small scaled tilt-rotor UAV [25], (b) Dual tilt wing UAV HARVee [26].

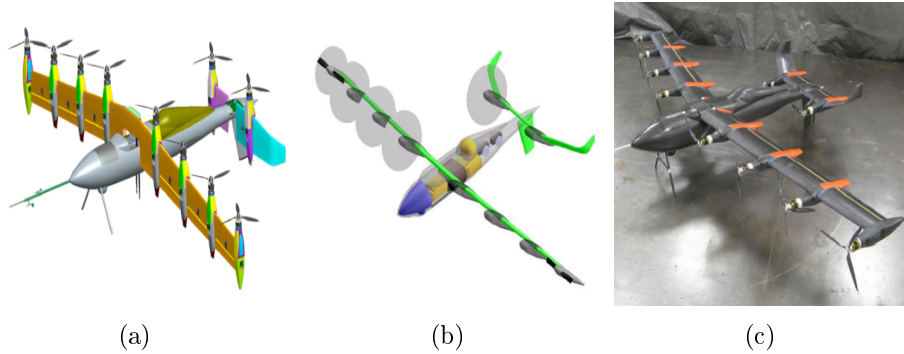


Figure 2.2: CAD models showing (a) vertical and (b) transition modes and prototype aircraft in (c) horizontal mode.

front and rear wings. Thanks to their additional two wings, they do not show the disadvantage of cyclic control requirements that can be encountered in dual tilt-rotors. There are three flight modes of a QTW UAV; (1): vertical mode where UAV has the capability of VTOL, (2): horizontal mode where it can fly like a fixed-wing UAV and this mode is suitable for long-distance, energy efficient flight, (3): transition where UAV changes its wing configuration from vertical to transition and vice-versa.

Various research groups have been working on QTW UAVs. Muraoka et al. [28] constructed and tested a proof-of-concept QTW UAV which is

remotely controlled with an RC system by a pilot (Figure 2.3 (a)). They also investigated the transition mode of the QTW [29]. Suzuki et al. [30] designed a model-based attitude controller of a QTW UAV and its effectiveness was validated by flight experiments. SUAVI [22, 31–35] is another example that was designed, manufactured and flight tested at Sabanci University, which will be discussed in more detail in Chapter 3.



Figure 2.3: Examples of QTW UAVs

## 2.2 UAV Flight Control Systems

The main challenges that make the control of tilt-wing UAVs a difficult task which requires advanced controllers are: (1) the coupling between the translational and rotary motions, (2) highly nonlinear multi-input multi-output system dynamics, (3) various uncertainty sources as in the work of Dydek et al. [36]. These authors introduced a propeller cut during the flight which results in the loss-of-thrust. In addition, unpredictable damages and actuator malfunctions can be possible uncertainty sources. A rich literature exists on the closed loop control of UAVs offering a variety of controllers to handle these changes. A comprehensive literature survey about the guidance,

navigation and control of rotary UAVs can be found in [37] and in this survey flight control systems are classified as:

- Linear flight control systems.
- Model-based nonlinear controllers.
- Learning-based flight controllers.

Flight controllers will be discussed based on this classification below.

### 2.2.1 Linear Flight Control Systems

Some examples of controllers proposed in the literature are PID type. PID technique which utilizes simplified dynamics and LQ based control approach based on a complete model of an autonomous UAV is proposed in [38]. In the work of Pounds et al. [39], dynamic load disturbances were introduced by instantaneously payload mass to small-scale UAV helicopters and quadrotors and these disturbances were compensated with a PID. PID controllers were also used in flight simulations that were done in the context of OS4 project which was initiated in Autonomous System Laboratory (EPFL) to design a fully autonomous UAV [40]. Furthermore, position control of the STARMAC (Stanford Testbed of Autonomous Aircraft for Multi-Agent Control) quadrotor helicopter was achieved by PID [41]. There are also PD<sup>2</sup> controllers where a proportional and two derivative actions were used [42].

Linear-quadratic regulator (LQR) or linear-quadratic gaussian (LQG) is also a widely used optimal control technique which has been applied to various UAVs. On a simplified quadrotor model, the LQR was used to track the reference trajectory in the presence of disturbances [43]. The LQR was also

implemented in MIT Real-Time Indoor Autonomous Vehicle Test Environment's (RAVEN) quadrotors, to optimize the vehicle's hover capabilities [44]. Besides, an LQR controller was used to stabilize the right hand poles of a Yamaha RMAX helicopter system [45]. Here a feedback linearization controller was used to linearize the system and PID controllers were used for trajectory tracking.

The  $H_\infty$  approach is a model based robust control method. Civita et al. [46] implemented a gain scheduled  $H_\infty$  loop shaping controller to test flight of a Yamaha R-50 robotic helicopter. Besides, a robust  $H_\infty$  control for muFly, which is a coaxial helicopter with a mass of 95 g, was designed and its attitude and heave control have been tested [47]. Furthermore, Gadewadikar et al. [48] presented an  $H_\infty$  approach for helicopter control and disturbance accommodation.

In gain scheduling approach, a nonlinear model of UAV is linearized about one or more operating points. Then linear controllers provide satisfactory control around each operating point. A gain-scheduled PID control (GS-PID) was investigated in the presence of fault(s) in one or more actuator during the flight and experimentally tested on a Qball-X4 quadrotor [49]. In the method of Gillula et al. [50], the behavior of the system was approximated as a collection of simplified hybrid modes, which represent a particular operating regime defined by a region of the state space. Linear control tools were then used to design control laws and to construct aggressive manoeuvres, such as a backflip on a STARMAC quadrotor.

### 2.2.2 Model-based Nonlinear Controllers

Feedback linearization is a widely used technique which transforms the variables of the system into a new coordinate system, where dynamics are linear. It achieves exact state transformation rather than linear approximations. Dynamic inversion is a specific case of feedback linearization where the nonlinear plant dynamics are inverted and used as feedback. Helicopter controller design based on input-output linearization was performed by Koo and Sastry [51]. They showed that input-output linearization results in unstable zero dynamics. Voos [52] used a nested quadrotor control structure, which consists of velocity and attitude control. Attitude control problem was solved with a feedback linearization approach and for velocity control a proportional controller was used. Peng et al. [53] proposed a hierarchical control for the autonomous flight of a UAV helicopter which consists of a composite nonlinear feedback control for the inner loop and dynamic inversion for the outer loop. A commercial Raptor 90 helicopter was able to achieve take-off, hovering and landing with the proposed controller.

Feedback linearization techniques can be vulnerable to uncertainties and modeling errors. Adaptive control techniques offer a robust solution for the unknown or change in time system parameters. Since the adaptation mechanism updates the parameters of the adjustable controller and generates an auxiliary control to maintain the performance [54]. A feedback linearizing nonlinear adaptive controller was designed for multiple UAV formation flight [55]. In addition, variable-structure and a parametric identification approaches were combined in an adaptive control law for an autopilot of the UAV [56]. In order to overcome the sensor noise and modeling uncertainties of a quadrotor helicopter, an adaptive sliding mode controller approach was pre-

sented in [57]. Generally sliding mode controllers use large control inputs to overcome various uncertainties, however with the proposed approach control inputs do not reach large magnitudes. In [58] a direct approximate-adaptive control, using cerebellar model articulation controller (CMAC) approach was used on a quadrotor helicopter and uniform ultimate boundedness of all signals was ensured with a Lyapunov stability proof. In the work of Palunko and Fierro [59], an adaptive controller based on output feedback linearization was used to compensate the dynamic changes in center of gravity (CoG). In the first stage a cascade PD controller was implemented but it could not stabilize the system due to uncertain center of gravity changes. Therefore an adaptive feedback linearization controller was used and its stability was proven with Lyapunov theory.

Model Predictive Control (MPC) approach uses an explicit model of the plant to predict the future evolution of the plant to optimize the control inputs. A flight control system based on a nonlinear MPC was used in [60] to avoid input/output saturation over the flight envelope. The controller was validated with experimental results which consist of way-point navigation, pursuit-evasion game and tracking of a moving target. Shim, Kim and Sastri [61] presented a nonlinear model predictive control (NMPC) for multiple autonomous UAVs. In their framework, collision avoidance in a dynamic complex three-dimensional space has also been considered. The NMPC approach was also used in [62] as a high level controller of a fixed wing UAV. The performance of the approach was tested through hardware in the loop simulations.

Backstepping is a recursive control methodology which describes some of the state variables as virtual controls. Then, intermediate control laws are

designed for these virtual controls [63]. In order to achieve global asymptotic stability a backstepping controller was designed for a generic quadrotor UAV model in [64]. The controller was designed specifically for the hovering condition of the UAV in the presence of reduced actuation and turbulent gust disturbances. There are also experimental works of backstepping approach: A novel backstepping landing controller was flight tested on a commercial EAGLE helicopter [65]. An innovative extension was applied to backstepping which is a correction control to compensate for the flapping and servo dynamics. Furthermore, in the work carried by Lee et al. [66], an exponentially stable backstepping controller was applied on a quadrotor UAV and tested experimentally. In this work UAV tracks the trajectory of the Cartesian virtual point which is teleoperated over the internet.

### **2.2.3 Learning-based Flight Controllers**

Fuzzy logic control (FLC) is one of the learning-based controller which has been successfully applied to variety of unmanned aerial systems. The main idea of FLC is designing a controller based on human operator experience with a collection of fuzzy control rules. Sugeno et al. [67] designed a FLC to control an unmanned helicopter. Expert knowledge and training data was used to generate fuzzy rules base and the proposed approach was flight tested on a Yamaha R-50 helicopter. The later successfully executed hovering and forward flight with voice activated commands. On a full scale UH1-H helicopter a fuzzy logic controller was implemented in [68]. Individual fuzzy logic controllers were used for a set of tasks that are necessary to fly the aircraft and a genetic algorithm set the rules for the each FLC. Furthermore, in a recent study of Santos et al. [69] a PID-like fuzzy intelligent control

approach was proposed for a quadrotor. Decisions of the controller is based on four motions of a quadrotor, which are height, pitch, roll and yaw.

Artificial neural networks (ANN) consist of statistical learning models which are inspired by human brain. Kim and Calise [70] developed a neural-network based flight controller. They used the neural networks to represent the nonlinear inverse transformation needed for feedback linearization. In another approach developed by Buskey et al. [71], ANN generated hover commands for an autonomous helicopter by using the data obtained from inertial navigation system (INS) and these commands manipulated the servos. INS to actuator relation is learned with a feedforward network using the back propagation regime. A finite impulse response (FIR) approximator, which approximates the response of a  $PI^{\lambda}D^{\mu}$  controller, is trained with neural networks in [72]. This controller implemented on a quadrotor UAV with a promising tracking results.

Human based learning approach is also promising for UAV control. Gavrillets et al. [73] collected input/output data from a human operated helicopter to determine intuitive control strategies. The aim of this study was to extract input sequences that a human pilot uses to perform aggressive manoeuvres with the MIT's Xcell-60 helicopter. The intuition that was developed with this paper was used in [74] for the automatic execution of maneuvers that is inspired by the human pilot. This controller was flight tested with aggressive maneuvers such as hammerhead and  $360^{\circ}$  axial roll.

# Chapter III

## 3 Mathematical Model of SUAVI

SUAVI is a novel tandem wing QTW UAV. It is a highly coupled nonlinear system, which changes its wing angles during the flight (Fig. 3.1). Evolution of wing angles affects the model significantly due to the change of moment of inertias, lift and drag forces.



Figure 3.1: SUAVI in different wing configurations; (Left) Horizontal, (Middle) Transition, (Right) Vertical [75].

Nonlinear dynamics of the SUAVI are described in this chapter. Additionally, a reference flight trajectory and an example scenario are generated to test the proposed controllers developed in Chapter III. According to the test scenario a failure occurs at the right wings during the horizontal flight. Hence, evolution of principal moment of inertias and mass due to this failure and change of wing angles are examined. Besides, center of gravity variation due to failure is also taken into account.

### 3.1 System Model

In deriving dynamical model of the aerial vehicle the following assumptions are made:

- The aerial vehicle is a 6 DOF rigid body.
- Downwash effect of the front wings on the rear wings is neglected.
- Same angles for the front and rear wings are used.

World  $W : (O_w, x_w, y_w, z_w)$  and body  $B : (O_b, x_b, y_b, z_b)$  reference frames are utilized in order to model the aerial vehicle (see Fig. 3.2).

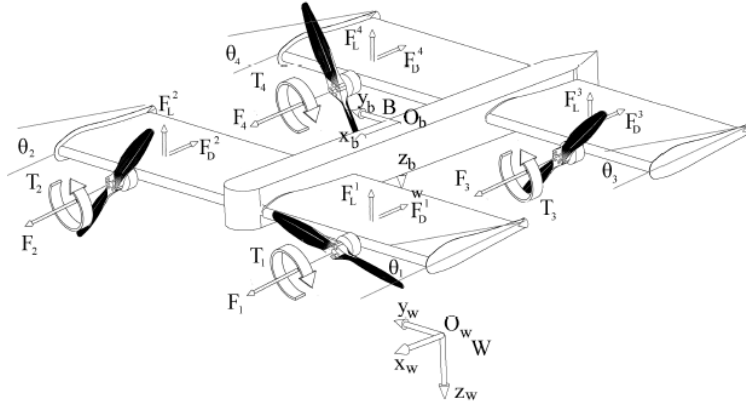


Figure 3.2: Coordinate frames, forces and momets on SUAVI.

UAV's attitude and its time derivative in the world frame are defined as

$$\alpha_w = [\phi, \theta, \psi]^T, \quad \Omega_w = \dot{\alpha}_w = [\dot{\phi}, \dot{\theta}, \dot{\psi}]^T \quad (1)$$

where  $\phi$ ,  $\theta$  and  $\psi$  are roll, pitch and yaw angles, respectively.

Position and linear velocity of the vehicle's center of mass in the world frame are defined as

$$P_w = [X, Y, Z]^T, \quad V_w = \dot{P}_w = [\dot{X}, \dot{Y}, \dot{Z}]^T \quad (2)$$

The orientation of the body frame with respect to the world frame is defined by the  $R_{wb}(\phi, \theta, \psi)$  rotation matrix where

$$R_{wb}(\phi, \theta, \psi) = \begin{bmatrix} c_\psi c_\theta & s_\phi s_\theta c_\psi - c_\phi s_\psi & c_\phi s_\theta c_\psi + s_\phi s_\psi \\ s_\psi c_\theta & s_\phi s_\theta s_\psi + c_\phi c_\psi & c_\phi s_\theta s_\psi - s_\phi c_\psi \\ -s_\theta & s_\phi c_\theta & c_\phi c_\theta \end{bmatrix} \quad (3)$$

For simplicity, in this and the following equations  $c(\cdot)$  and  $s(\cdot)$  denote  $\cos(\cdot)$  and  $\sin(\cdot)$ , respectively. Linear velocity transformation between the world and the body frames is given as

$$V_b = \begin{bmatrix} v_x \\ v_y \\ v_z \end{bmatrix} = R_{wb}^T(\phi, \theta, \psi) \cdot \begin{bmatrix} \dot{X} \\ \dot{Y} \\ \dot{Z} \end{bmatrix} = R_{bw}(\phi, \theta, \psi) \cdot V_w \quad (4)$$

The following transformation gives the relationship between  $p, q, r$  which are angular velocities around  $x, y, z$  axis of the vehicle and the time derivative of the attitude angles:

$$\Omega_w = \mathbb{E}^{-1}(\alpha_w)\Omega_b = \mathbb{B}(\alpha_w) \begin{bmatrix} p \\ q \\ r \end{bmatrix} \quad (5)$$

where  $\mathbb{E}$  is the velocity transformation matrix and  $\mathbb{B}$  is inverse of the velocity transformation.  $\mathbb{E}$  is given as

$$\mathbb{E}(\alpha_w) = \begin{bmatrix} 1 & 0 & -s_\theta \\ 0 & c_\phi & s_\phi c_\theta \\ 0 & -s_\phi & c_\phi c_\theta \end{bmatrix} \quad (6)$$

Overall dynamics equations of the system are given as

$$\begin{bmatrix} mI_{3 \times 3} & 0_{3 \times 3} \\ 0_{3 \times 3} & I_b \end{bmatrix} \begin{bmatrix} \dot{V}_w \\ \dot{\Omega}_b \end{bmatrix} + \begin{bmatrix} 0 \\ \Omega_b \times (I_b \Omega_b) \end{bmatrix} = \begin{bmatrix} F_t \\ M_t \end{bmatrix} \quad (7)$$

where  $m$  and  $I_b$  are mass and moment of inertia matrix in body frame, respectively.  $V_w$  is the linear velocity in the world frame and  $\Omega_b$  is the angular velocity in the body frame.  $F_t$  and  $M_t$  are the net forces and moments applied on the UAV.

The net force acting on the system  $F_t$  consists of the motor thrusts  $F_{th}$ , aerodynamic forces  $F_w$ , gravity on the UAV  $F_g$  and external disturbances  $F_d$  such as winds. These forces are transformed to the world frame as follows:

$$F_t = R_{wb}(F_{th} + F_w + F_g + F_d) \quad (8)$$

where motor thrust forces  $F_{th}$  are defined as

$$F_{th} = \begin{bmatrix} c_{\theta_1} & c_{\theta_2} & c_{\theta_3} & c_{\theta_4} \\ 0 & 0 & 0 & 0 \\ -s_{\theta_1} & -s_{\theta_2} & -s_{\theta_3} & -s_{\theta_4} \end{bmatrix} \begin{bmatrix} k\omega_1^2 \\ k\omega_2^2 \\ k\omega_3^2 \\ k\omega_4^2 \end{bmatrix}$$

where  $i = 1, 2, 3, 4$  and  $\theta_i$  denotes wing angles with respect to body (See Fig. 3.2). Motor thrusts are modeled as

$$F_i = k\omega_i^2 \quad (9)$$

where  $k$  is the motor thrust constant and  $\omega_i$  is the each rotor's rotational speed. For simplicity, all of the wings are tilted together, leading to the relations  $\theta_1 = \theta_2 = \theta_3 = \theta_4$ .

Wing forces  $F_w$  is denoted as

$$F_w = \begin{bmatrix} (F_D^1 + F_D^2 + F_D^3 + F_D^4) \\ 0 \\ (F_L^1 + F_L^2 + F_L^3 + F_L^4) \end{bmatrix}$$

Lift forces  $F_L^i(\theta_i, v_x, v_z)$  and drag forces  $F_D^i(\theta_i, v_x, v_z)$  are functions of linear velocities  $v_x$  and  $v_z$ , and the wing angle of attacks  $\theta_i$ . These functions are given as

$$\begin{bmatrix} F_D^i \\ 0 \\ F_L^i \end{bmatrix} = R(\theta_i - \alpha_i) \begin{bmatrix} -\frac{1}{2}c_D(\alpha_i)\rho Av_\alpha^2 \\ 0 \\ -\frac{1}{2}c_L(\alpha_i)\rho Av_\alpha^2 \end{bmatrix} \quad (10)$$

where  $\rho$  is the air density,  $A$  is the wing planform area,  $R(\theta_i - \alpha_i)$  is the rotation matrix for the rotation around y axis that decomposes the forces on the wings onto the body axes. Defining  $\beta = \theta_i - \alpha_i$ ,  $R(\beta)$  becomes

$$R(\beta) = \begin{bmatrix} c_\beta & 0 & s_\beta \\ 0 & 1 & 0 \\ -s_\beta & 0 & c_\beta \end{bmatrix} \quad (11)$$

$v_\alpha$  is the airstream velocity which is defined by

$$v_\alpha = \sqrt{v_x^2 + v_z^2} \quad (12)$$

where  $v_x$  and  $v_z$  are UAV's velocities along  $X$  and  $Y$  of the body coordinate frame.  $\alpha_i$  is the effective angle of attack (Fig. 3.3) which is defined as

$$\alpha_i = \theta_i - (-atan2(v_z, v_x)) \quad (13)$$

$C_L$  and  $C_D$  are the lift and drag coefficients, respectively, which are obtained

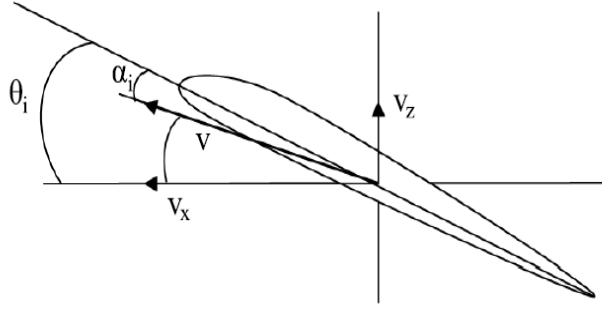


Figure 3.3: Effective angle of attack,  $\alpha_i$ .

from wind tunnel tests' data [76]. Cubic polynomial curves were fitted to lift and drag coefficient data which are shown in Figure 3.4 and expressed in equations (14) and (15).

$$C_L(\alpha_i) = -3\alpha_i^4 + 9.6\alpha_i^3 - 11\alpha_i^2 + 5.4\alpha_i + 0.0013 \quad (14)$$

$$C_D(\alpha_i) = -0.52\alpha_i^3 + 1.1\alpha_i^2 + 0.23\alpha_i + 0.012 \quad (15)$$

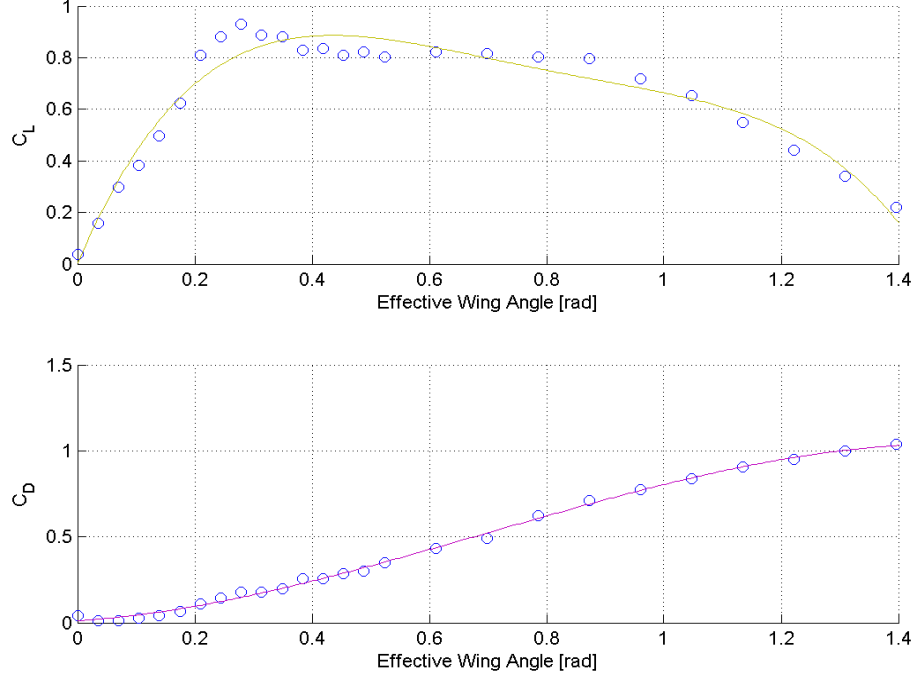


Figure 3.4: Cubic polynomial curve fitting to the lift and drag coefficients' wind tunnel data.

The total moment  $M_t$  can be defined as:

$$M_t = M_{th} + M_w + M_{gyro} + M_d \quad (16)$$

where  $M_{th}$  is the moments generated by the rotors:

$$M_{th} = l_s \begin{bmatrix} s_{\theta_1} - \frac{\lambda_1}{l_s} c_{\theta_1} & -s_{\theta_2} - \frac{\lambda_2}{l_s} c_{\theta_2} & s_{\theta_3} - \frac{\lambda_3}{l_s} c_{\theta_3} & -s_{\theta_4} - \frac{\lambda_4}{l_s} c_{\theta_4} \\ \frac{l_l}{l_s} s_{\theta_1} & \frac{l_l}{l_s} s_{\theta_2} & -\frac{l_l}{l_s} s_{\theta_3} & -\frac{l_l}{l_s} s_{\theta_4} \\ c_{\theta_1} + \frac{\lambda_1}{l_s} s_{\theta_1} & -c_{\theta_2} + \frac{\lambda_2}{l_s} s_{\theta_2} & c_{\theta_3} + \frac{\lambda_3}{l_s} s_{\theta_3} & -c_{\theta_4} + \frac{\lambda_4}{l_s} s_{\theta_4} \end{bmatrix} \begin{bmatrix} k\omega_1^2 \\ k\omega_2^2 \\ k\omega_3^2 \\ k\omega_4^2 \end{bmatrix}$$

$M_w$  is the moments generated by the aerodynamic forces:

$$M_w = \begin{bmatrix} l_s(F_L^1 - F_L^2 + F_L^3 - F_L^4) \\ l_l(F_L^1 + F_L^2 - F_L^3 - F_L^4) \\ l_s(-F_D^1 + F_D^2 - F_D^3 + F_D^4) \end{bmatrix}$$

$M_{gyro}$  is the moments produced by the gyroscopic effects of the propellers:

$$M_{gyro} = \sum_{i=1}^4 J_{prop} [\eta_i \Omega_b \times \begin{bmatrix} c\theta_i \\ 0 \\ -s\theta_i \end{bmatrix} \omega_i]$$

$M_d$  is the moments due to the external disturbances.

In these expressions,  $l_s$  and  $l_l$  denote the rotor distance to center of gravity along y and x axis, respectively.  $J_{prop}$  is the rotational inertia of the rotors about their rotation axes and  $\eta_{(1,2,3,4)} = 1, -1, -1, 1$ . The rotor reaction torques are modeled as

$$T_i = \lambda_i k \omega_i^2 \quad (17)$$

where  $\lambda_i$  are torque/force ratios. For clockwise rotating propellers,  $\lambda_{2,3} = -\lambda$  whereas for counterclockwise rotating propellers  $\lambda_{1,4} = \lambda$ .

Using vector-matrix notation, (7) can be written as follows:

$$M\dot{\zeta} + C(\zeta)\zeta = G + O(\zeta)\omega + E(\xi)\omega^2 + W(\zeta) + D(\zeta, \xi) \quad (18)$$

where  $\zeta = [\dot{X}, \dot{Y}, \dot{Z}, p, q, r]^T$  and  $\xi = [X, Y, Z, \phi, \theta, \psi]^T$ .  $M$ , the inertia matrix,  $C$ , Coriolis-centripetal matrix and  $G$ , the gravity term, are given as

follows:

$$M = \begin{bmatrix} mI_{3 \times 3} & 0_{3 \times 3} \\ 0_{3 \times 3} & \text{diag}(I_{xx}, I_{yy}, I_{zz}) \end{bmatrix} \quad (19)$$

$$C(\zeta) = \begin{bmatrix} 0 & 0 & 0 & 0 & 0 & 0 \\ 0 & 0 & 0 & 0 & 0 & 0 \\ 0 & 0 & 0 & 0 & 0 & 0 \\ 0 & 0 & 0 & 0 & I_{zz}r & -I_{yy}q \\ 0 & 0 & 0 & -I_{zz}r & 0 & I_{xx}p \\ 0 & 0 & 0 & I_{yy}q & -I_{xx}p & 0 \end{bmatrix} \quad (20)$$

$$G = \begin{bmatrix} 0 & 0 & mg & 0 & 0 & 0 \end{bmatrix}^T \quad (21)$$

where  $I_{xx}, I_{yy}$  and  $I_{zz}$  are the moments of inertia of the aerial vehicle around its body frame axes.

$$O(\zeta)\omega = J_{prop} \left( \begin{array}{c} 0_{3 \times 1} \\ \sum_{i=1}^4 [\eta_i \Omega_b \times \begin{bmatrix} c_{\theta_i} \\ 0 \\ -s_{\theta_i} \end{bmatrix} \omega_i] \end{array} \right) \quad (22)$$

Lift and drag forces produced by the wings and the resulting moments due

to these forces for different wing angles are defined as

$$W(\zeta) = \begin{bmatrix} W_x \\ W_y \\ W_z \\ 0 \\ W_t \\ 0 \end{bmatrix} = \begin{bmatrix} R_{wb} \begin{bmatrix} F_D^1 + F_D^2 + F_D^3 + F_D^4 \\ 0 \\ F_L^1 + F_L^2 + F_L^3 + F_L^4 \\ 0 \\ l_l(F_L^1 + F_L^2 - F_L^3 - F_L^4) \\ 0 \end{bmatrix} \end{bmatrix} \quad (23)$$

$W_x$ ,  $W_y$  and  $W_z$  are aerodynamic forces along  $X$ ,  $Y$ ,  $Z$  axis of world coordinate frame and  $W_t$  is the moment produced by aerodynamic forces around  $Y$  axis of body fixed coordinate frame.

When aerodynamic downwash effects of the front wings on the rear wings are neglected and same angles are used for front and rear wings, system actuator vector,  $E(\xi)\omega^2$ , can be given as

$$E(\xi)\omega^2 = \begin{bmatrix} (c_\psi c_\theta c_{\theta_f} - (c_\phi s_\theta c_\psi + s_\phi s_\psi) s_{\theta_f}) u_1 \\ (s_\psi c_\theta c_{\theta_f} - (c_\phi s_\theta s_\psi - s_\phi c_\psi) s_{\theta_f}) u_1 \\ (-s_\theta c_{\theta_f} - c_\phi c_\theta s_{\theta_f}) u_1 \\ s_{\theta_f} u_2 - c_{\theta_f} u_4 \\ s_{\theta_f} u_3 \\ c_{\theta_f} u_2 + s_{\theta_f} u_4 \end{bmatrix} \quad (24)$$

where  $\theta_f$  denotes the front wing angle. Control inputs  $u_1$ ,  $u_2$ ,  $u_3$  and  $u_4$  in (24) are given as:

$$u_1 = k(\omega_1^2 + \omega_2^2 + \omega_3^2 + \omega_4^2) \quad (25)$$

$$u_2 = kl_s(\omega_1^2 - \omega_2^2 + \omega_3^2 - \omega_4^2) \quad (26)$$

$$u_3 = kl_l(\omega_1^2 + \omega_2^2 - \omega_3^2 - \omega_4^2) \quad (27)$$

$$u_4 = k\lambda(\omega_1^2 - \omega_2^2 - \omega_3^2 + \omega_4^2) \quad (28)$$

In light of equation (18) dynamics of the aerial vehicle can be written as

$$\begin{aligned} \ddot{X} &= \frac{1}{m} [(c_\psi c_\theta c_{\theta_f} - (c_\phi s_\theta c_\psi + s_\phi s_\psi) s_{\theta_f}) u_1 + W_x] \\ \ddot{Y} &= \frac{1}{m} [(s_\psi c_\theta c_{\theta_f} - (c_\phi s_\theta s_\psi - s_\phi c_\psi) s_{\theta_f}) u_1 + W_y] \\ \ddot{Z} &= \frac{1}{m} [(-s_\theta c_{\theta_f} - c_\phi c_\theta s_{\theta_f}) u_1 + mg + W_z] \\ \dot{p} &= \frac{u_2}{I_{xx}} + \frac{I_{yy} - I_{zz}}{I_{xx}} qr - \frac{J_{prop}}{I_{xx}} q \omega_p s_{\theta_f} \\ \dot{q} &= \frac{u_3}{I_{yy}} + \frac{I_{zz} - I_{xx}}{I_{yy}} pr + \frac{J_{prop}}{I_{yy}} (p s_{\theta_f} + r c_{\theta_f}) \omega_p + W_t \\ \dot{r} &= \frac{u_4}{I_{zz}} + \frac{I_{xx} - I_{yy}}{I_{zz}} pq - \frac{J_{prop}}{I_{zz}} q \omega_p c_{\theta_f} \end{aligned} \quad (29)$$

where  $\omega_p = \omega_1 - \omega_2 - \omega_3 + \omega_4$ .

In order to design attitude controllers, attitude dynamics of the UAV should be expressed in world coordinate frame. The attitude dynamics of the UAV in body fixed coordinate frame is given in Eqn. (7) as:

$$\dot{\Omega}_b = I_b^{-1} (-\Omega_b \times (I_b \Omega_b) + M_t) \quad (30)$$

and the derivative of Eqn. (5) is

$$\dot{\Omega}_w = \mathbb{B} \dot{\Omega}_b + \mathbb{B} \dot{\Omega}_b \quad (31)$$

By using Eqn. (5) and substituting Eqn. (30) into Eqn. (31), the following equation is obtained

$$\dot{\Omega}_w = \dot{\mathbb{B}}\mathbb{E}\Omega_w - \mathbb{B}I_b^{-1}(\mathbb{E}\Omega_w \times I_b\mathbb{E}\Omega_w) + \mathbb{B}I_b^{-1}M_t \quad (32)$$

Multiplying both sides of Eqn. (32) by the matrix  $\mathbb{M}(\alpha_w) = \mathbb{E}^T I_b \mathbb{E}$  and using the fact  $\dot{\mathbb{E}} = -\mathbb{E}\dot{\mathbb{B}}\mathbb{E}$ , the following equation is obtained:

$$\mathbb{M}(\alpha_w)\dot{\Omega}_w = -\mathbb{E}^T I_b \dot{\mathbb{E}}\Omega_w - \mathbb{E}^T(\mathbb{E}\Omega_w \times I_b\mathbb{E}\Omega_w) + \mathbb{E}^T M_t \quad (33)$$

Coriolis terms in above equation can be written with a  $\mathbb{C}$  matrix as

$$\mathbb{C}(\alpha_w, \Omega_w) = \mathbb{E}^T I_b \dot{\mathbb{E}} + \mathbb{E}^T S(\mathbb{E}\Omega_w) I_b \mathbb{E}$$

where  $S(\cdot)$  is the skew-symmetric matrix that replaces the cross-product. The attitude dynamics expressed in the world frame can be written as follows

$$\mathbb{M}(\alpha_w)\dot{\Omega}_w + \mathbb{C}(\alpha_w, \Omega_w)\Omega_w = \mathbb{E}^T M_t \quad (34)$$

The modified inertia matrix  $\mathbb{M}(\alpha_w)$  in (34) is given as

$$\mathbb{M}(\alpha_w) = \begin{bmatrix} I_{xx} & 0 & -I_{xx}s\theta \\ 0 & I_{yy}c_\phi^2 + I_{zz}s_\phi^2 & \mathbb{M}_{23} \\ -I_{xx}s\theta & \mathbb{M}_{23} & \mathbb{M}_{33} \end{bmatrix} \quad (35)$$

where,

$$\mathbb{M}_{23} = I_{yy}c_\phi s_\phi c_\theta - I_{zz}c_\phi s_\phi c_\theta \quad (36)$$

$$\mathbb{M}_{33} = I_{xx}s_\theta^2 + I_{yy}s_\phi^2 c_\theta^2 + I_{zz}c_\phi^2 c_\theta^2 \quad (37)$$

and the Coriolis Matrix,  $\mathbb{C}(\alpha_w, \Omega_w)$  is given as

$$\mathbb{C}(\alpha_w, \Omega_w) = \begin{bmatrix} 0 & \mathbb{C}_{12} & \mathbb{C}_{13} \\ I_{xx}d & I_{yy}f + I_{zz}g & \mathbb{C}_{23} \\ I_{xx}e & I_{yy}h + I_{zz}k & \mathbb{C}_{33} \end{bmatrix}. \quad (38)$$

In (38),  $\mathbb{C}_{ij}$ s are defined as

$$\mathbb{C}_{12} = -I_{yy}s_3c_\phi - I_{zz}s_2s_\phi \quad (39)$$

$$\mathbb{C}_{13} = -I_{xx}c_\theta\dot{\theta} - I_{yy}s_3s_\phi c_\theta + I_{zz}s_2c_\phi c_\theta \quad (40)$$

$$\mathbb{C}_{23} = I_{xx}mm + I_{yy}n + I_{zz}P \quad (41)$$

$$\mathbb{C}_{33} = I_{xx}Q + I_{yy}R + I_{zz}\epsilon, \quad (42)$$

where,

$$\begin{aligned} s_1 &= \dot{\phi} - s_\theta\dot{\psi}, & s_2 &= c_\phi\dot{\theta} + s_\phi c_\theta\dot{\psi}, & s_3 &= -s_\phi\dot{\theta} + c_\phi c_\theta\dot{\psi}, \\ d &= s_3c_\phi + s_2s_\phi, & e &= s_3s_\phi c_\theta - s_2c_\phi c_\theta, & f &= -s_\phi\dot{\phi}c_\phi - s_1c_\phi s_\phi, \\ g &= s_1s_\phi c_\phi + c_\phi\dot{\phi}s_\phi, & mm &= -s_3s_\theta c_\phi - s_2s_\theta s_\phi, & a &= c_\phi\dot{\phi}c_\theta - s_\phi s_\theta\dot{\theta}, \\ n &= ac_\phi - s_1s_\phi^2 c_\theta, & b &= -s_\phi\dot{\phi}c_\theta - c_\phi s_\theta\dot{\theta}, & P &= -s_1c_\phi^2 c_\theta - bs_\phi, \\ h &= s_3c_\phi s_\theta - s_\phi^2\dot{\phi}c_\theta + s_1c_\phi^2 c_\theta, & k &= s_2s_\phi s_\theta + s_1s_\phi^2 c_\theta - c_\phi^2\dot{\phi}c_\theta, \\ \epsilon &= -s_2c_\phi c_\theta s_\theta - s_1c_\phi c_\theta^2 s_\phi + bc_\phi c_\theta, & Q &= c_\theta\dot{\theta}s_\theta - s_3s_\theta s_\phi c_\theta + s_2s_\theta c_\phi c_\theta, \\ R &= s_3s_\phi c_\theta s_\theta + as_\phi c_\theta + s_1s_\phi c_\theta^2 c_\phi. \end{aligned}$$

## 3.2 Example Flight Scenario

To analyze the behavior of the tilt-wing UAV during vertical, horizontal and transition modes, a flight scenario is created as shown in Fig. 3.5. According to the scenario:

1. The UAV takes off vertically with  $90^\circ$  wing angles (0s - 10s).
2. After reaching a desired altitude it changes its wing angles to  $20^\circ$  (10s - 20s).
3. Then, it flies in horizontal mode for about 650 meters (20s - 65s).
4. During level flight, two batteries, wing lower covers and winglets fall, all from the right wings (At  $t = 61$  s).
5. After level flight it changes its wing angles back to  $90^\circ$ , while slowing down (65s - 100s).
6. Then, it lands as a quadrotor (100s - 110s).

In the remaining of this Chapter, a trajectory generation method to obtain a zero pitch angle during horizontal motion is given. Additionally, the changes in mass, moment of inertia and center of gravity due to wing movements and failure are investigated.

### 3.2.1 Trajectory Generation for Pitch Angle Minimization

QTW UAV tilts its wings for long duration flights to benefit from the lift forces and flies in horizontal mode as depicted in Figure 3.5. However, position reference along the X axis of world coordinate frame may force the

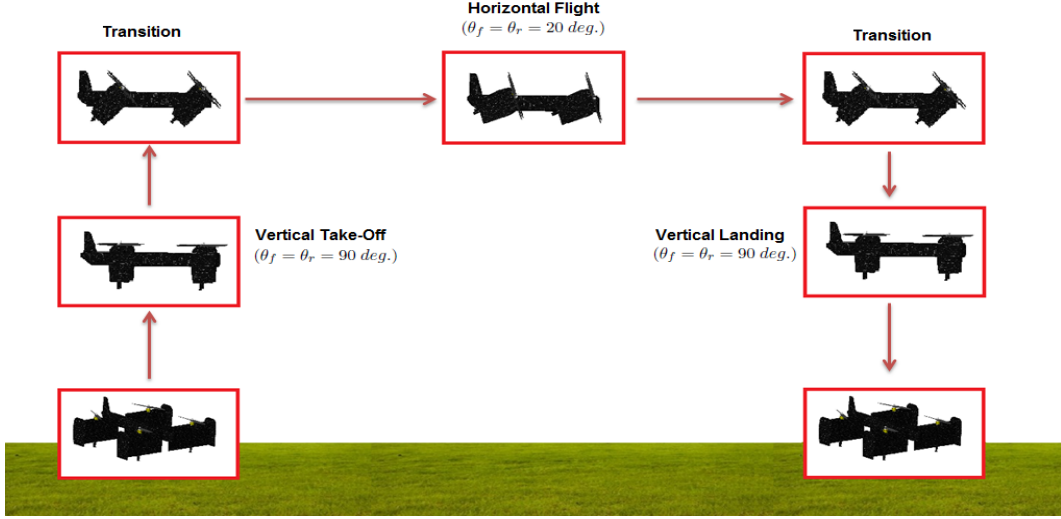


Figure 3.5: Implemented flight scenario.

vehicle to fly with relatively slow velocities which results in a dramatic increase at the pitch angle. Therefore a minimum forward velocity and a suitable reference trajectory that minimizes pitch angle during horizontal flight should be developed.

1) *Minimum forward velocity:* In order to obtain the minimum forward velocity that will lead to a zero degree pitch angle during horizontal flight, UAV dynamics along the  $Z$  axis is recalled:

$$\ddot{Z} = \frac{1}{m} [(-s_{\theta}c_{\theta_f} - c_{\phi}c_{\theta}s_{\theta_f})u_1 + mg + W_z] \quad (43)$$

There should be a zero net force along the  $Z$  axis (i.e.  $m\ddot{Z} = 0$ ) for a level flight. Additionally, pitch angle should be set to zero which results in,

$$W_z = c_{\phi}s_{\theta_f}u_1 - mg \quad (44)$$

Recall the aerodynamic forces along X, Y, Z axis of the world coordinate frame:

$$W(\zeta) = \begin{bmatrix} W_x \\ W_y \\ W_z \end{bmatrix} = \begin{bmatrix} R_{wb} \begin{bmatrix} F_D^1 + F_D^2 + F_D^3 + F_D^4 \\ 0 \\ F_L^1 + F_L^2 + F_L^3 + F_L^4 \end{bmatrix} \end{bmatrix} \quad (45)$$

To simplify the analysis all wing angles are assumed to be equal. Therefore, lift and drag forces are defined as

$$\begin{aligned} F_L^1 &= F_L^2 = F_L^3 = F_L^4 \\ F_D^1 &= F_D^2 = F_D^3 = F_D^4 \end{aligned}$$

From (45), wing forces along Z axis becomes

$$W_z = -s_\theta(4F_D) + c_\phi c_\theta(4F_L)$$

If the pitch angle is set to zero then  $W_z$  becomes

$$W_z = c_\phi(4F_L)$$

Substituting  $W_z$  in (44) the lift force that is necessary for a level flight can be found as

$$F_L = \frac{c_\phi s_{\theta_f} u_1 - mg}{4c_\phi} \quad (46)$$

Using (10), (11) and (46) it is obtained that

$$-2s_\beta C_D \rho A v_\alpha^2 + 2c_\beta C_L \rho A v_\alpha^2 = \frac{c_\phi s_{\theta_f} u_1 - mg}{c_\phi} \quad (47)$$

The minimum forward velocity in the body coordinate frame that can achieve zero degree pitch angle is obtained using (12) and (47) as

$$v_x = \sqrt{\frac{c_\phi s_{\theta_f} u_1 - mg}{2c_\beta c_\phi C_L \rho A - 2s_\beta c_\phi C_D \rho A}} - v_z^2 \quad (48)$$

Using the transformation of linear velocities between the body and world frames,  $V_w = R_{wb}V_b$ , minimum forward velocity in the world frame that can achieve zero degree pitch angle can be identified as

$$\dot{X} = c_\psi c_\theta v_x + s_\phi s_\theta c_\psi v_y - c_\phi s_\psi v_y + c_\phi s_\theta c_\psi v_z + s_\phi s_\psi v_z \quad (49)$$

2) *Trajectory Generation*: If minimum forward velocity, that is given in (49), is achieved then it creates the lift forces to sustain its level flight. Therefore, a suitable trajectory is generated along the X axis by using so called Linear Segments with Parabolic Blends (LSPB). A more detailed analysis of LSPB can be found in [77].

LSPB type trajectory consists of three parts: In the first part, it is a quadratic polynomial which results in a ramp velocity profile. Then, at the blending time it blends with a linear function. After this linear segment which creates a constant velocity, it again switches to a quadratic polynomial. Therefore, the resulting velocity profile is trapezoidal.

### 3.2.2 Moment of Inertia and Mass Variations During Transition Mode and Component Failure

UAV's CAD model was designed in Solidworks which is shown in Figure 3.6 (a). Then it was used to extract the principal moment of inertia changes

during transition and failure. For the transition from vertical to horizontal mode, wing angles were changed from  $90^\circ$  to  $0^\circ$  with  $5^\circ$  intervals and for each interval principal moments of inertias were calculated in Solidworks. Minimum and maximum values and percent changes due to wing movements are given in Table 3.1.

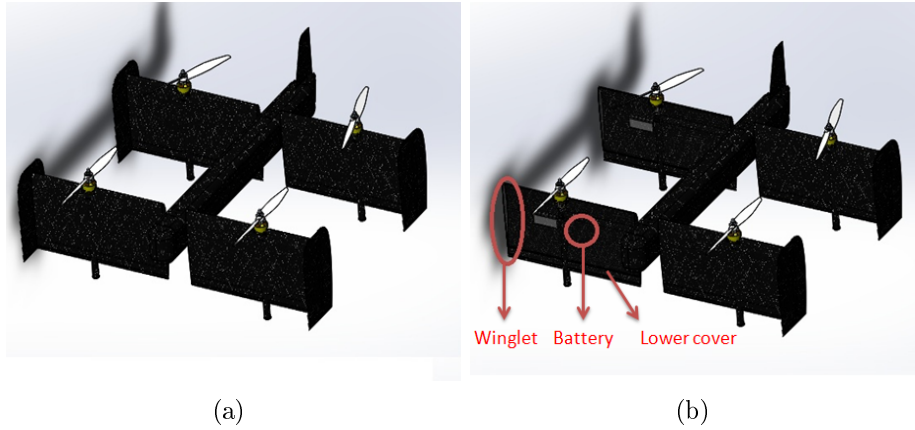


Figure 3.6: (a) CAD model of SUAVI (b) Model after failure (Fallen components' places are indicated for front right wing).

	$I_{xx}$	$I_{yy}$	$I_{zz}$
Minimum	0.239547	0.450649	0.677345
Maximum	0.248038	0.452372	0.684241
Percent change (%)	3.5446	0.3823	1.018

Table 3.1: Minimum, maximum values and percent changes of the principal moments of inertias due to wing movement (Before failure).

Moment of inertias are modeled by fitting cubic polynomial curves to data calculated by Solidworks. The resulting curves are shown in Figure 3.7 and corresponding polynomials are given in Equations (50) - (52).

$$I_{xx_i} = -0.005\theta_i^3 + 0.012\theta_i^2 - 0.0011\theta_i + 0.24 \quad (50)$$

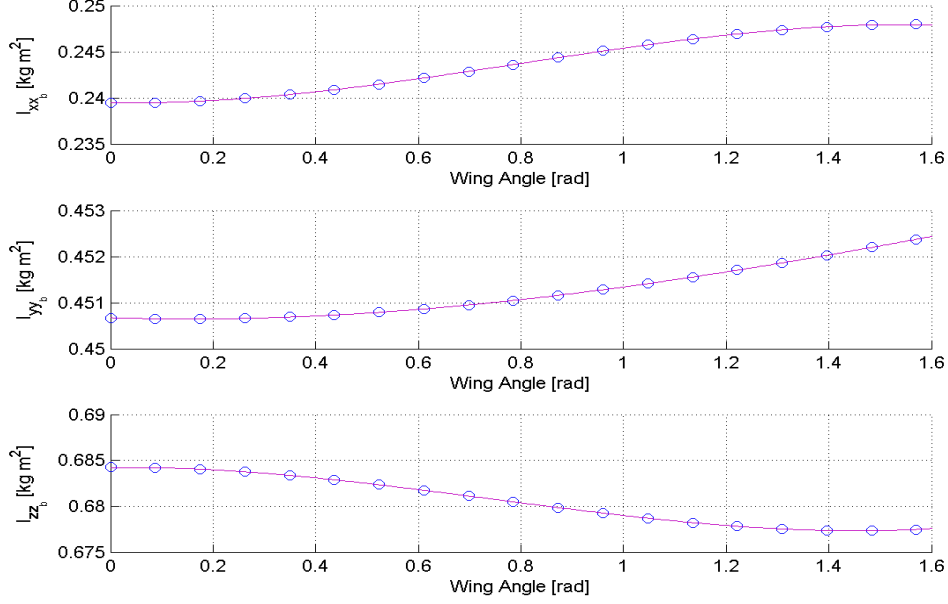


Figure 3.7: Evolution of principal moment of inertias due to wing movement, before the failure.

$$I_{yy_b} = -0.00019\theta_i^3 + 0.0012\theta_i^2 - 0.00037\theta_i + 0.45 \quad (51)$$

$$I_{zz_b} = 0.0048\theta_i^3 - 0.011\theta_i^2 + 0.00074\theta_i + 0.68 \quad (52)$$

where  $I_{xx_b}$ ,  $I_{yy_b}$  and  $I_{zz_b}$  are the UAV's principal moment of inertias before the failure around its body axes. Since all the wing angles are assumed to be equal during the flight, they are shown with  $\theta_i$ .

The same procedure is used to calculate the variations in the moment of inertias during the transition from the fixed-wing mode to quadrotor mode. However, during this transition the UAV model is different from the one in the first transition due to the missing parts that are lost at the moment of

failure at  $t = 61$  which is shown in Fig. 3.6 (b). Note that, right front and rear wings' lower covers, winglets and two batteries fall at the failure instant. Minimum and maximum values and percent changes due to wing movements after failure are given in Table 3.2.

	$I_{xx}$	$I_{yy}$	$I_{zz}$
Minimum	0.208271	0.417153	0.61305
Maximum	0.216098	0.418437	0.619631
Percent change (%)	3.758	0.3078	1.073

Table 3.2: Minimum, maximum values and percent changes of the principal moments of inertias due to wing movement (After failure).

Cubic polynomial curves were fitted to this data. The resulting curves are illustrated in Figure 3.8 and corresponding polynomials for these curves are given in Equations (53) - (55).

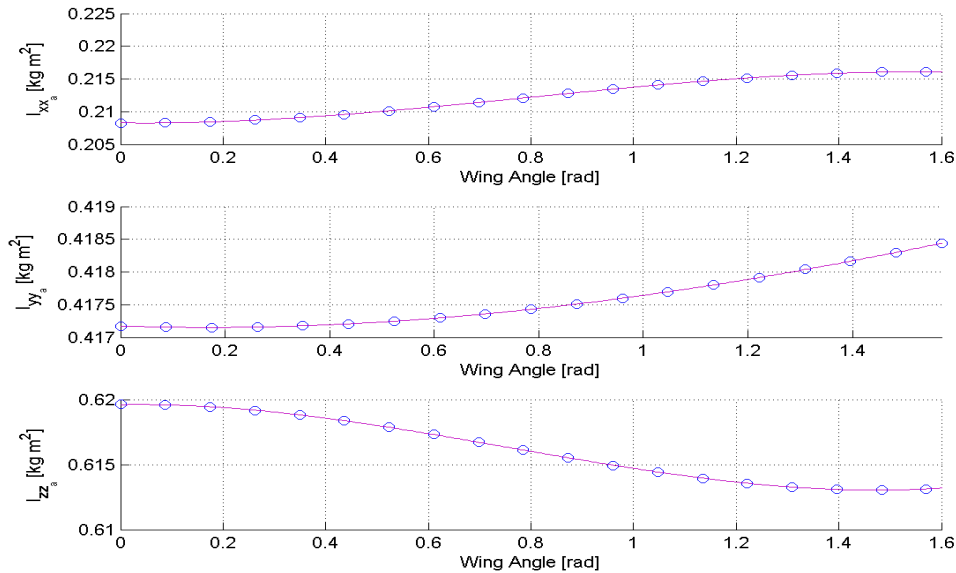


Figure 3.8: Evolution of principal moment of inertias due to wing movement, after the failure.

$$I_{xx_a} = -0.0046\theta_i^3 + 0.011\theta_i^2 - 0.001\theta_i + 0.21 \quad (53)$$

$$I_{yy_a} = 9.6 \times 10^{-5}\theta_i^3 + 0.00084\theta_i^2 - 0.00027\theta_i + 0.42 \quad (54)$$

$$I_{zz_a} = 0.0044\theta_i^3 - 0.01\theta_i^2 + 0.00072\theta_i + 0.62 \quad (55)$$

where  $I_{xx_a}$ ,  $I_{yy_a}$  and  $I_{zz_a}$  are the UAV's principal moment of inertias after the failure around its body frame. Data, that is used for fitting the curves, are given in Appendix. To get a better fit, wing angles' units were taken as radian. Norm of the residuals for the resulting fits are shown in Table 3.3.

	$I_{xx_b}$	$I_{yy_b}$	$I_{zz_b}$	$I_{xx_a}$	$I_{yy_a}$	$I_{zz_a}$
Norm of the residuals ( $\times 10^{-5}$ )	6.7	1	6.4	6.2	0.82	5.9

Table 3.3: Norm of the residuals for the inertia curve fitting results.

Mass is also an important parameter that changes at the failure instant. UAV's mass decreases approximately 0.36 kg at the failure instant; therefore, UAV's mass drops by 7.4% due to the failure. UAV's and each components' masses are given in Table 3.4.

	Mass [kg]
UAV (before failure)	4.891
Batteries (x2)	0.294
Lower covers (x2)	0.04
Winglets (x2)	0.03
UAV (after failure)	4.527

Table 3.4: Mass of the UAV and missing components.

In the simulations, polynomials obtained from the curve fitting were used

to simulate the parameter changes during the transition stages and during the failure. Overall percent changes in these system parameters due to wing movement and failure are presented in Table 3.5

	$I_{xx}$ [kg m <sup>2</sup> ]	$I_{yy}$ [kg m <sup>2</sup> ]	$I_{zz}$ [kg m <sup>2</sup> ]
Percent change [%] (After failure)	15.65	7	7.93
Percent change [%] (Overall)	22.2	6.55	8.78

Table 3.5: Percent changes of principal moment of inertias due to wing movement and failure.

### 3.2.3 Center of Gravity Variation Due to the Failure

In addition to moment of inertia and mass changes, center of gravity of UAV changes with the failure. This change is modeled as an external disturbance to UAV position dynamics which consists of the moments  $M_x$ ,  $M_y$  and  $M_z$  calculated as

$$\begin{bmatrix} M_x \\ M_y \\ M_z \end{bmatrix} = \begin{bmatrix} r_x \\ r_y \\ r_z \end{bmatrix} \times \begin{bmatrix} F_x \\ F_y \\ F_z \end{bmatrix}, \quad \begin{bmatrix} F_x \\ F_y \\ F_z \end{bmatrix} = R_{bw} \begin{bmatrix} 0 \\ 0 \\ m_{af}g \end{bmatrix} \quad (56)$$

where,  $R_{bw}$  is the rotation matrix that gives the orientation of the world frame with respect to the body frame,  $g$  is the gravitational acceleration,  $m_{af}$  is the mass of the UAV after the failure and  $r_x$ ,  $r_y$  and  $r_z$  are the distances of the center of gravity to the original position before the failure, measured along the axes.

# Chapter IV

## 4 Nonlinear Hierarchical Adaptive Control

Two different hierarchical control approaches will be discussed in this chapter. First approach is based on feedback linearization and PID which was also used in earlier works [22]. The second approach is based on nonlinear adaptive controllers. Both of the controllers are synthesized on the QTW-UAV model, whose nonlinear dynamics were given in Chapter 3.

### 4.1 Feedback Linearization Approach

In order to design flight controllers, dynamics of the UAV are divided into two subsystems, which are position and attitude. A PID based controller which utilizes the nonlinear transformation based on dynamic inversion resides for the position subsystem, which can also be called upper level controller. For the attitude subsystem, or the lower level controller, a feedback linearization method is used. For simplicity, the downwash effects of the front wings on rear wings will be neglected; therefore, equal front and rear wing angles will be assumed, i.e.  $\theta_f = \theta_r$ . Control calculations will be based on front wing angles.

#### 4.1.1 PID Based Controllers via Dynamic Inversion

To design position controllers, first the aerial vehicle position ( $X$ ,  $Y$  and  $Z$ ) dynamics which are given in Eqn. (29) is recalled; i.e

$$\ddot{X} = \frac{1}{m}[(c_\psi c_\theta c_{\theta_f} - (c_\phi s_\theta c_\psi + s_\phi s_\psi) s_{\theta_f})u_1 + W_x] \quad (57)$$

$$\ddot{Y} = \frac{1}{m}[(s_\psi c_\theta c_{\theta_f} - (c_\phi s_\theta s_\psi - s_\phi c_\psi) s_{\theta_f})u_1 + W_y] \quad (58)$$

$$\ddot{Z} = \frac{1}{m}[(-s_\theta c_{\theta_f} - c_\phi c_\theta s_{\theta_f})u_1 + mg + W_z] \quad (59)$$

The aerial vehicle has to produce required accelerations along  $X, Y$  and  $Z$  axes, to track the desired trajectory. These accelerations can be generated by the following virtual control inputs:

$$\mu_1 = \ddot{X}_d + K_{pX}e_X + K_{iX} \int_0^t e_X dt + K_{dX}\dot{e}_X \quad (60)$$

$$\mu_2 = \ddot{Y}_d + K_{pY}e_Y + K_{iY} \int_0^t e_Y dt + K_{dY}\dot{e}_Y \quad (61)$$

$$\mu_3 = \ddot{Z}_d + K_{pZ}e_Z + K_{iZ} \int_0^t e_Z dt + K_{dZ}\dot{e}_Z \quad (62)$$

where position tracking errors are defined as  $e_q = q_d - q$  for  $q = X, Y, Z$  and subscript  $d$  refers to the desired trajectory. In order to calculate the reference attitude angles and total motor thrust, dynamic inversion approach is utilized. Therefore, by equating virtual control inputs to position dynamics the following equations are obtained

$$\tilde{\mu}_1 \triangleq m\mu_1 - W_x = (c_{\psi_d} c_{\theta_d} c_{\theta_f} - (c_{\phi_d} s_{\theta_d} c_{\psi_d} + s_{\phi_d} s_{\psi_d}) s_{\theta_f})u_1 \quad (63)$$

$$\tilde{\mu}_2 \triangleq m\mu_2 - W_y = (s_{\psi_d} c_{\theta_d} c_{\theta_f} - (c_{\phi_d} s_{\theta_d} s_{\psi_d} - s_{\phi_d} c_{\psi_d}) s_{\theta_f})u_1 \quad (64)$$

$$\tilde{\mu}_3 \triangleq m\mu_3 - W_z - mg = (-s_{\theta_d} c_{\theta_f} - c_{\phi_d} c_{\theta_d} s_{\theta_f})u_1 \quad (65)$$

where  $\tilde{\mu}_1$ ,  $\tilde{\mu}_2$  and  $\tilde{\mu}_3$  are new virtual inputs. Equations (63)-(65) are solved for the total thrust  $u_1$ , desired roll ( $\phi_d$ ) and pitch ( $\theta_d$ ) angles as

$$u_1 = \sqrt{\tilde{\mu}_1^2 + \tilde{\mu}_2^2 + \tilde{\mu}_3^2} \quad (66)$$

$$\phi_d = \arcsin\left(\frac{-\gamma_1}{u_1 s_{\theta_f}}\right) \quad (67)$$

$$\theta_d = \arcsin\left(\frac{-\tilde{\mu}_3 u_1 c_{\theta_f} - u_1 \gamma_2 s_{\theta_f} c_{\phi_d}}{\gamma_2^2 + \tilde{\mu}_3^2}\right) \quad (68)$$

where  $\gamma_1$  and  $\gamma_2$  are the auxiliary variables and they are defined as

$$\gamma_1 = \tilde{\mu}_1 \cdot s_{\psi_d} - \tilde{\mu}_2 \cdot c_{\psi_d} \quad (69)$$

$$\gamma_2 = \tilde{\mu}_1 \cdot c_{\psi_d} + \tilde{\mu}_2 \cdot s_{\psi_d} \quad (70)$$

Desired roll, pitch angles and total thrust to hover the UAV at a desired altitude can be computed using Eqns. (66) - (68). These equations produce references for the attitude subsystem. It should be noted that the desired yaw angle can be set to any reference value.

#### 4.1.2 Feedback Linearization Based Attitude Controllers

For the attitude control of SUAVI a feedback linearization approach is used. Desired attitude angles given in Eqns. (67) - (68) are used as the reference angles. In order to design the attitude controllers, Eqn. (34) can be rewritten as

$$\mathbb{M}(\alpha_w)\dot{\Omega}_w + \mathbb{C}(\alpha_w, \Omega_w)\Omega_w = \mathbb{E}^T(M_{th} + M_w) \quad (71)$$

where  $M_t \approx M_{th} + M_w$ . Since gyroscopic effects on propellers are small enough to be neglected, these moments are not considered in controller design. The attitude dynamics given in Eqn. (71) is fully actuated, therefore it is feedback linearizable. Consider the following transformation for feedback linearization:

$$\tilde{\eta} = M_{th} = I_b \mathbb{E} \eta + \mathbb{E}^{-T} \mathbb{C}(\alpha_w, \Omega_w) \Omega_w - M_w \quad (72)$$

where  $\tilde{\eta}$  is a new virtual control input vector and  $\eta$  is the virtual control input vector for attitude subsystem. These control inputs have 3 components and they are defined as

$$\tilde{\eta} = \begin{bmatrix} \tilde{\eta}_1 & \tilde{\eta}_2 & \tilde{\eta}_3 \end{bmatrix}^T, \quad \eta = \begin{bmatrix} \eta_1 & \eta_2 & \eta_3 \end{bmatrix}^T \quad (73)$$

In light of Eqns. (24), (72) and (73), it follows that

$$\tilde{\eta}_1 = s_{\theta_f} u_2 - c_{\theta_f} u_4 \quad (74)$$

$$\tilde{\eta}_2 = s_{\theta_f} u_3 \quad (75)$$

$$\tilde{\eta}_3 = c_{\theta_f} u_2 + s_{\theta_f} u_4 \quad (76)$$

The following PID controllers are designed to generate virtual control inputs,  $\eta_1, \eta_2, \eta_3$ ; i.e.

$$\eta_1 = \ddot{\phi}_d + K_{p\phi} e_\phi + K_{i\phi} \int_0^t e_\phi dt + K_{d\phi} \dot{e}_\phi \quad (77)$$

$$\eta_2 = \ddot{\theta}_d + K_{p\theta} e_\theta + K_{i\theta} \int_0^t e_\theta dt + K_{d\theta} \dot{e}_\theta \quad (78)$$

$$\eta_3 = \ddot{\psi}_d + K_{p\psi}e_\psi + K_{i\psi} \int_0^t e_\psi dt + K_{d\psi}\dot{e}_\psi \quad (79)$$

where attitude tracking errors are defined as  $e_q = q_d - q$  for  $q = \phi, \theta, \psi$ .

It is well known that physical inputs for quadrotor type aerial vehicles are motor voltages which creates specified rotor rotational speeds that generate motor thrusts. The relationship between control inputs and rotor speeds is given through Eqns. (25)-(28). The total thrust  $u_1$  generated by rotors is given in Eqn. (66). Other control inputs can be found by using Eqns. (74)-(76) as,

$$u_3 = \frac{\tilde{\eta}_2}{s_{\theta_f}} \quad (80)$$

$$\begin{bmatrix} u_2 \\ u_4 \end{bmatrix} = \begin{bmatrix} s_{\theta_f} & -c_{\theta_f} \\ c_{\theta_f} & s_{\theta_f} \end{bmatrix}^{-1} \begin{bmatrix} \tilde{\eta}_1 \\ \tilde{\eta}_3 \end{bmatrix} \quad (81)$$

## 4.2 Nonlinear Adaptive Control Approach

Apart from the feedback linearization approach, a hierarchical nonlinear adaptive control approach is developed that can adapt its parameters online to control the QTW UAV. On the upper level, a Model Reference Adaptive Controller (MRAC) [78] provides virtual control inputs to control the position of the UAV. These control inputs are converted to desired attitude angles which are then fed to the lower level attitude controller. A nonlinear adaptive controller [79] is employed as the attitude controller so that uncertainties can be compensated without the need for linearization of system dynamics. Closed loop control system structure is presented in Fig. 4.1 and upper and lower level controllers are described below.

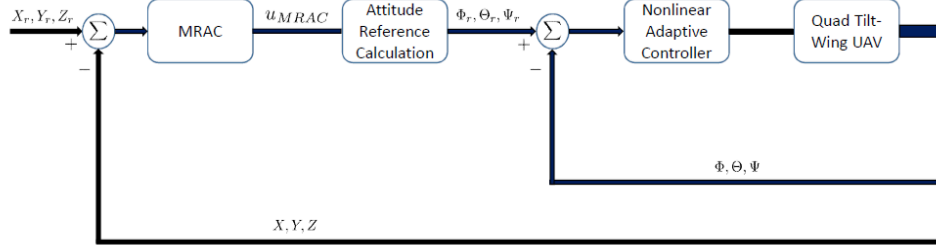


Figure 4.1: Closed loop control system block diagram.

#### 4.2.1 MRAC Design

A Model Reference Adaptive Controller (MRAC), that resides in the upper level of the hierarchy, is designed to control the position of the SUAVI, assuming that the system is a simple mass. This controller calculates the required forces that need to be created, by the lower level nonlinear controller, in the  $X, Y$  and  $Z$  directions, to make the UAV follow the desired trajectory. No information is used about the actual mass of the UAV during the design and this uncertainty in the mass is handled by online modification of control parameters based on the trajectory error. It is noted that the uncertainties in moment of inertia are handled by the lower level attitude controller, which is explained in the next section.

Consider the following system dynamics:

$$\begin{aligned} \dot{\underline{X}}(t) &= A\underline{X}(t) + B_n \Lambda(u_{MRAC}(t) + D + \mu_1 \Upsilon_D(\phi, \theta, \psi, \alpha) + \mu_2 \Upsilon_L(\phi, \theta, \psi, \alpha) + \pi(t)) \\ y(t) &= C\underline{X}(t), \end{aligned} \quad (82)$$

where,  $\underline{X} = [X, Y, Z, \dot{X}, \dot{Y}, \dot{Z}]^T \in \mathfrak{R}^6$  is the state vector,  $u_{MRAC} \in \mathfrak{R}^3$  is the position controller signal (see Fig. 4.1),  $\mu_1 \Upsilon_D(\phi, \theta, \psi, \alpha) \in \mathfrak{R}^3$  is the drag

force vector where  $\mu_1$  is an unknown constant and  $\Upsilon_D(\cdot)$  is a known bounded function,  $\mu_2 \Upsilon_L(\phi, \theta, \psi, \alpha) \in \mathfrak{R}^3$  is the lift force vector where  $\mu_2$  is an unknown constant and  $\Upsilon_L(\cdot)$  is a known bounded function,  $\pi(t) \in \mathfrak{R}^3$  is a bounded, time-varying, unknown disturbance,  $y \in \mathfrak{R}^3$  is the plant output,

$$A = \begin{bmatrix} 0_{3 \times 3} & I_{3 \times 3} \\ 0_{3 \times 3} & 0_{3 \times 3} \end{bmatrix} \quad (83)$$

$$B_n = \begin{bmatrix} 0_{3 \times 3} \\ I_{3 \times 3} \end{bmatrix} \frac{1}{m_n} \quad (84)$$

$$\Lambda = \frac{m_n}{m} \quad (85)$$

$$D = \begin{bmatrix} 0_{2 \times 1} \\ mg \end{bmatrix} \quad (86)$$

$$C = \begin{bmatrix} I_{3 \times 3} & 0_{3 \times 3} \end{bmatrix}, \quad (87)$$

where  $m$  is the actual mass of the UAV that is assumed to be unknown,  $m_n$  is the nominal mass,  $g$  is the gravitational acceleration and  $\Lambda$  represents the uncertainty in the UAV mass. It is noted that from now on, time dependence of the parameters will not be emphasized unless necessary and therefore “t” will be dropped from the expressions. In addition, arguments of the vectors  $\Upsilon_D$  and  $\Upsilon_L$  will be dropped.

**Remark 1.** The model introduced in (82) represents a simple mass being controlled via virtual control inputs acting in the direction of three axes of the world frame in the presence of lift and drag forces, gravity and unknown

and bounded time-varying disturbances. It is noted that this representation would be accurate if the inner loop controller, which controls the attitude of the UAV, had infinite bandwidth, which is of course not the case.

**Remark 2.** The lift and drag coefficients are modelled via linear regression using the data obtained from wind tunnel tests. For the controller design, in (82), the uncertainty in these models (together with constants) are represented by two coefficients  $\mu_1$  and  $\mu_2$ , one for each coefficient. A more accurate representation would be distributing the uncertainty to each of the regression parameters (instead of using them in a single coefficient).

### Reference Model Design

Consider the following control law, which is to be used for the nominal system dynamics, where  $\Lambda = 1, D = D_n = [0_{1 \times 2} \ m_n g]^T$ ,  $\mu_1$  and  $\mu_2$  are known and  $\pi(t) = 0$ :

$$u_n = K_x^T \underline{X} + K_r^T r - D_n - \mu_1 \Upsilon_D - \mu_2 \Upsilon_L \quad (88)$$

where  $r \in R^3, K_x \in R^{6 \times 3}$  and  $K_r \in R^{3 \times 3}$  are the reference input ( $X_r, Y_r, Z_r$ ), control gain for the states and control gain for the reference input, respectively. When (88) is used for the nominal system, the nominal closed loop dynamics is obtained, which is given below:

$$\dot{\underline{X}}_n = (A + B_n K_x^T) \underline{X}_n + B_n K_r^T r. \quad (89)$$

In (89),  $K_x$  can be determined by any linear control design method, such as pole placement or LQR. Defining  $A_m = A + B_n K_x^T$ , nominal plant output is

obtained as

$$y_n = C(sI - A_m)^{-1}B_nK_r^T r. \quad (90)$$

For a constant  $r$ , the steady state plant output can be calculated as

$$y_{ss} = -CA_m^{-1}B_nK_r^T r. \quad (91)$$

Using  $K_r^T = -(CA_m^{-1}B_n)^{-1}$ , it is obtained that

$$\lim_{t \rightarrow \infty} (y_n - r) = 0. \quad (92)$$

As a result, the reference model dynamics is determined as

$$\dot{\underline{X}}_m = A_m \underline{X}_m + B_m r \quad (93)$$

where,

$$A_m = A + B_n K_x^T \quad (94)$$

and

$$B_m = B_n K_r^T \quad (95)$$

$$= -B_n (CA_m^{-1}B_n)^{-1}. \quad (96)$$

## Adaptive Controller Design

When uncertainties are considered in the system dynamics (82), the fixed controller gains introduced in (88) must be replaced with their corresponding adaptive estimates. Since the uncertainty in nonlinear aerodynamic forces  $\Upsilon_D$  and  $\Upsilon_L$  appears linearly in system dynamics, designing adaptive con-

troller terms for these forces does not create a problem. For example, the following adaptive controller

$$u_{MRAC} = \hat{K}_x^T \underline{X} + \hat{K}_r^T r + \hat{D} + \hat{\mu}_1 \Upsilon_D + \hat{\mu}_2 \Upsilon_L \quad (97)$$

with the adaptive laws given below can be shown to result in a stable closed loop system [80]

$$\dot{\hat{K}}_x = -\Gamma_x (\underline{X} e^T P B_n + \sigma_x \|e\| \hat{K}_x), \quad (98)$$

$$\dot{\hat{K}}_r = -\Gamma_r (r e^T P B_n + \sigma_r \|e\| \hat{K}_r), \quad (99)$$

$$\dot{\hat{D}}^T = -\Gamma_d (e^T P B_n + \sigma_D \|e\| \hat{D}), \quad (100)$$

$$\dot{\hat{\mu}}_1 = -\Gamma_{\mu_1} (\Upsilon_D e^T P B_n + \sigma_{\mu_1} \|e\| \hat{\mu}_1) \quad (101)$$

$$\dot{\hat{\mu}}_2 = -\Gamma_{\mu_2} (\Upsilon_L e^T P B_n + \sigma_{\mu_2} \|e\| \hat{\mu}_2) \quad (102)$$

where  $e = \underline{X} - \underline{X}_m$ ,  $\Gamma_x \in \Re^{6 \times 6}$ ,  $\Gamma_r \in \Re^{3 \times 3}$ ,  $\Gamma_d \in \Re$ ,  $\Gamma_{\mu_1} \in \Re^{3 \times 3}$  and  $\Gamma_{\mu_2} \in \Re^{3 \times 3}$  are adaptive gains,  $\sigma_x, \sigma_r, \sigma_D, \sigma_{\mu_1}, \sigma_{\mu_2}$  are positive scalar gains of e-modification terms and  $P \in \Re^{6 \times 6}$  is the symmetric solution of the Lyapunov equation

$$A_m^T P + P A_m = -Q \quad (103)$$

where  $Q \in \Re^{6 \times 6}$  is a positive definite matrix. It is noted that in the adaptive

laws, e-modification [78], [80] is used. It can be shown that, the system defined by (97) - (103) is stable [80].

To summarize, for the position controller design, the following plant dynamics is used:

$$\begin{aligned}\dot{\underline{X}}(t) &= A\underline{X}(t) + B_n\Lambda(u_{MRAC}(t) + D + \pi(t)) \\ y(t) &= C\underline{X}(t),\end{aligned}\tag{104}$$

The adaptive controller designed for (104) is given as

$$u_{MRAC} = \hat{K}_x^T \underline{X} + \hat{K}_r^T r + \hat{D}\tag{105}$$

with the adaptive laws

$$\dot{\hat{K}}_x = -\Gamma_x(\underline{X}e^T P B_n + \sigma_x \|e\| \hat{K}_x + \gamma_x \|e\|^2 \hat{K}_x),\tag{106}$$

$$\dot{\hat{K}}_r = -\Gamma_r(r e^T P B_n + \sigma_r \|e\| \hat{K}_r),\tag{107}$$

$$\dot{\hat{D}}^T = -\Gamma_d(e^T P B_n + \sigma_D \|e\| \hat{D}),\tag{108}$$

#### 4.2.2 Attitude Reference Calculation

From (7) and (24), we obtain that

$$m\ddot{X} = (c_\psi c_\theta c_{\theta_f} - (c_\phi s_\theta c_\psi + s_\phi s_\psi) s_{\theta_f}) u_1\tag{109}$$

$$m\ddot{Y} = (s_\psi c_\theta c_{\theta_f} - (c_\phi s_\theta s_\psi - s_\phi c_\psi) s_{\theta_f}) u_1\tag{110}$$

$$m\ddot{Z} = (-s_\theta c_{\theta_f} - c_\phi c_\theta s_{\theta_f}) u_1 + mg.\tag{111}$$

Right hand sides of (109)-(111) correspond to the forces determined by the MRAC position controller:

$$u_{MRAC}^1 = (c_\psi c_\theta c_{\theta_f} - (c_\phi s_\theta c_\psi + s_\phi s_\psi) s_{\theta_f}) u_1 \quad (112)$$

$$u_{MRAC}^2 = (s_\psi c_\theta c_{\theta_f} - (c_\phi s_\theta s_\psi - s_\phi c_\psi) s_{\theta_f}) u_1 \quad (113)$$

$$u_{MRAC}^3 = (-s_\theta c_{\theta_f} - c_\phi c_\theta s_{\theta_f}) u_1. \quad (114)$$

It is important to note that the  $D$  term in (82) addresses the gravitational force  $mg$ . From (112)-(114), it is obtained that

$$u_1 = \sqrt{(u_{MRAC}^1)^2 + (u_{MRAC}^2)^2 + (u_{MRAC}^3)^2} \quad (115)$$

$$\phi_d = \arcsin\left(\frac{-\rho_1}{u_1 s_{\theta_f}}\right) \quad (116)$$

$$\theta_d = \arcsin\left(\frac{-u_{MRAC}^3 u_1 c_{\theta_f} - u_1 \rho_2 s_{\theta_f} c_{\phi_d}}{(\rho_2)^2 + (u_{MRAC}^3)^2}\right) \quad (117)$$

where,

$$\rho_1 = u_{MRAC}^1 s_{\psi_d} - u_{MRAC}^2 c_{\psi_d} \quad (118)$$

$$\rho_2 = u_{MRAC}^1 c_{\psi_d} + u_{MRAC}^2 s_{\psi_d}. \quad (119)$$

It is noted that, different from similar works in the literature, the desired attitude angles are functions of the wing angles.  $\psi_d$ , the desired yaw angle, can be chosen by the UAV operator that would be appropriate for the mission at hand. These required attitude angles are given to the lower level attitude controller as references.

### 4.2.3 Nonlinear Adaptive Control Design

To force the UAV follow the requested attitude angles, in the presence of uncertainties, a nonlinear adaptive controller [81] is employed. Defining  $u' = \mathbb{E}^T M_t$ , (34) can be rewritten as

$$\mathbb{M}(\alpha_w)\dot{\Omega}_w + \mathbb{C}(\alpha_w, \Omega_w)\Omega_w = u'. \quad (120)$$

Equation (120), which describes the rotational dynamics of SUAVI, can be parameterized in a way such that the moment of inertia of the UAV,  $I_{UAV} = [I_{xx}, I_{yy}, I_{zz}]^T$ , appears linearly. This transformation is needed so that the uncertain moment of inertia terms appears in a form that is suitable for the adaptive control design:

$$Y(\alpha_w, \dot{\alpha}_w, \ddot{\alpha}_w)I_{UAV} = u'. \quad (121)$$

Consider the following definition

$$s = \dot{\tilde{\alpha}}_w + \Lambda_s \tilde{\alpha}_w \quad (122)$$

where  $\tilde{\alpha}_w = \alpha_w - \alpha_{wd}$ ,  $\alpha_{wd}$  is the desired value of  $\alpha_w$  and  $\Lambda_s \in R^{3 \times 3}$  is a symmetric positive definite matrix. Equation (122) can be modified as

$$s = \dot{\alpha}_w - \dot{\alpha}_{wr} \quad (123)$$

where

$$\dot{\alpha}_{wr} = \dot{\alpha}_{wd} - \Lambda_s \tilde{\alpha}_w. \quad (124)$$

A matrix  $Y' = Y'(\alpha_w, \dot{\alpha}_w, \dot{\alpha}_{wr}, \ddot{\alpha}_{wr})$  can be defined, to be used in linear parameterization, as in the case of (121), such that

$$\mathbb{M}(\alpha_w)\ddot{\alpha}_{wr} + \mathbb{C}(\alpha_w, \Omega_w)\dot{\alpha}_r = Y'(\alpha_w, \dot{\alpha}_w, \dot{\alpha}_{wr}, \ddot{\alpha}_{wr})I_{UAV}. \quad (125)$$

It can be shown that the following nonlinear controller,

$$u_{Nadp} = Y'\hat{I}_{UAV} - K_D s \quad (126)$$

where  $K_D \in R^{3 \times 3}$  is positive definite matrix and  $\hat{I}$  is an estimate of the uncertain parameter  $I$ , with an adaptive law

$$\dot{\hat{I}}_{UAV} = -\Gamma_I Y'^T s \quad (127)$$

where  $\Gamma_I$  is the adaptation rate, stabilizes the closed loop system and makes the error  $\tilde{\alpha}_w$  converge to zero.

The total thrust  $u_1$  is provided in (115). The rest of the control inputs in (24) can be calculated [22] by first defining  $u'' = (\mathbb{E}(\alpha_w)^T)^{-1} u'$  and performing the following operations:

$$u_3 = \frac{u_2''}{s_{\theta_f}} \quad (128)$$

$$\begin{bmatrix} u_2 \\ u_4 \end{bmatrix} = \begin{bmatrix} s_{\theta_f} & -c_{\theta_f} \\ c_{\theta_f} & s_{\theta_f} \end{bmatrix}^{-1} \begin{bmatrix} u_1'' \\ u_3'' \end{bmatrix}. \quad (129)$$

Once these control inputs are determined, the thrusts created by the rotors can be calculated using linear relationships given in (25)-(28).

# Chapter V

## 5 Simulation Results

Performance of the proposed controllers is investigated with the flight trajectory that was designed in Section 3.2. Four different scenarios are investigated for a comprehensive comparison between the fixed controller and the proposed adaptive controller:

- **Normal Flight Scenario:** UAV completes the example flight scenario.
- **Failure Scenario:** In this scenario, component failure that was explained in Section 3.2 is introduced to the system. In addition to this, a 10% uncertainty assumed in the actuator powers. Also, a 20 % actuator power loss is assumed due to the failure at  $t = 61$  s.
- **Wind Disturbance Added Failure Scenario:** Dryden wind turbulence model is added to the first scenario to simulate wind disturbances along  $X, Y$  and  $Z$  axes. This model provides realistic atmospheric wind to simulations [82, 83].
- **Full Flight Scenario:** As well as the failure, actuator uncertainties and wind disturbances, sensor measurement noises are also added to this scenario. Therefore, this can be referred as the most realistic scenario with respect to first and second scenarios.

All the above scenarios are investigated with feedback linearization and non-linear adaptive control approaches. Note that, for all the scenarios flight

trajectory and change of the wing angles shown in Figure 5.1 are the same. Since principle of moment of inertias are functions of wing angles, evolution of them during the flight is the same for all scenarios. Change of the principle moment of inertias are shown in Fig. 5.2.

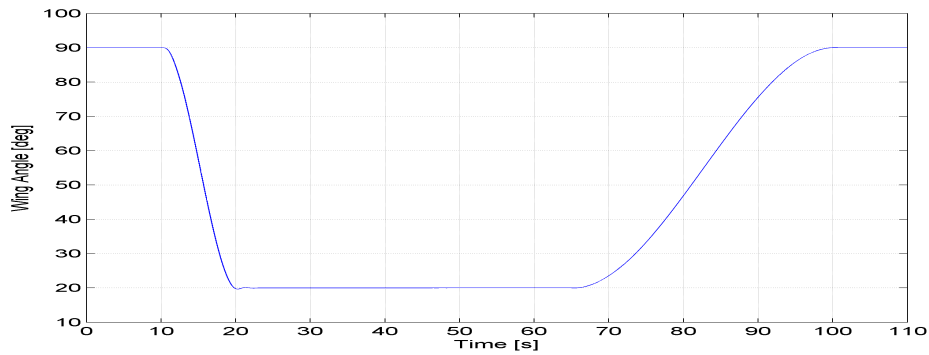


Figure 5.1: Evolution of wing angles.

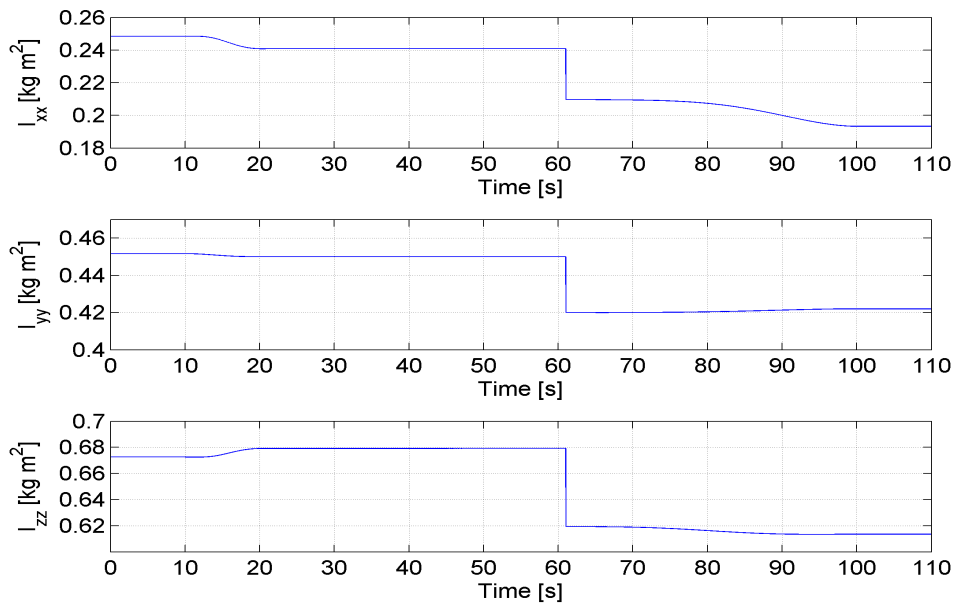


Figure 5.2: Changes in principal moment of inertias.

## 5.1 Normal Flight Scenario

UAV tracks the desired trajectory which is proposed in example flight scenario in chapter 3. UAV takes off vertically as a quadrotor and reaches a desired altitude. Then, it undergoes a transition from vertical to horizontal mode by changing its wing angles and flies like a fixed wing airplane. After this period, it again changes its wing angles and transforms to vertical mode and completes its vertical landing.

### Feedback Linearization Approach

Position tracking of the UAV is shown in Figures 5.3 - 5.6. Since there are no external disturbances UAV tracks the trajectory approximately zero tracking errors. Tracking errors along  $X$  and  $Z$  are caused by the change of wing angles.

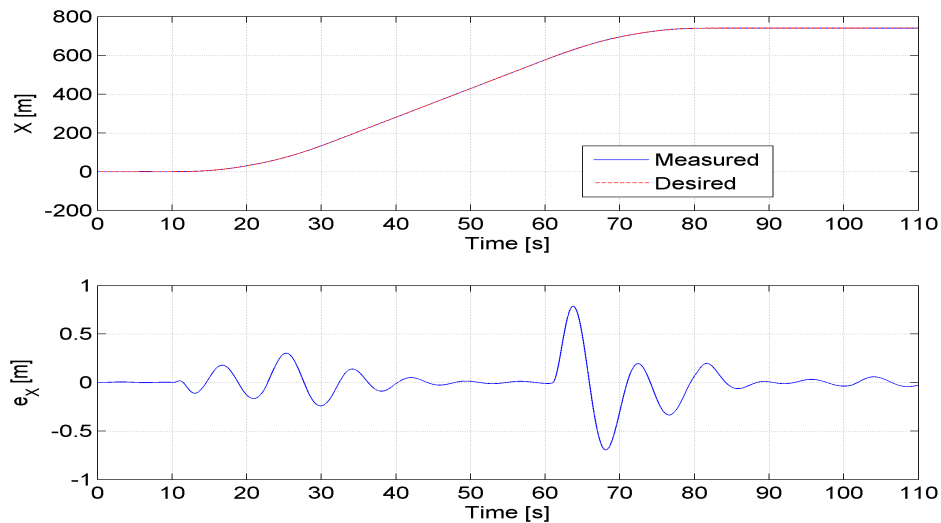


Figure 5.3: X tracking (top), tracking error (bottom).

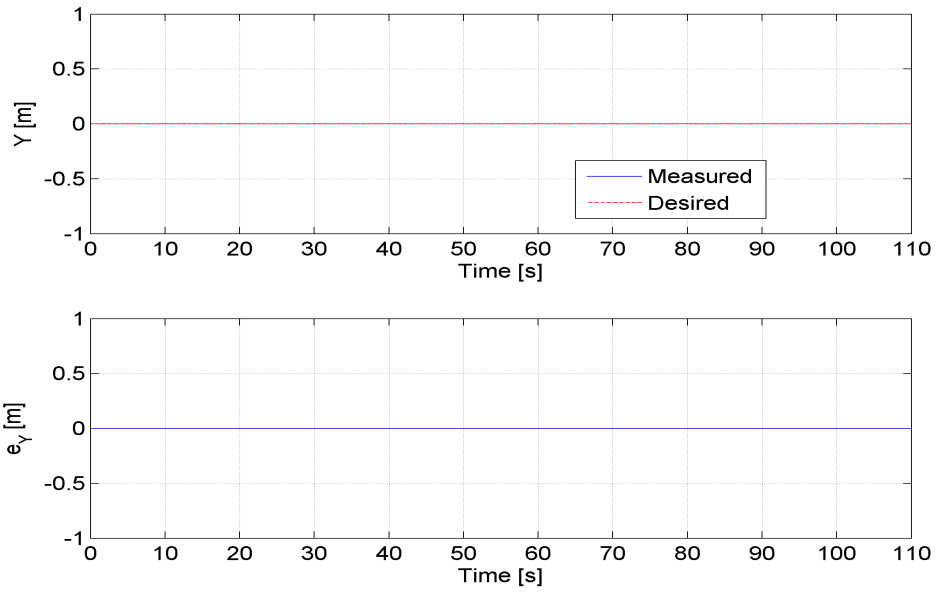


Figure 5.4: Y tracking (top), tracking error (bottom).

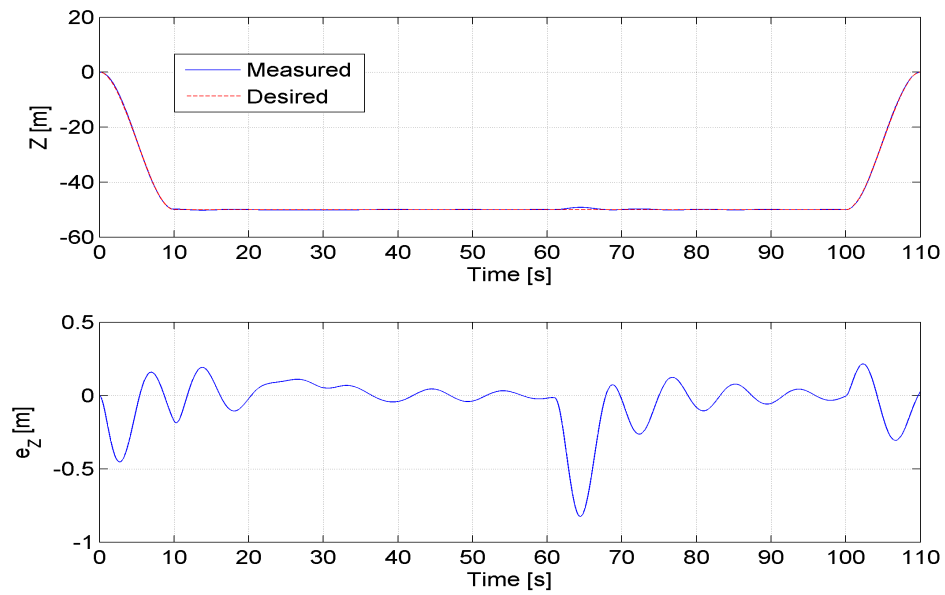


Figure 5.5: Z tracking (top), tracking error (bottom).

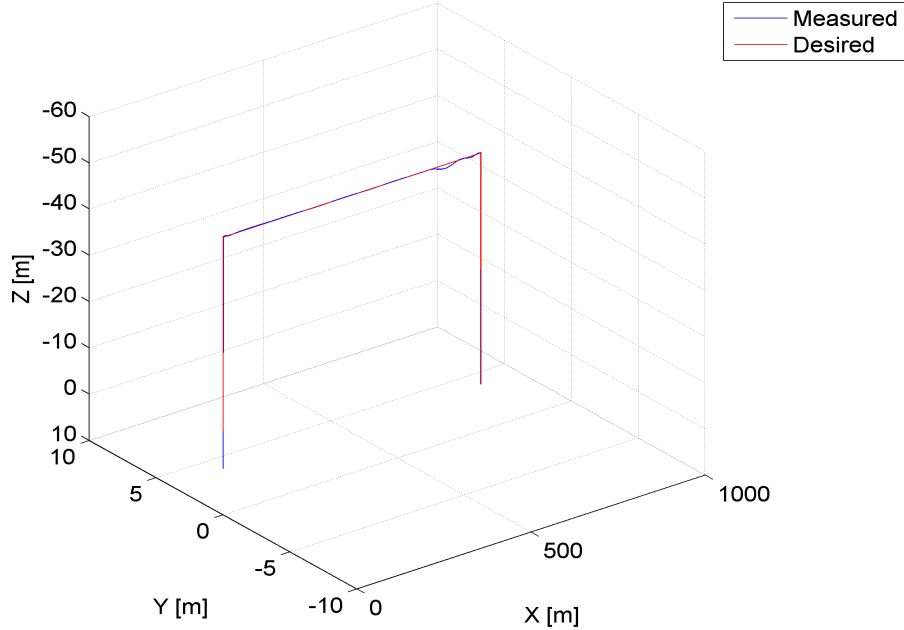


Figure 5.6: Trajectory tracking of the UAV.

Attitude tracking performance of the UAV is shown in Figures 5.7 - 5.9. Around roll ( $\phi$ ) and yaw ( $\psi$ ) angles there are no movement, since there is no disturbance. However, around pitch angle ( $\theta$ ), UAV reaches approximately 50 deg. at the transition instants to until an enough lift is created to achieve zero degree pitch angle.

Control efforts of the UAV is shown in 5.10. Until it achieves horizontal flight UAV's total thrust ( $u_1$ ) is approximately 40 N. However, at the horizontal flight ( $t = 30 - 60s.$ ) power consumption of the UAV dramatically decreases. There are no control effort in  $u_2$  and  $u_4$  because there is no movement around roll and yaw angles.  $\pm 5$  N control effort in  $u_3$  is caused by the transition instants at the beginning and at the end of the horizontal flight.

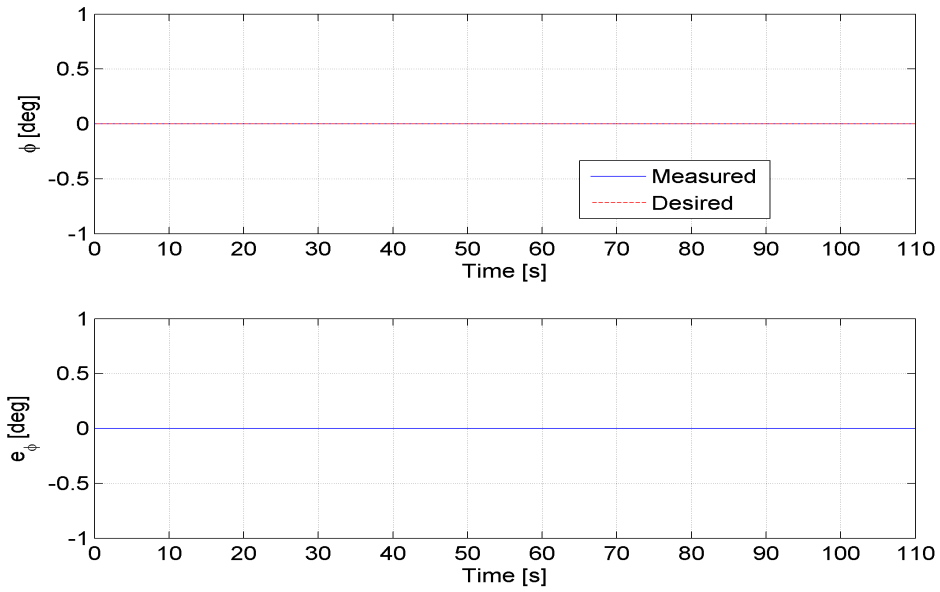


Figure 5.7:  $\phi$  tracking (top), tracking error (bottom).

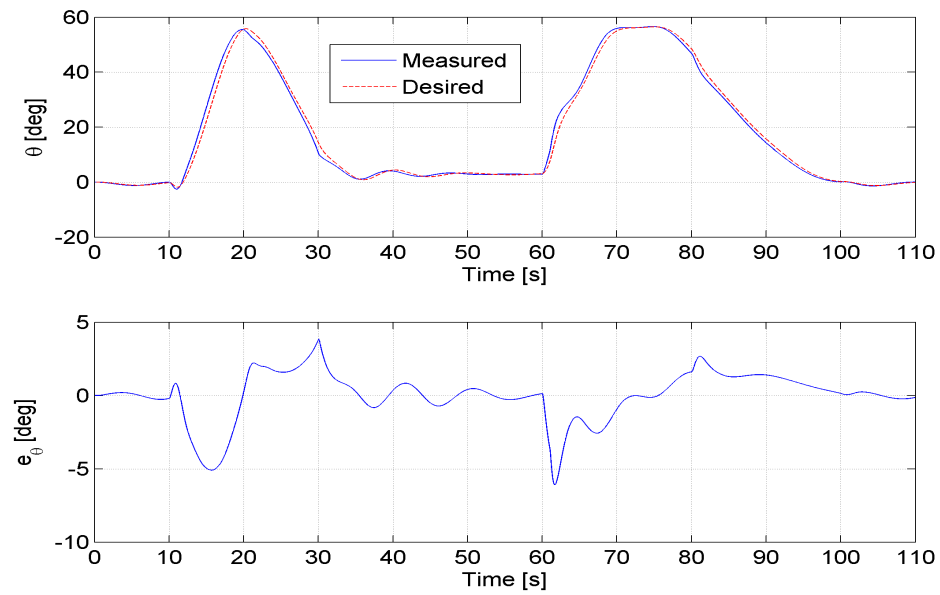


Figure 5.8:  $\theta$  tracking (top), tracking error (bottom).

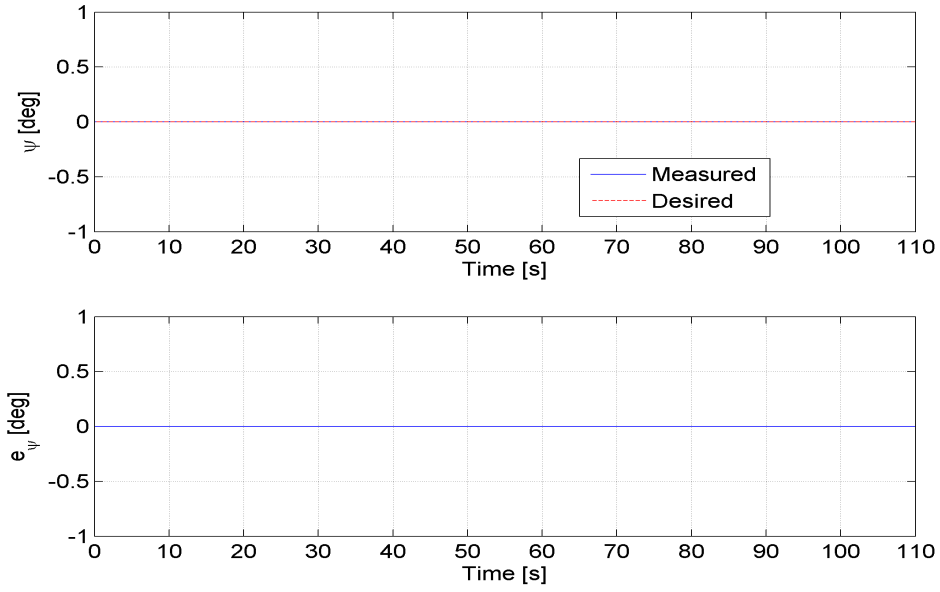


Figure 5.9:  $\psi$  tracking (top), tracking error (bottom).

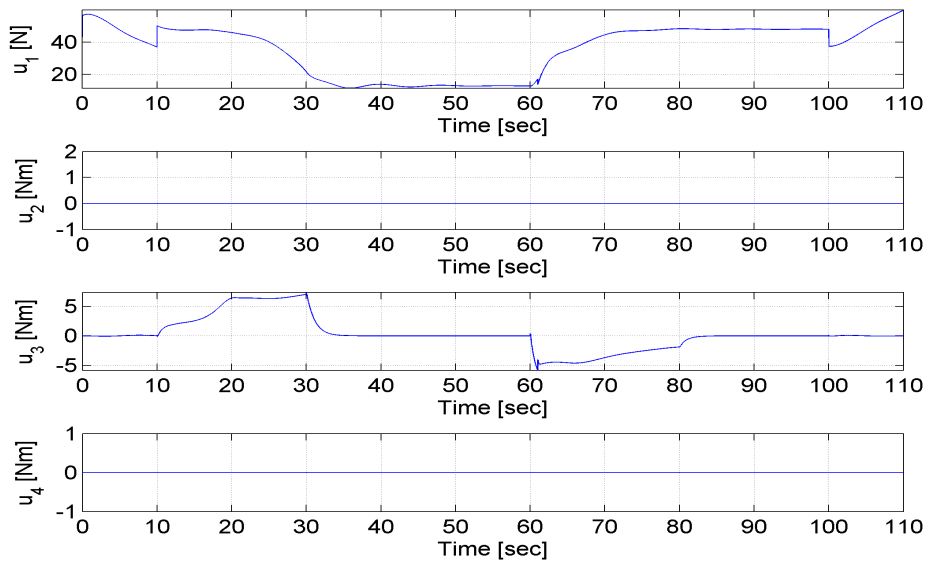


Figure 5.10: Control inputs.

## Adaptive Control Approach

Position tracking performance of the UAV is shown in Figures 5.11 - 5.14. There are tracking errors along  $X$  and  $Z$  axes, since MRAC position controller tracks the reference model. Along the  $Y$  axis, there is almost no tracking errors.

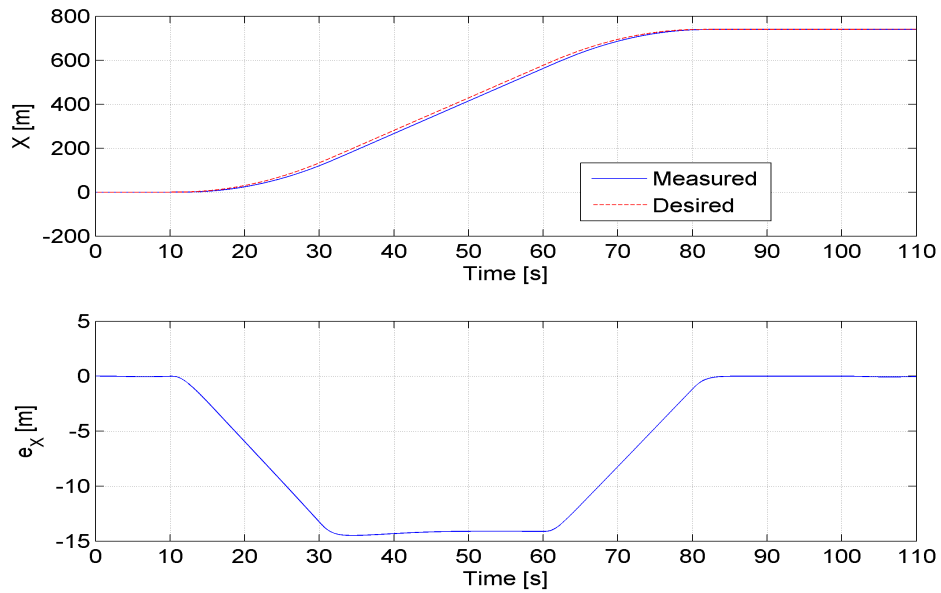


Figure 5.11: X tracking (top), tracking error (bottom).

Tracking performance around roll, pitch and yaw angles are shown in Figures 5.15 - 5.17. There are approximately zero tracking errors around roll and yaw angles. Tracking errors around pitch angle is caused by the transition mode, however, adaptive control tracks the pitch angle with smaller errors with respect to fixed controller. Control inputs of the adaptive controller is shown in Figure 5.18. Adaptive controller's efforts especially  $u_3$  is smaller than the fixed controller.

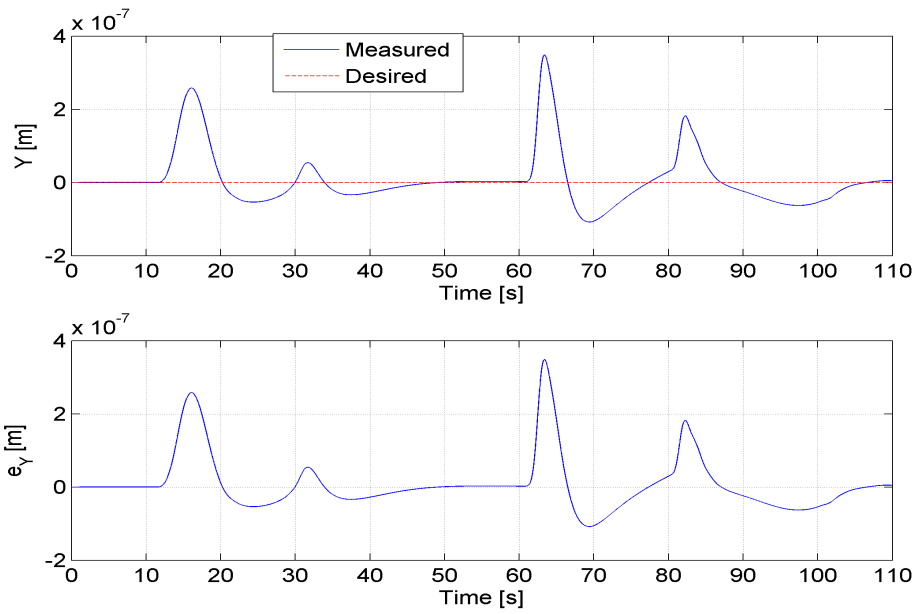


Figure 5.12: Y tracking (top), tracking error (bottom).

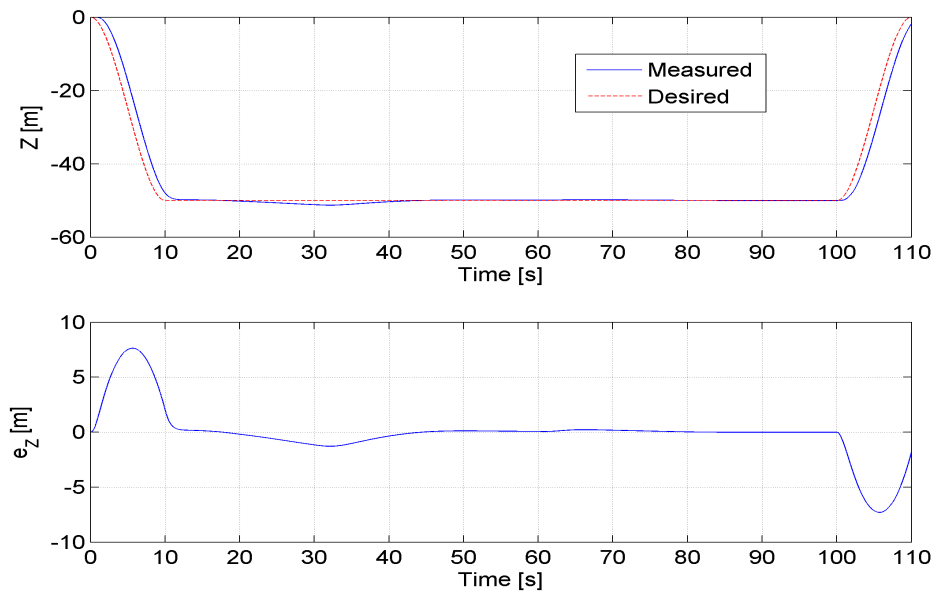


Figure 5.13: Z tracking (top), tracking error (bottom).

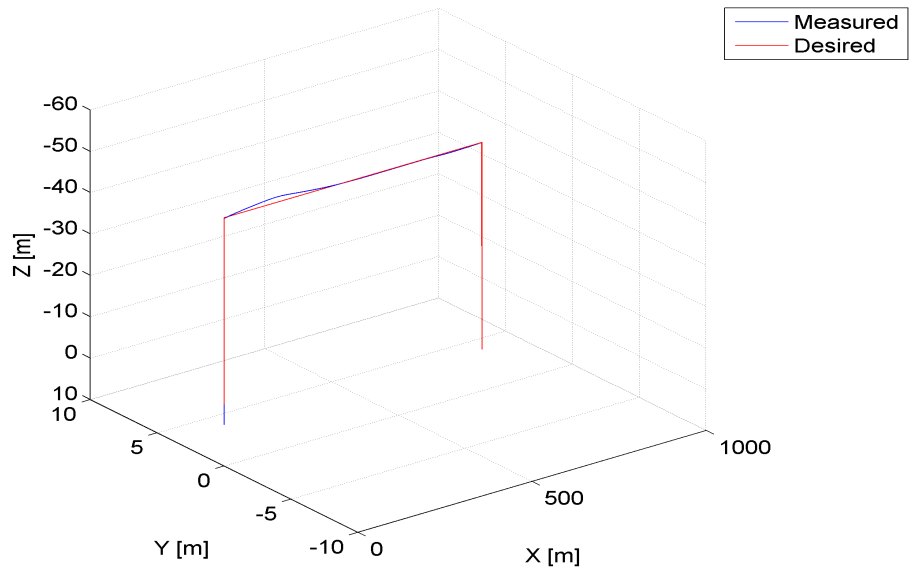


Figure 5.14: Trajectory tracking of the UAV.

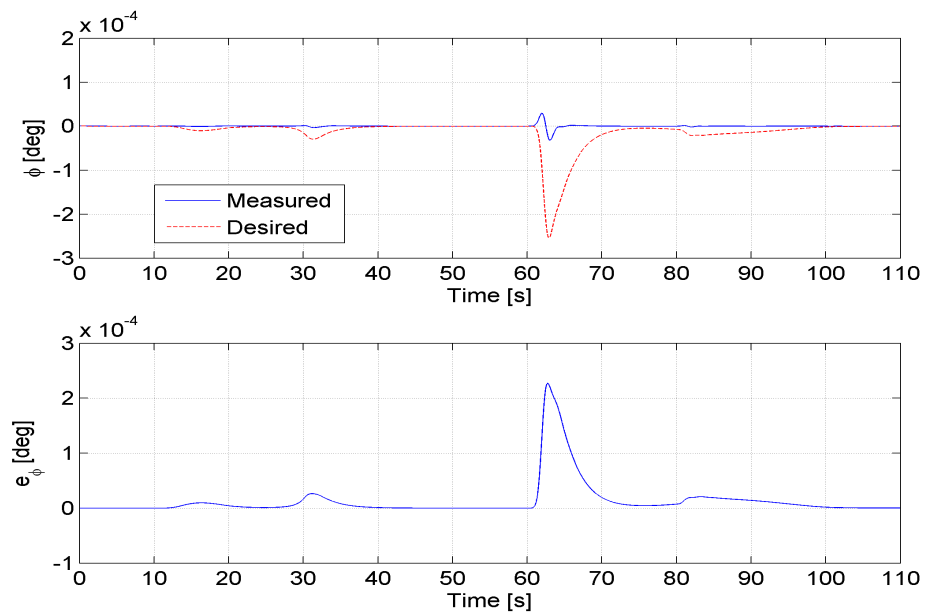


Figure 5.15:  $\phi$  tracking (top), tracking error (bottom).

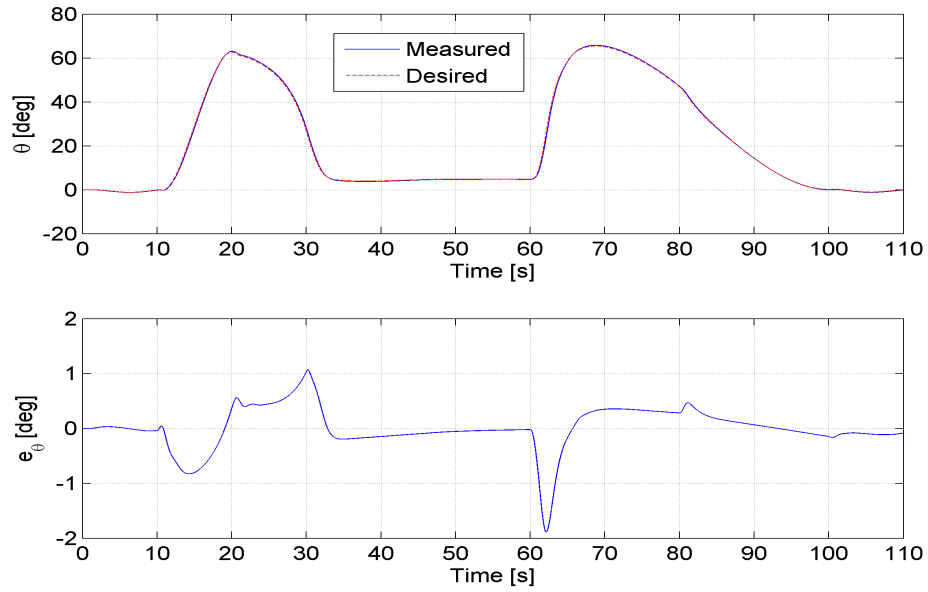


Figure 5.16:  $\theta$  tracking (top), tracking error (bottom).

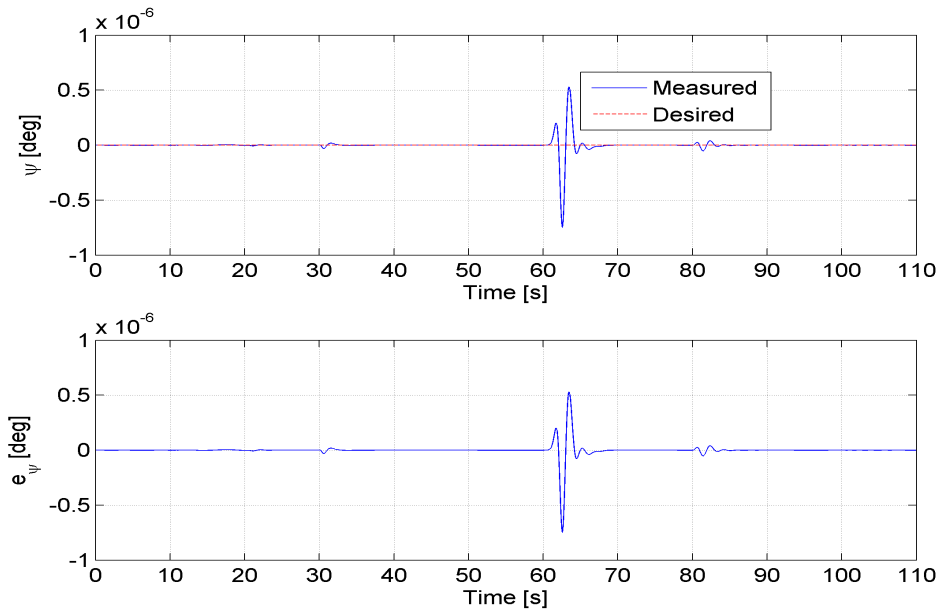


Figure 5.17:  $\psi$  tracking (top), tracking error (bottom).

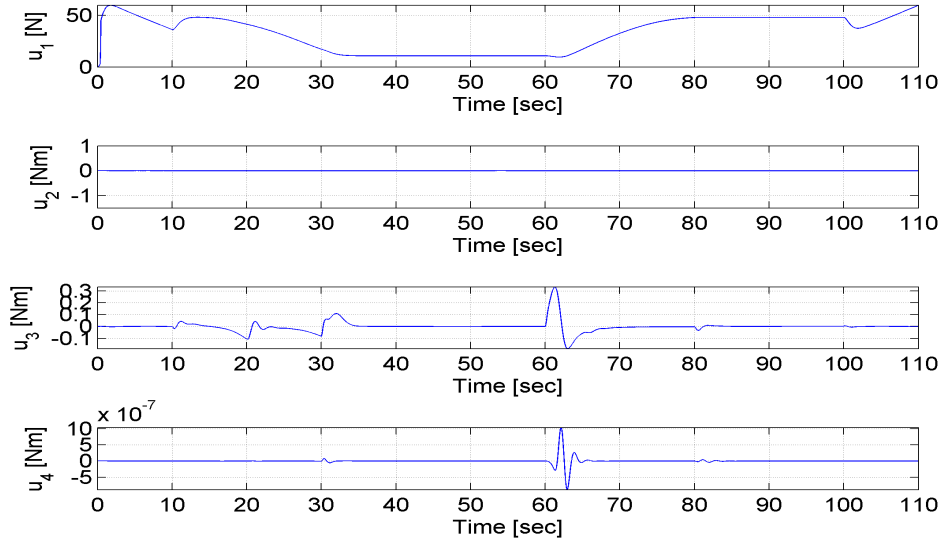


Figure 5.18: Control inputs.

## 5.2 Failure Scenario

In this scenario while UAV tracks the desired trajectory a component failure occurs at  $t = 61$ s. In the failure instant lower covers, winglets and one battery from each of the right wings fall down. In addition to this, 10% uncertainty at actuator powers and a 20 % actuator power loss after the failure is assumed. Therefore control inputs are multiplied by 0.9 until the failure and they are multiplied by 0.8 after the failure. Performance of the proposed controllers are given below.

### Feedback Linearization Approach

Controller's tracking performances along  $X, Y$  and  $Z$  axes are shown in Figs. 5.19 - 5.21.

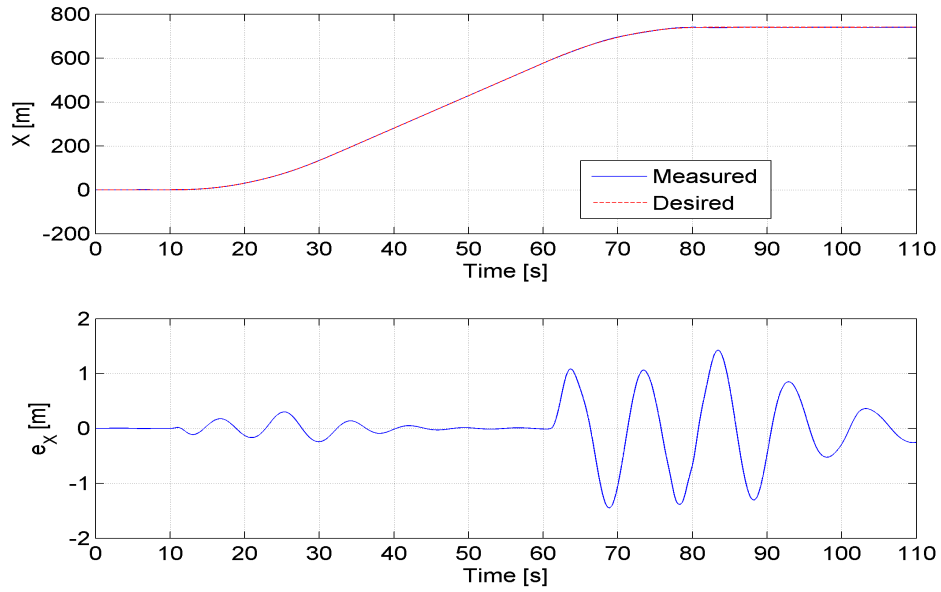


Figure 5.19: X tracking (top), tracking error (bottom).

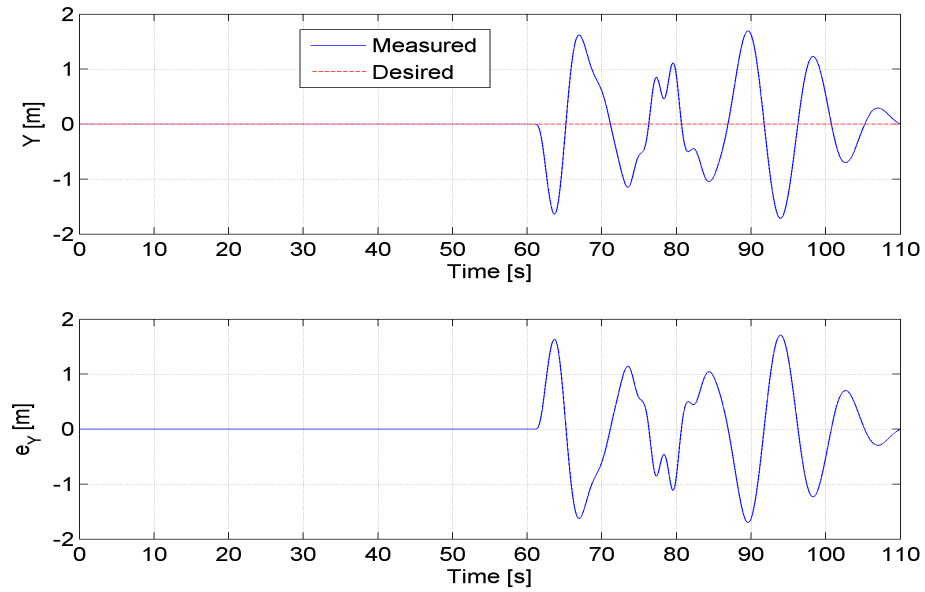


Figure 5.20: Y tracking (top), tracking error (bottom).

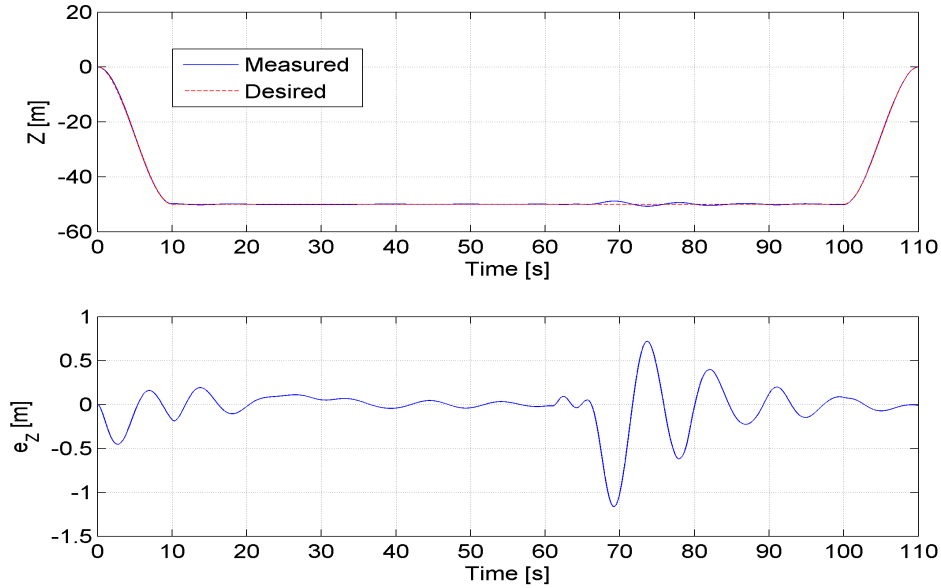


Figure 5.21: Z tracking (top), tracking error (bottom).

UAV tracks the desired trajectories with error values close to zero until the failure instant. There are small oscillations between 10 - 30 s. due to change of the wing angles. Additionally, in this period UAV starts to increase its velocity along  $X$  trajectory. However, after the failure UAV destabilizes and especially along  $X$  and  $Y$  axes continuous oscillations occurs. A 3D plot of the trajectory tracking curves is given in Figure 5.22.

Attitude tracking performance of the UAV is shown in Figure 5.23 - 5.25. Especially along the  $\phi$  and  $\psi$  axis, tracking performance drops dramatically after the failure. Error values increases approximately 45 degree. Since symmetry along the  $X$  axis changes less than the  $Y$  and  $Z$  axis,  $\theta$  tracking does not decrease severely. However, after the failure UAV oscillates along the pitch axis with a magnitude of approximately 4 degrees.

Control inputs of the UAV are shown in Figure 5.26. It is clear that

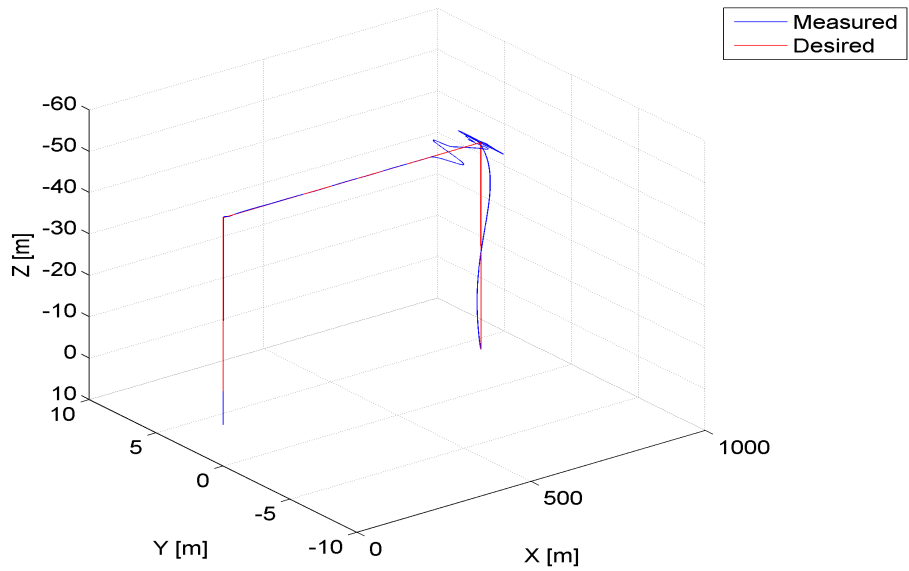


Figure 5.22: Trajectory tracking of the UAV.

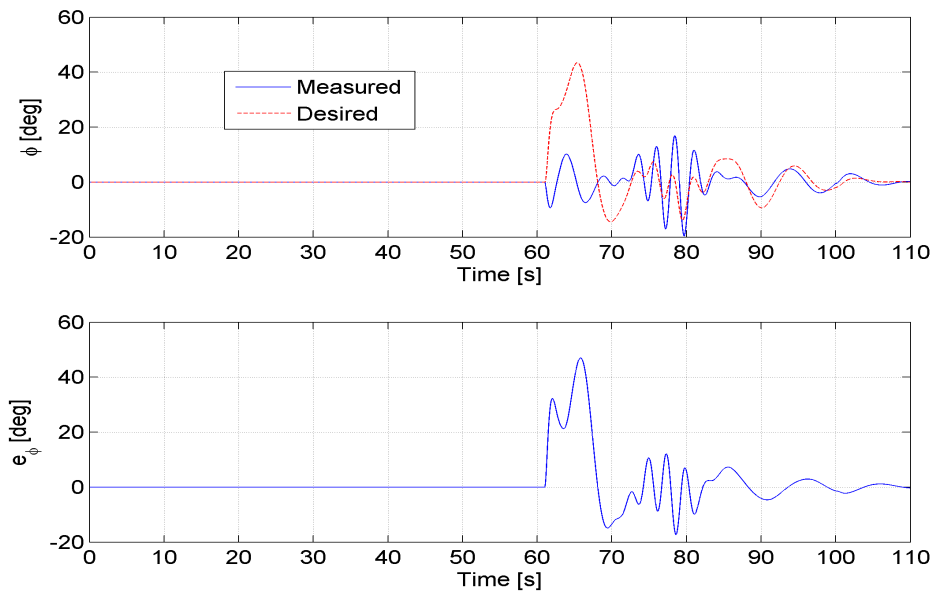


Figure 5.23:  $\phi$  tracking (top), tracking error (bottom).

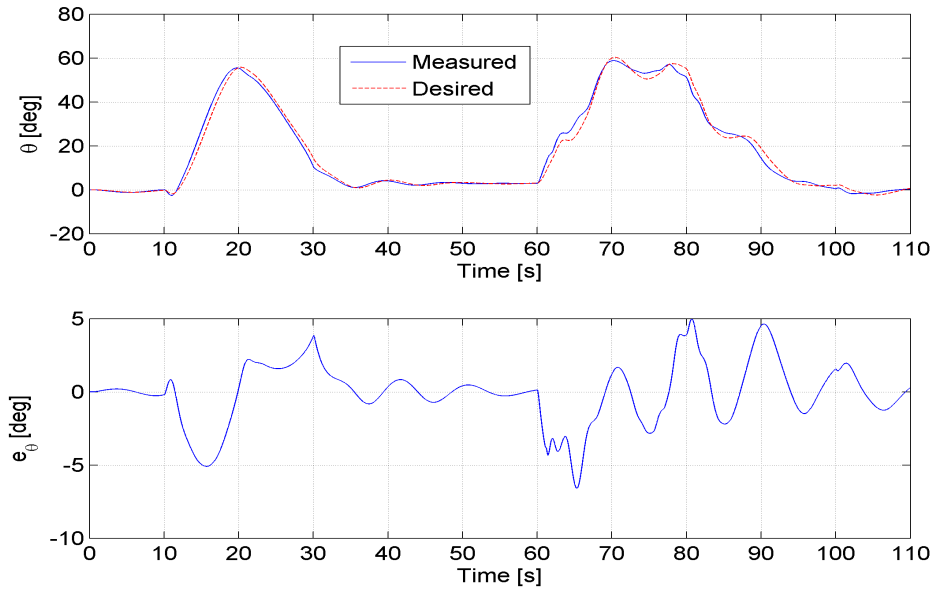


Figure 5.24:  $\theta$  tracking (top), tracking error (bottom).

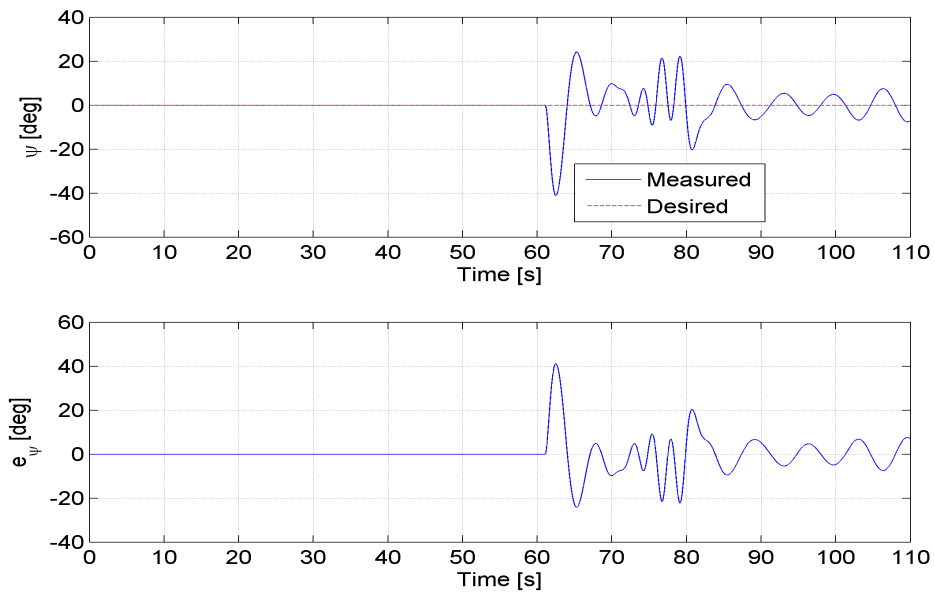


Figure 5.25:  $\psi$  tracking (top), tracking error (bottom).

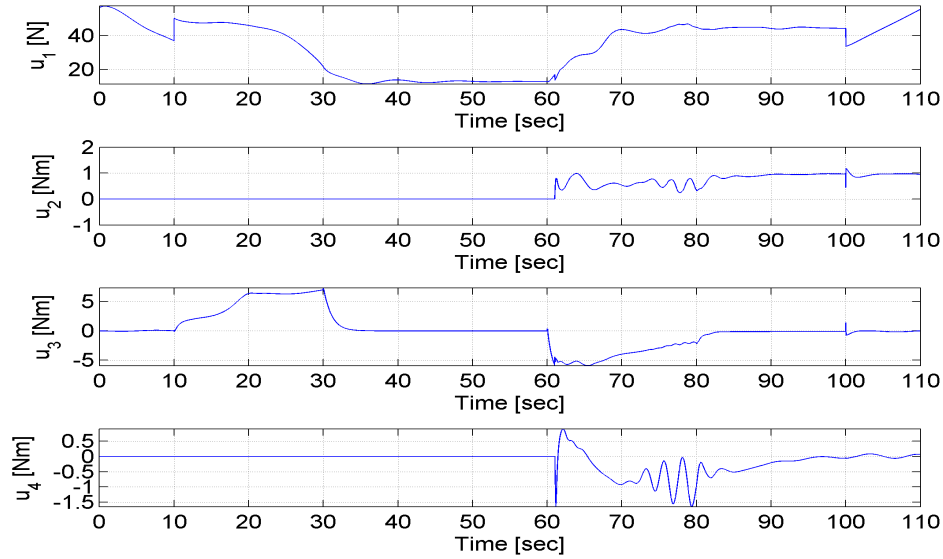


Figure 5.26: Control inputs.

during the horizontal flight total thrust of the UAV decreases.  $u_2$  and  $u_4$  have a magnitude of zero Nm until the failure instant. After failure their magnitudes increase approximately 1 Nm to stabilize the UAV around roll and yaw axis.  $u_3$  controls the UAV around pitch axis and it reaches to 5 Nm to achieve a pitch angle of approximately 60 degrees; and then until the failure it is zero Nm. When failure occurs it becomes -5 Nm which is due to the failure and pitch angle increases due to the velocity decrease along  $X$  axis.

### Adaptive Control Approach

Same failure scenario is also tested with the adaptive control approach. Tracking curves along  $X, Y$  and  $Z$  axes are shown in Figures 5.27 - 5.29.

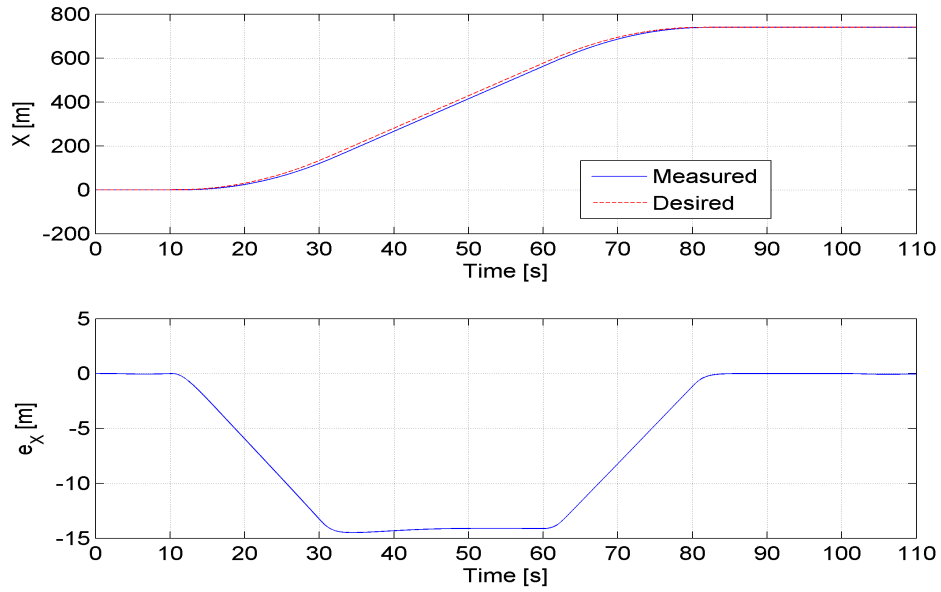


Figure 5.27: X tracking (top), tracking error (bottom).

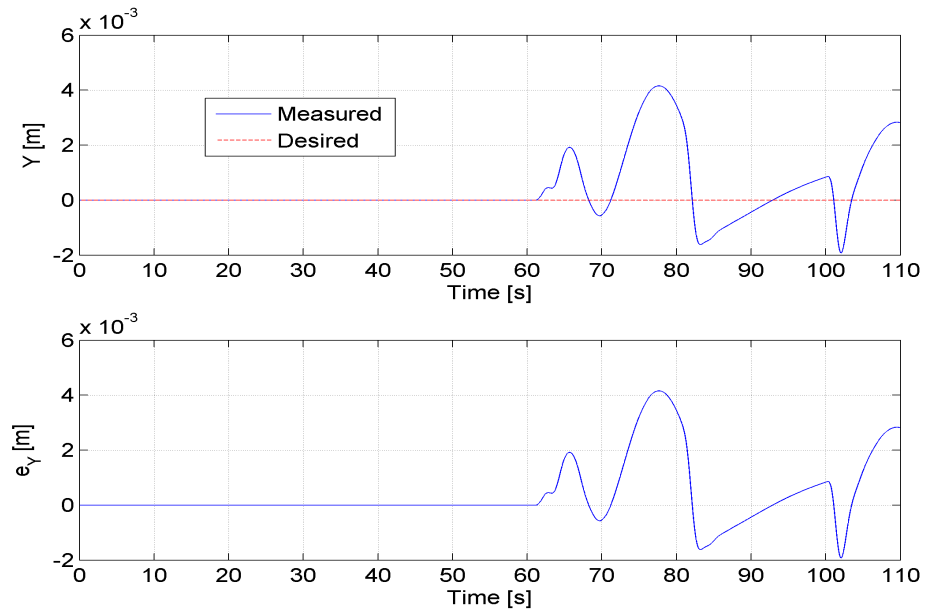


Figure 5.28: Y tracking (top), tracking error (bottom).

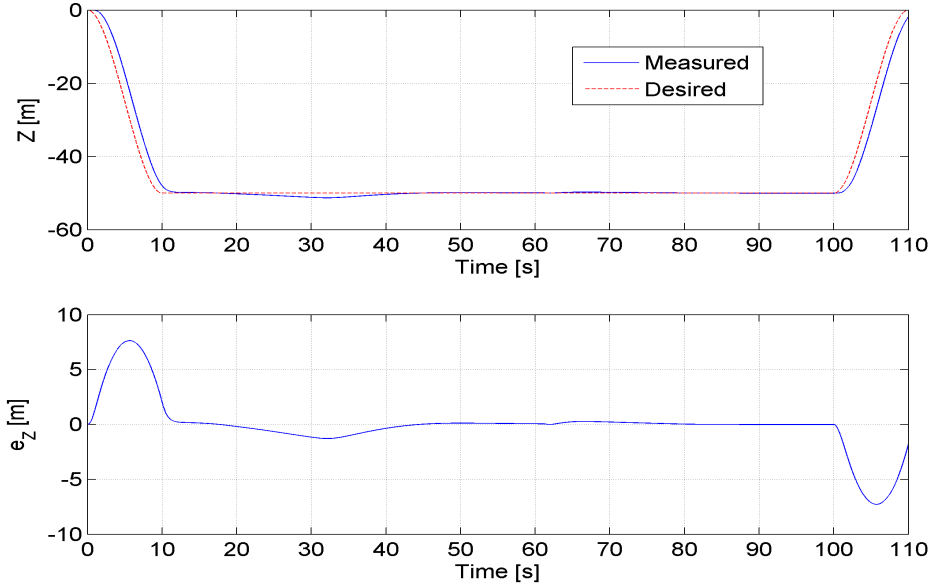


Figure 5.29:  $Z$  tracking (top), tracking error (bottom).

UAV deviates from the trajectory much less with respect to feedback linearization approach. Since, UAV tracks the reference model along the  $X$  axis there is a constant error especially at the linear segment. However, it does not oscillate severely after the failure instant. Additionally, along  $Y$  and  $Z$  axes UAV's tracking performance does not decrease as much as the fixed controller. Note that, in the fixed controller UAV deviates from the trajectory approximately 1 m. and 0.5 m. along the  $Y$  and  $Z$  axis, respectively. Tracking performances of the controllers can be compared with Figures 5.22 and 5.30 which show the 3D plots of the desired trajectories and tracking results.

Attitude tracking results of the UAV are shown in Figures 5.31 - 5.33. UAV's tracking errors around roll axis is less than  $1^\circ$  after the failure. It is much lower with respect to fixed controller whose error values around roll

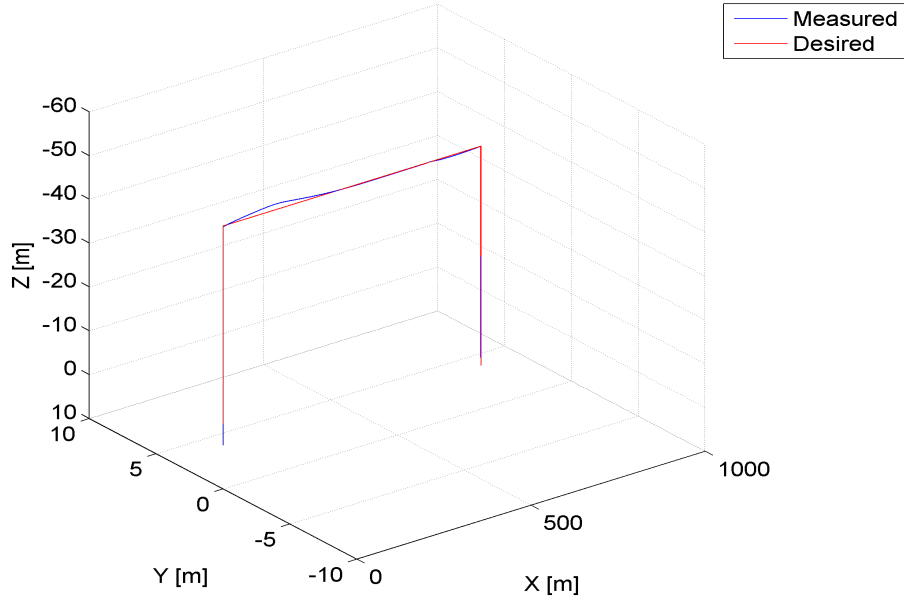


Figure 5.30: Trajectory tracking of the UAV.

axis reaches  $40^\circ$  after the failure. Additionally, around pitch and yaw axes tracking performance of the UAV outperforms the fixed controller. Around pitch axis tracking error becomes  $4^\circ$  and around yaw axis it becomes  $1^\circ$  at the failure instant.

Adaptive controller's inputs to the UAV are shown in Figure 5.34. Their magnitudes are similar to fixed controller's inputs.  $u_3$  increases to  $-10$  Nm. at the failure instant to stabilize the UAV at the pitch axis which takes negative values at the failure. On the other hand, except from this instant control inputs are smaller or similar to fixed controller's control inputs. Therefore, adaptive controller outperforms the fixed controller with achievable control input magnitudes.

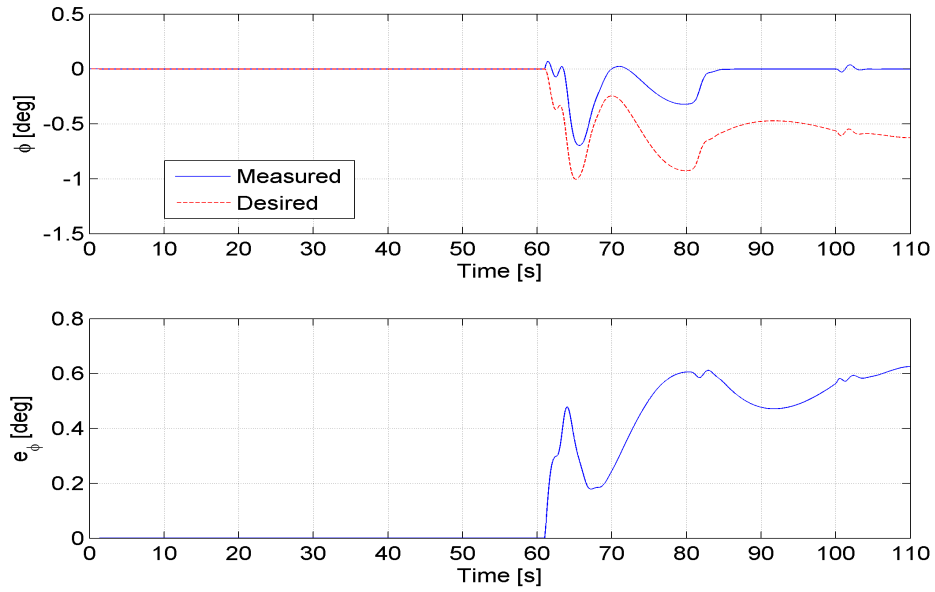


Figure 5.31:  $\phi$  tracking (top), tracking error (bottom).

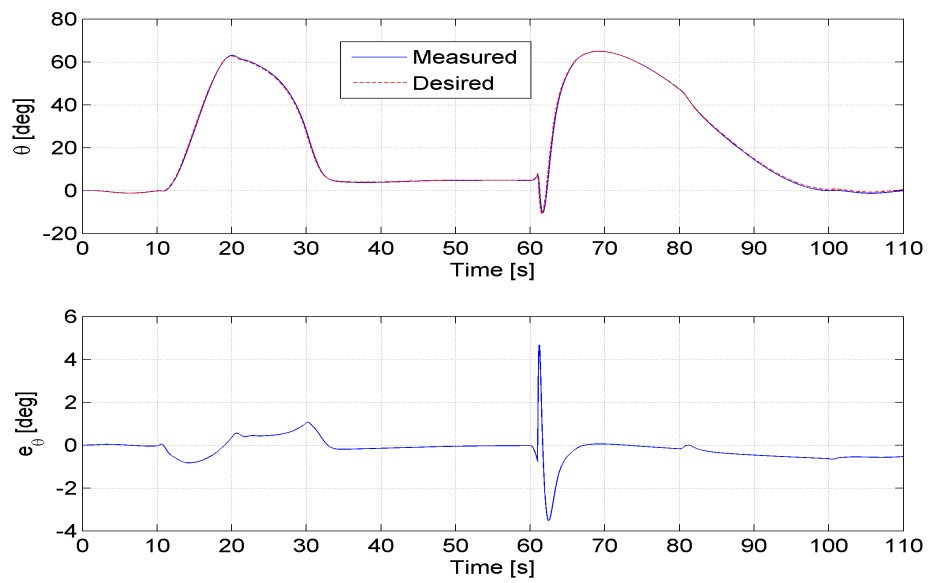


Figure 5.32:  $\theta$  tracking (top), tracking error (bottom).

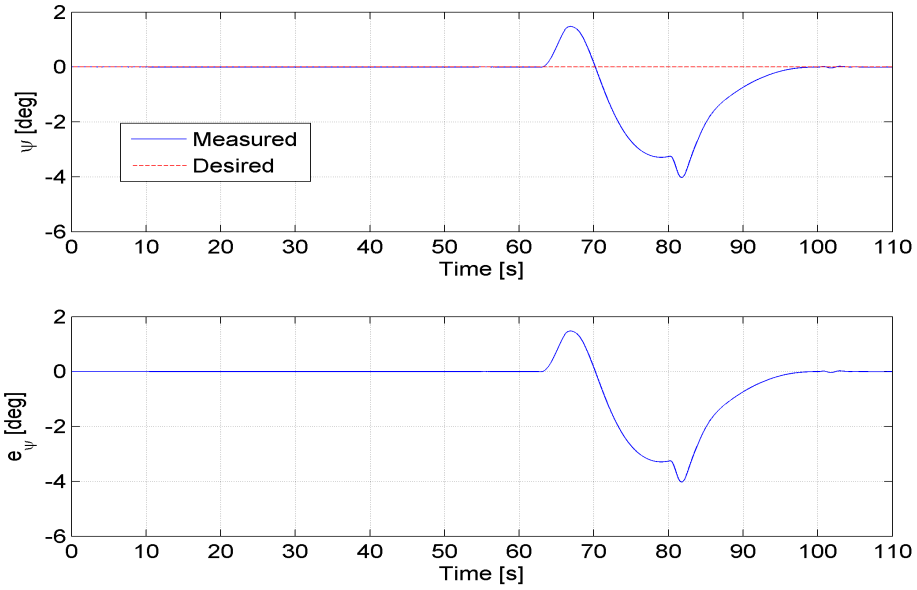


Figure 5.33:  $\psi$  tracking (top), tracking error (bottom).

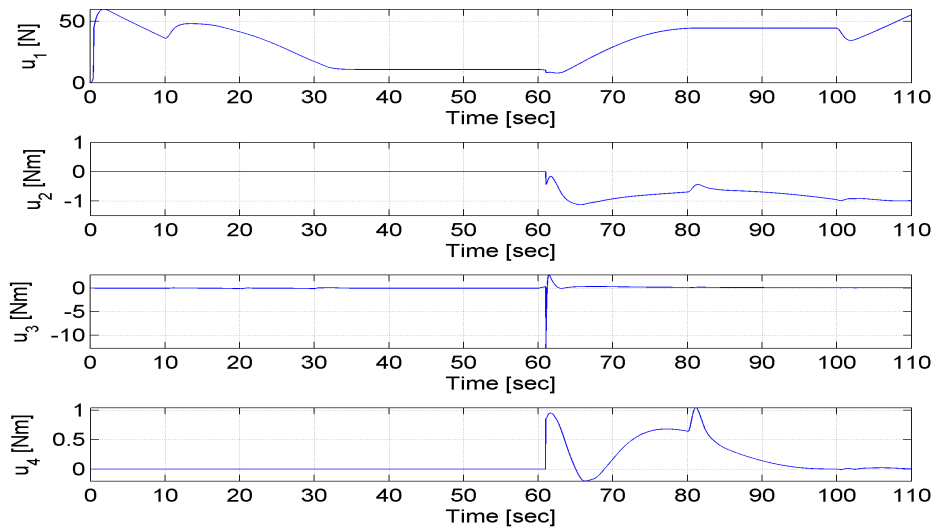


Figure 5.34: Control inputs.

### 5.3 Wind Disturbance Added Failure Scenario

In this scenario, a wind disturbance is added to the simulations in addition to the component failure and actuator power drops that occurs in the first scenario. A Dryden wind turbulence model is used to generate atmospheric turbulence. This model creates wind disturbances along  $X, Y$  and  $Z$  axes. Wind profile changes with respect to the magnitude of the UAV's velocity and attitude angles. UAV achieves the same velocity profile for the fixed and adaptive controller; however, their orientation are not same during the flight. Therefore, similar wind disturbances are applied for this scenario.

#### Feedback Linearization Approach

Wind profile that is applied for the fixed controller is shown in Figure 5.35.

Trajectory tracking performance of the fixed controller in the presence of the wind disturbances are shown in Figures 5.36 - 5.39. Wind magnitudes along  $X, Y$  and  $Z$  axes are in the envelope of  $\pm 0.8$  N. and this results in position tracking oscillations which can be seen in the tracking error plots until the failure instant. In addition to this, oscillations after the failure increases. For example, tracking errors are bigger in this scenario for the  $Y$  axis (Fig. 5.37) than the failure scenario (Fig. 5.20).

Attitude tracking performance is shown in Figures 5.40 - 5.42. There are approximately  $\pm 15^\circ$  oscillations between the  $t = 20 - 30$  s due to the wind disturbances. These oscillations are not severe in the pitch axis with respect to other attitude axes.

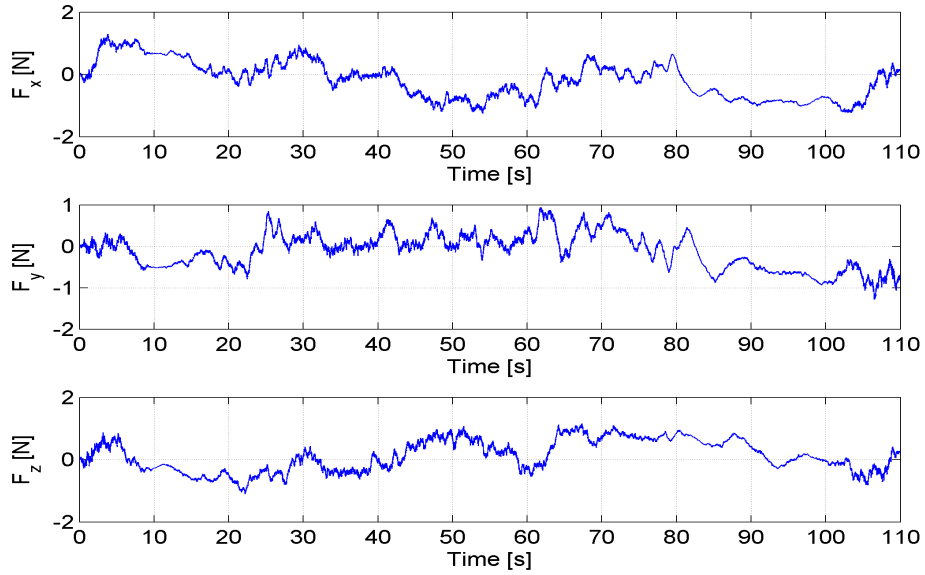


Figure 5.35: Wind Disturbances.

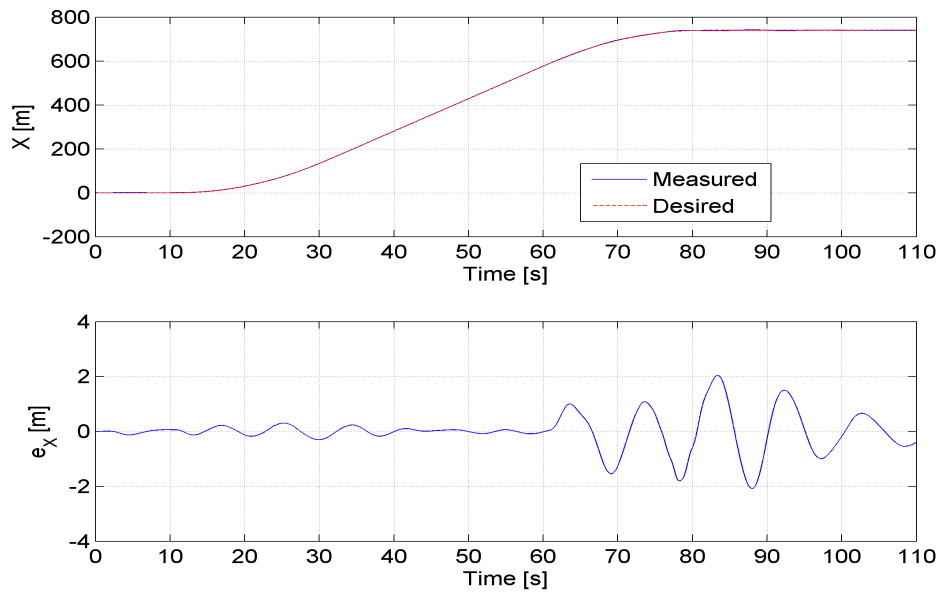


Figure 5.36: X tracking (top), tracking error (bottom).

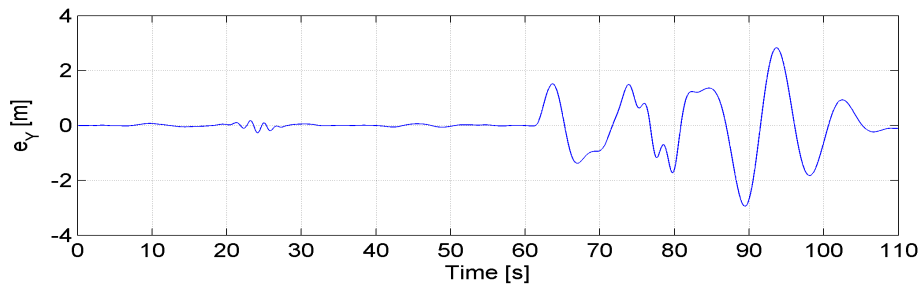
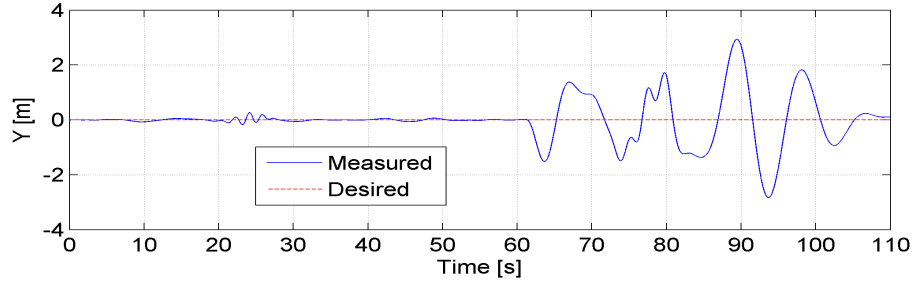


Figure 5.37: Y tracking (top), tracking error (bottom).

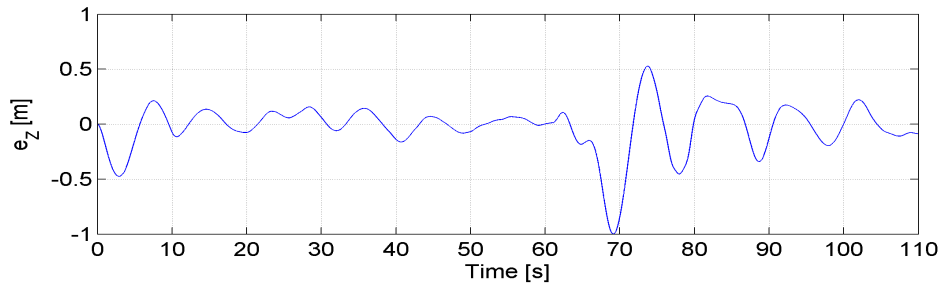
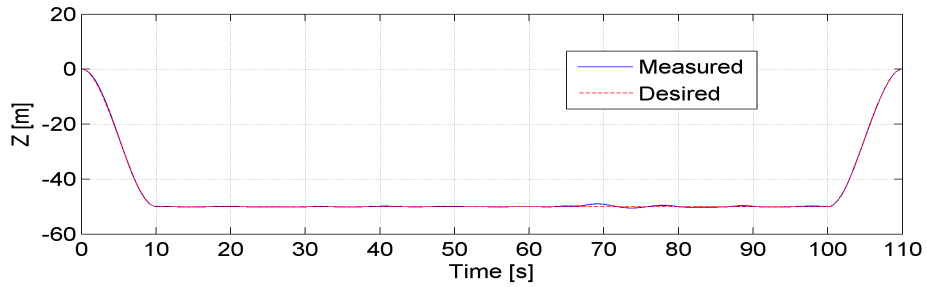


Figure 5.38: Z tracking (top), tracking error (bottom).

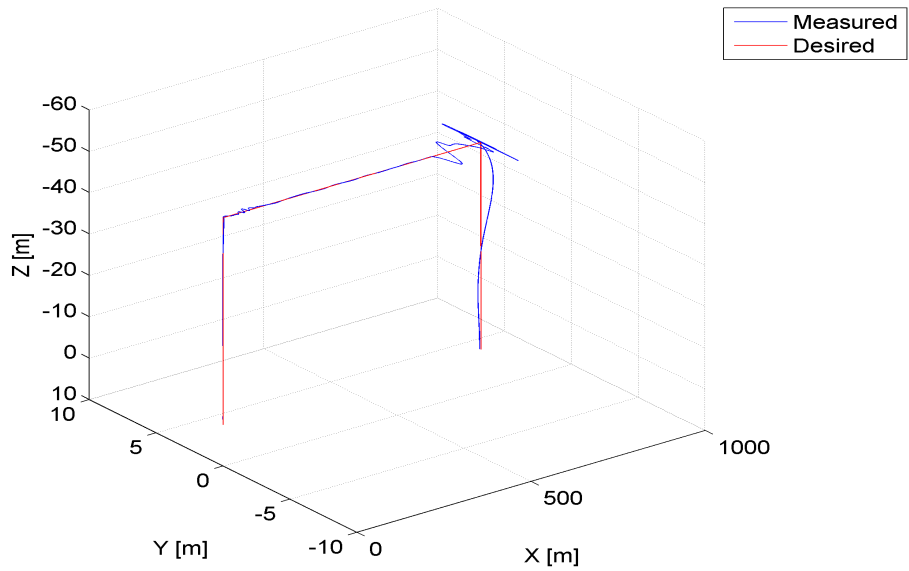


Figure 5.39: Trajectory tracking of the UAV.

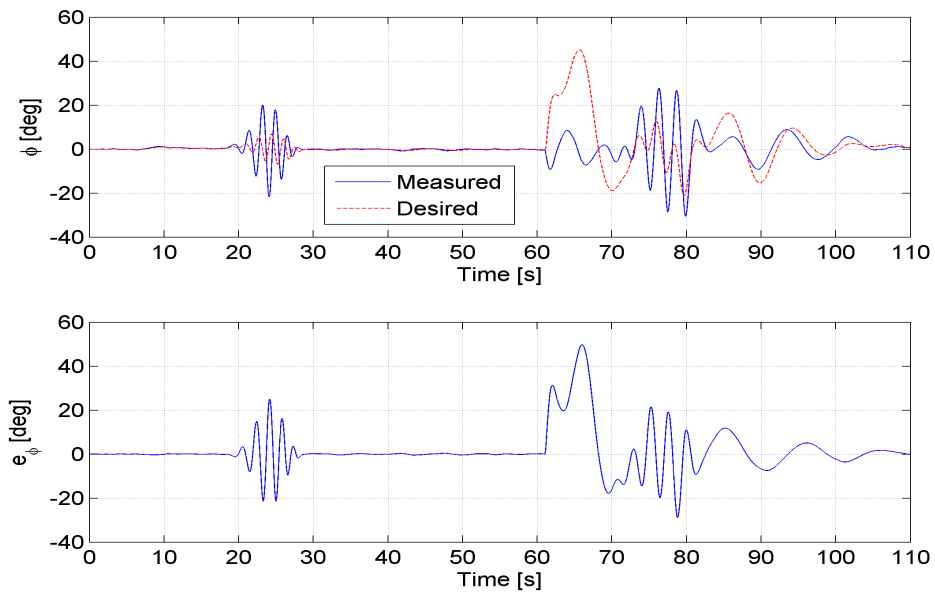


Figure 5.40:  $\phi$  tracking (top), tracking error (bottom).

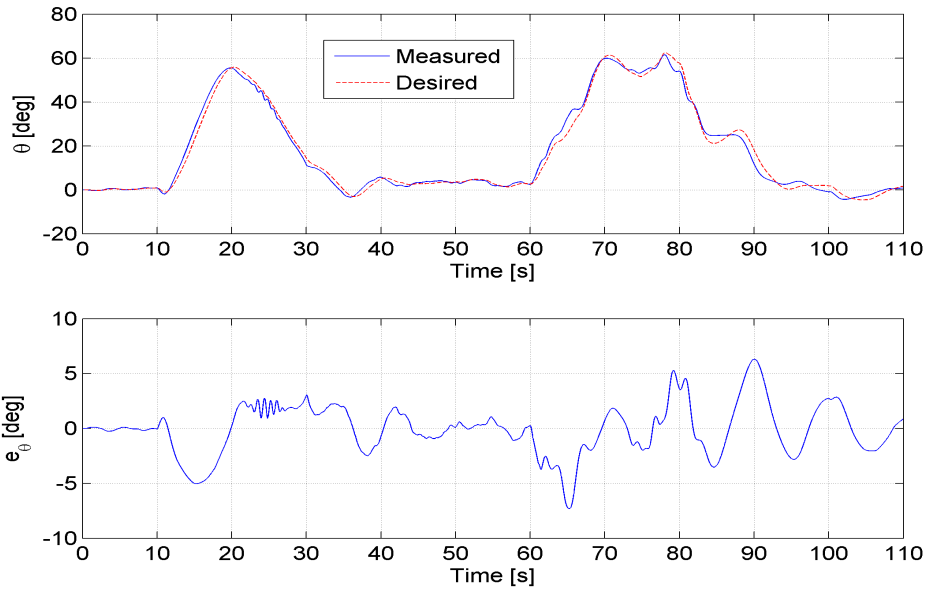


Figure 5.41:  $\theta$  tracking (top), tracking error (bottom).

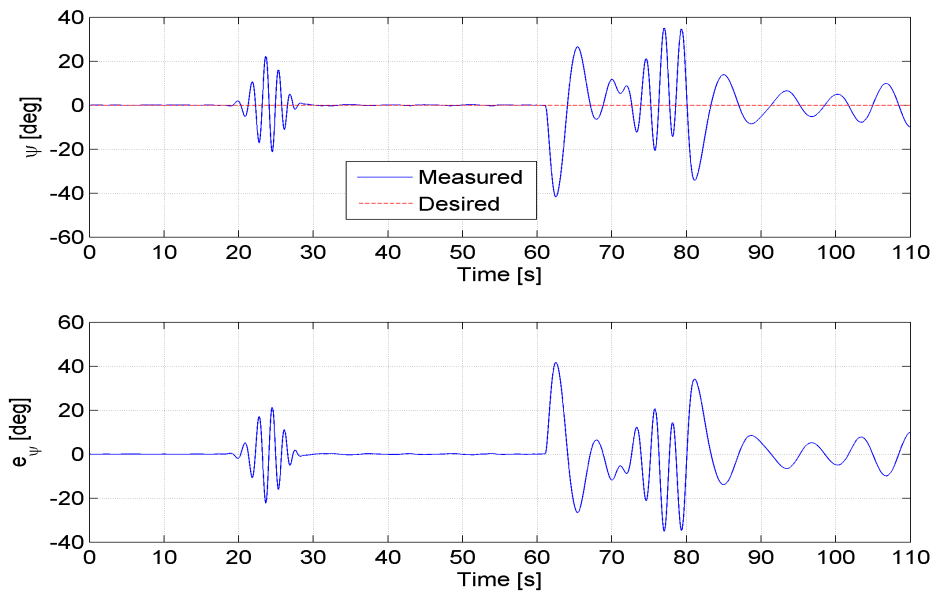


Figure 5.42:  $\psi$  tracking (top), tracking error (bottom).

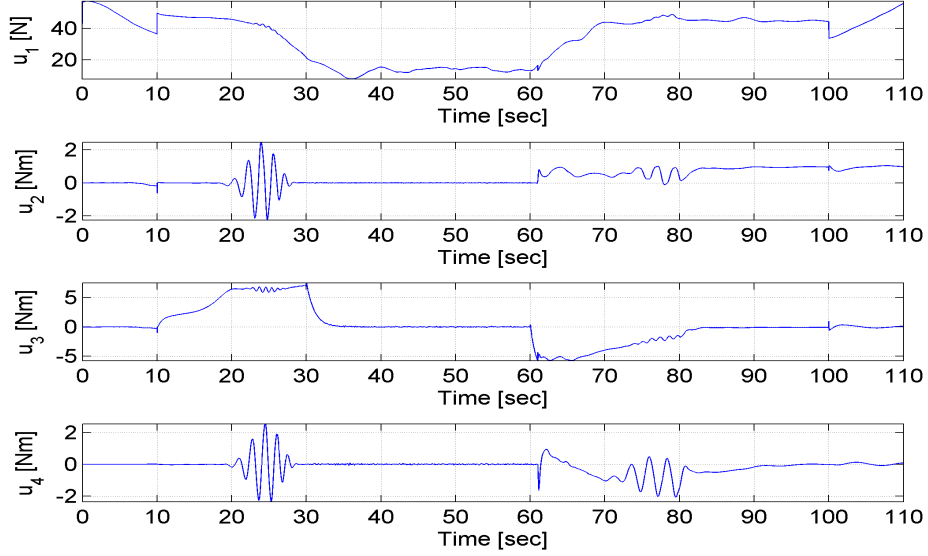


Figure 5.43: Control inputs.

After the failure instant, UAV attitude tracking errors are bigger than the failure scenario. To illustrate, for the failure scenario tracking errors around  $\phi$  were between  $\pm 10^\circ$  for  $t = 70 - 80$ s (Fig. 5.23) and in the presence of the disturbance this increases approximately to  $\pm 20^\circ$  (Fig. 5.40).

Control inputs for the fixed controller in the presence of wind disturbances are shown in Fig. 5.43. Oscillations do not exist in the failure scenario (Fig. 5.26) in  $u_2$  and  $u_4$  between the  $t = 20 - 30$  are created by the oscillations around roll and yaw axes which are caused by the wind.

### Adaptive Control Approach

Wind profile, which is the result of the attitude and velocity of the UAV, is shown in Figure 5.44. The minor differences of the wind profile in fixed con-

troller (Fig. 5.35) and adaptive controller are caused by the UAV's attitude during the flight.

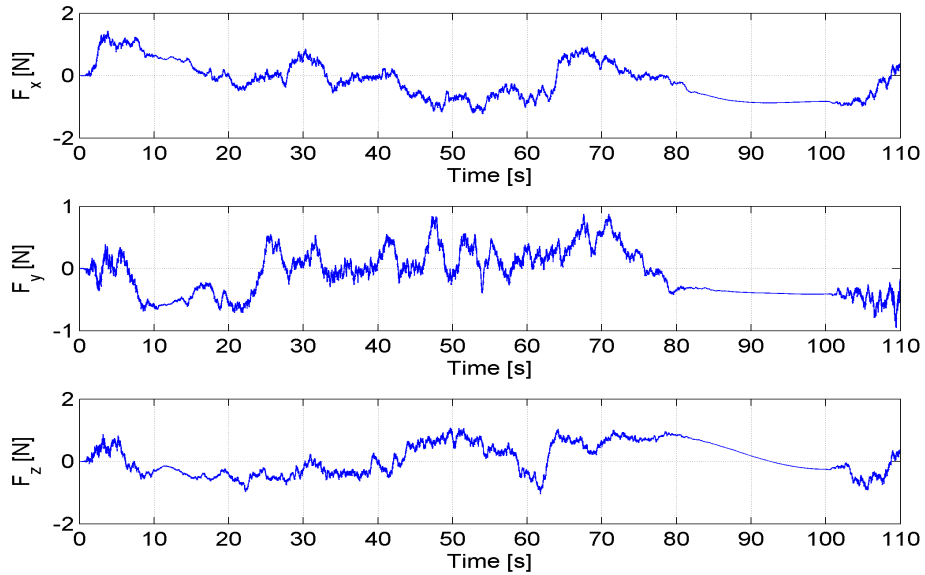


Figure 5.44: Wind Disturbances.

Position of the UAV along  $X, Y$  and  $Z$  axes are shown in Figures 5.45 - 5.47. UAV's tracking performance along the  $X, Y$  and  $Z$  axis does not decrease dramatically in the presence of disturbances. There are small oscillations in the measured signals which can be seen in Figure 5.46. However, fixed controller oscillations especially after the failure reaches up to  $3^\circ$ . Therefore adaptive controller especially after the failure outperforms the fixed controller.

Attitude tracking results for the adaptive controller are shown in Figure 5.49 - 5.51. Around the  $\phi, \theta$  and  $\psi$  axes UAV's tracking errors reach approximately  $4^\circ, 4.8^\circ$  and  $4^\circ$ , respectively. However, attitude tracking performance of the adaptive controller also outperforms the fixed controller.

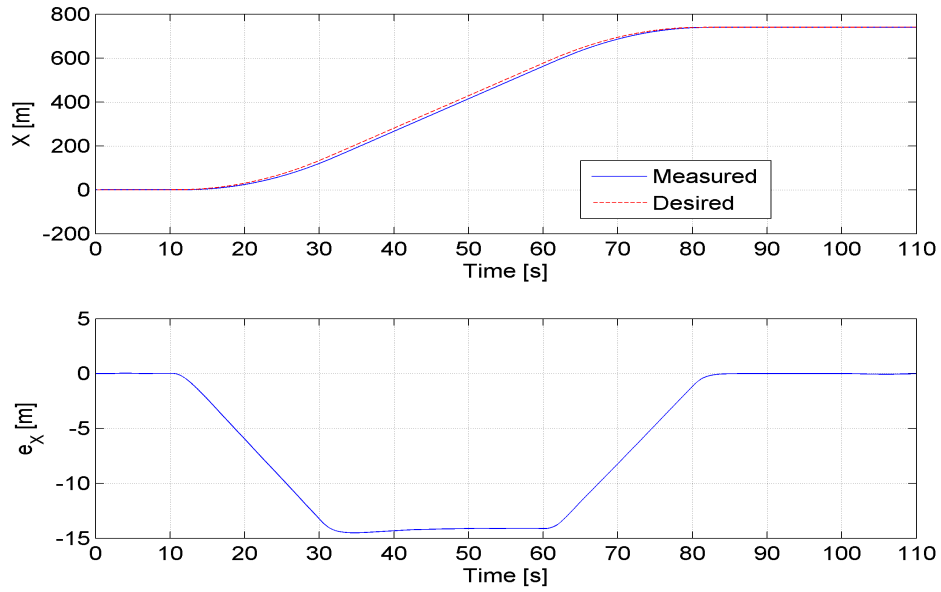


Figure 5.45: X tracking (top), tracking error (bottom).

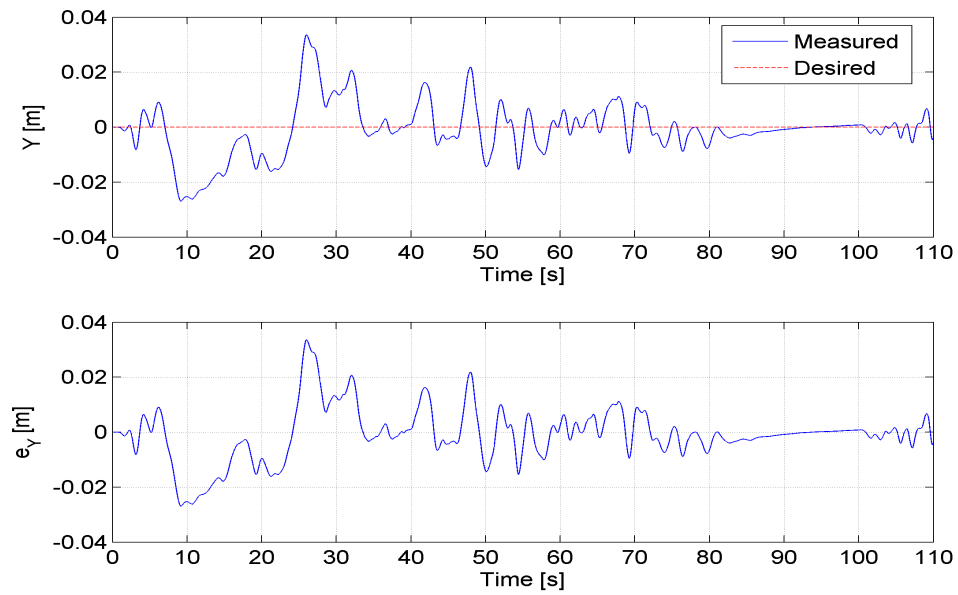


Figure 5.46: Y tracking (top), tracking error (bottom).

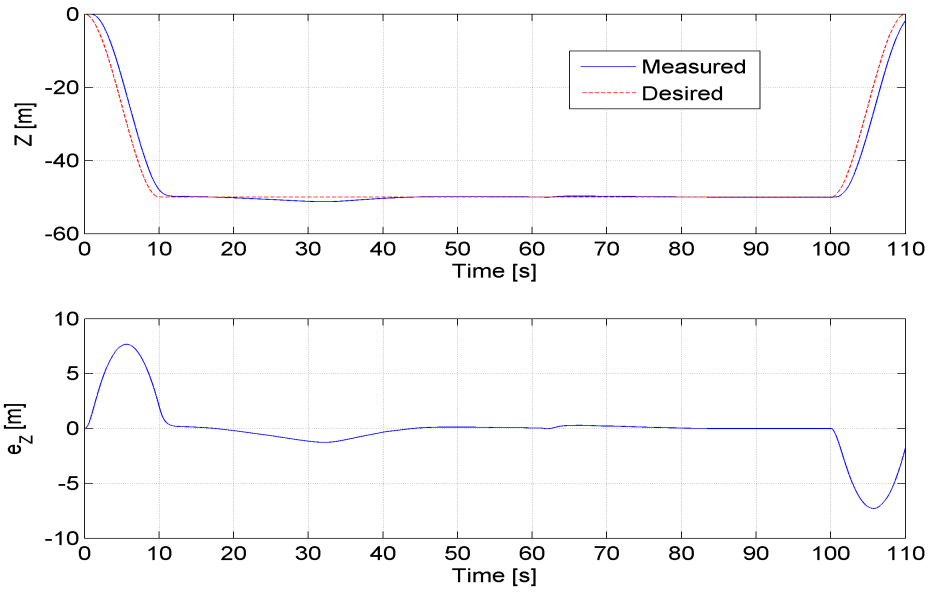


Figure 5.47: Z tracking (top), tracking error (bottom).

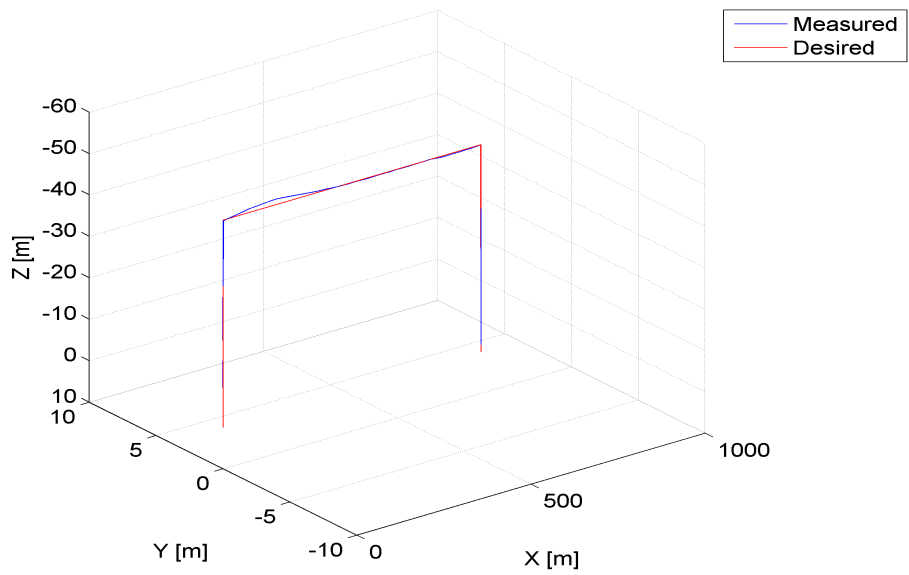


Figure 5.48: Trajectory tracking of the UAV.

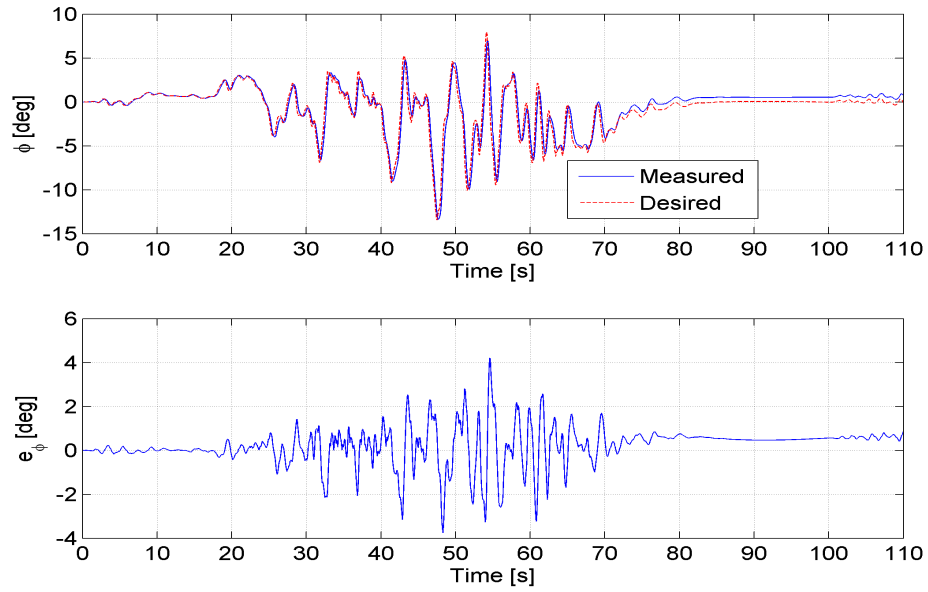


Figure 5.49:  $\phi$  tracking (top), tracking error (bottom).

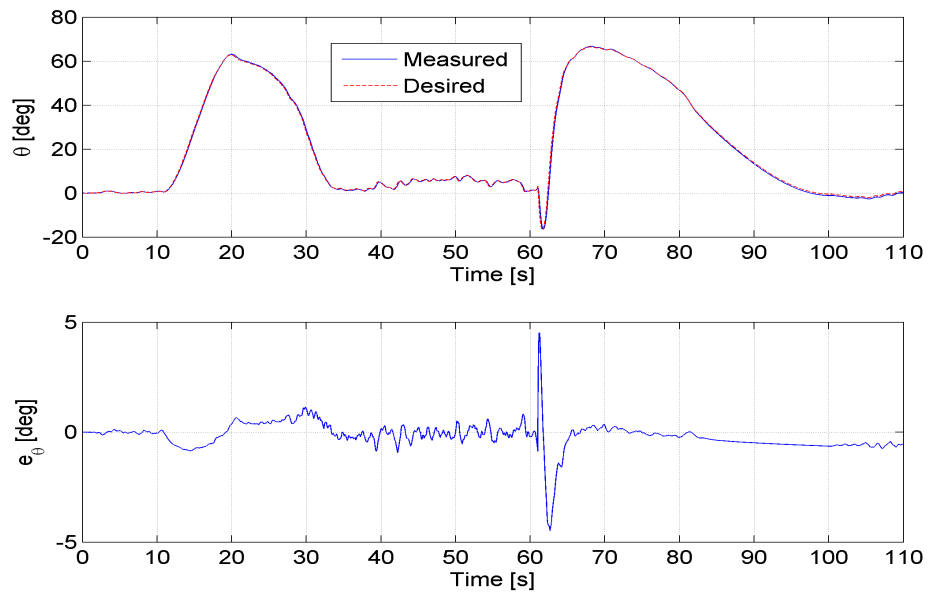


Figure 5.50:  $\theta$  tracking (top), tracking error (bottom).

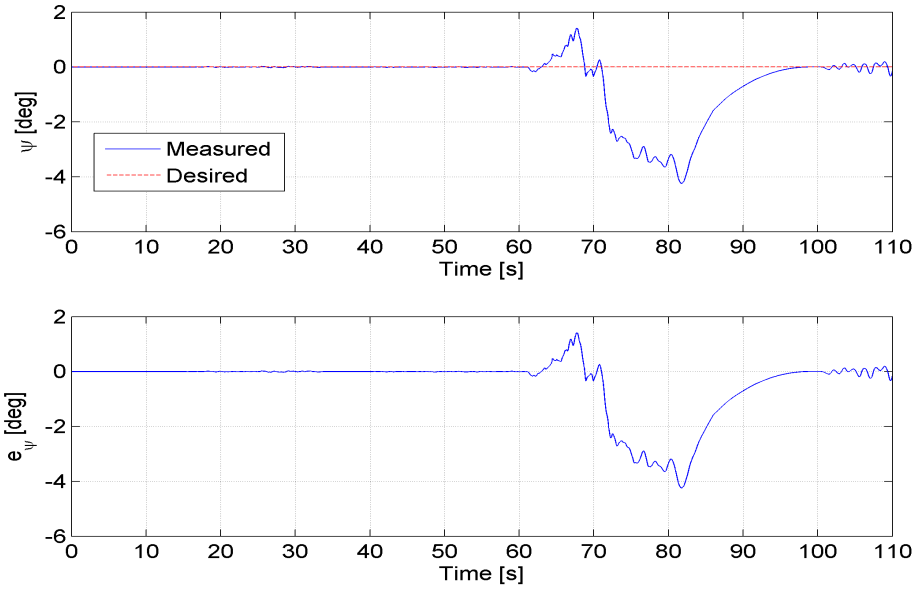


Figure 5.51:  $\psi$  tracking (top), tracking error (bottom).

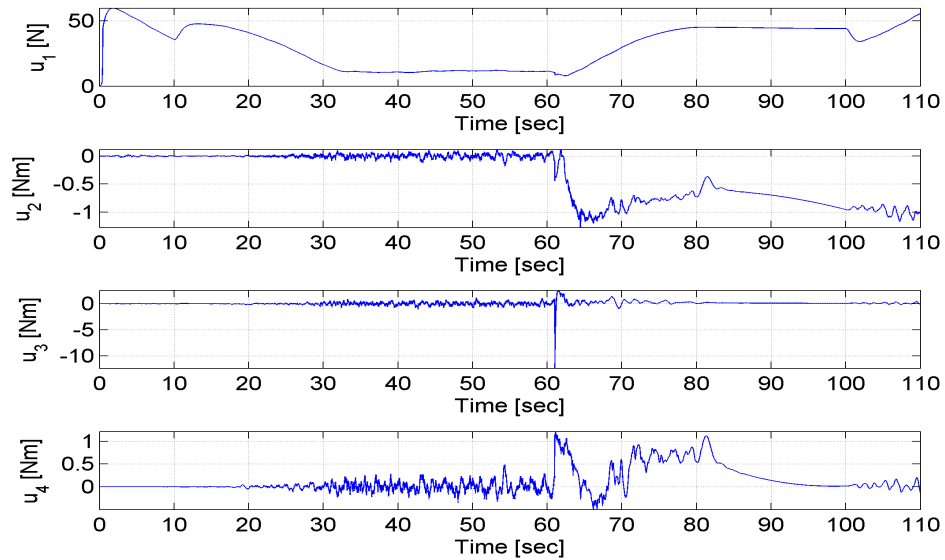


Figure 5.52: Control inputs.

Control inputs of the UAV are shown in Figures 5.52. Wind disturbance causes small chatterings on the control input signals. However, they are less than  $1^\circ$ . Therefore, adaptive controller tracking performance is achieved with small noises in control inputs.

## 5.4 Full Flight Scenario

In this scenario all the simulations are conducted with a high fidelity model, in the presence of uncertainties such as component failure and actuator power drops, wind disturbances and sensor measurement noises. Sensor measurement noises are depicted in Figure 5.53. Band limited white noise is used to simulate sensor noises. Attitude noises oscillate between  $\pm 0.5^\circ$  and position noises oscillate between  $\pm 0.1$  m. As expected, the adaptive controller outperforms the fixed controller due its adaptability to uncertainties which will be discussed below.

### Feedback Linearization Approach

The position tracking performance of the UAV is shown in Figures 5.54 - 5.57. Addition of the sensor measurement noise results in small oscillations in measured signals. These oscillations are in the range of  $\pm 0.2$  m. Tracking errors also increase due to the noise, for instance, maximum tracking error along the  $Y$  axis increases from 3 m to 5.4 m (see Fig. 5.37 and 5.55). It is noted that although its performance is not as good as the adaptive controller, the fixed controller can still keep the closed loop system.

Attitude tracking of the fixed control for the full scenario is shown in Figures 5.58 - 5.60. As it can be seen from the figures fixed controller tracks

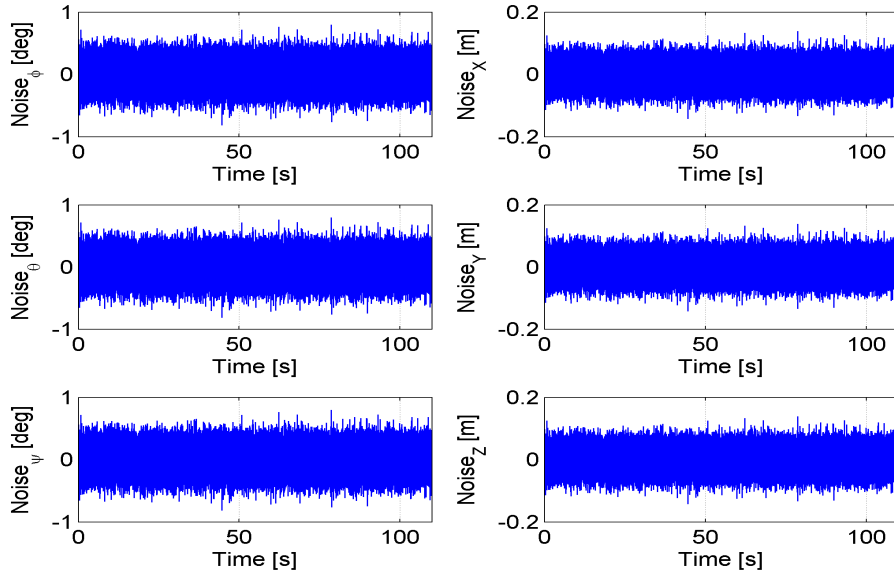


Figure 5.53: Additive measurement noises.

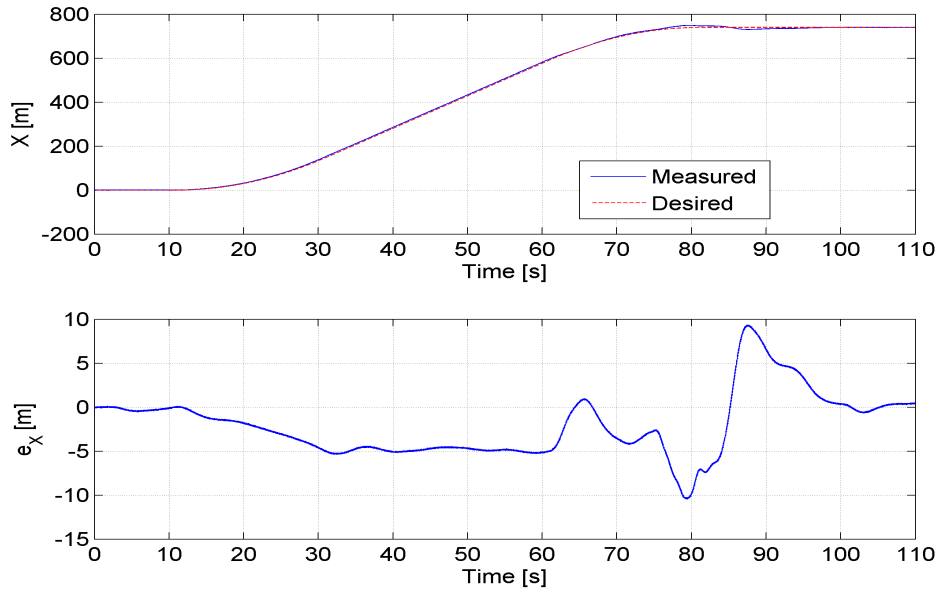


Figure 5.54: X tracking (top), tracking error (bottom).

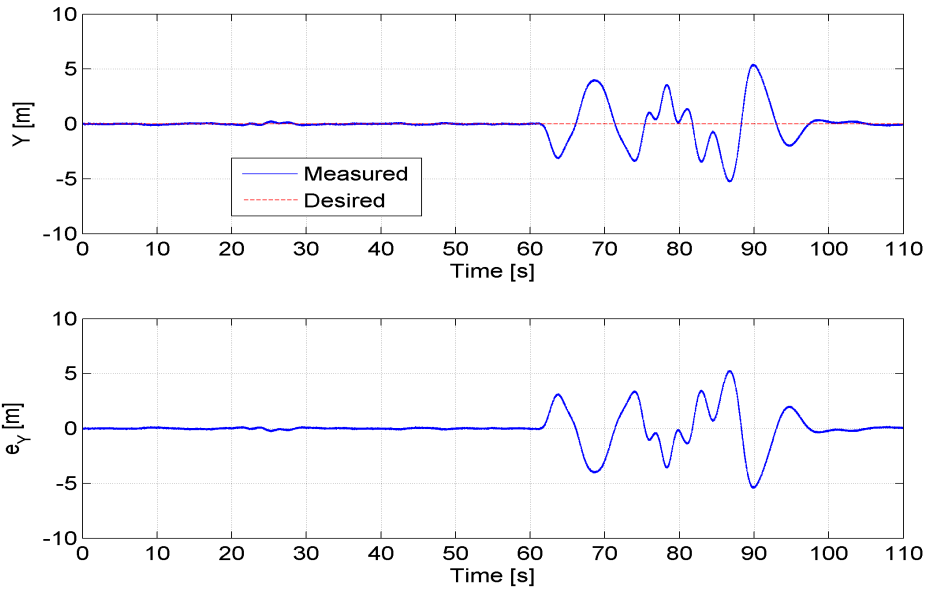


Figure 5.55: Y tracking (top), tracking error (bottom).

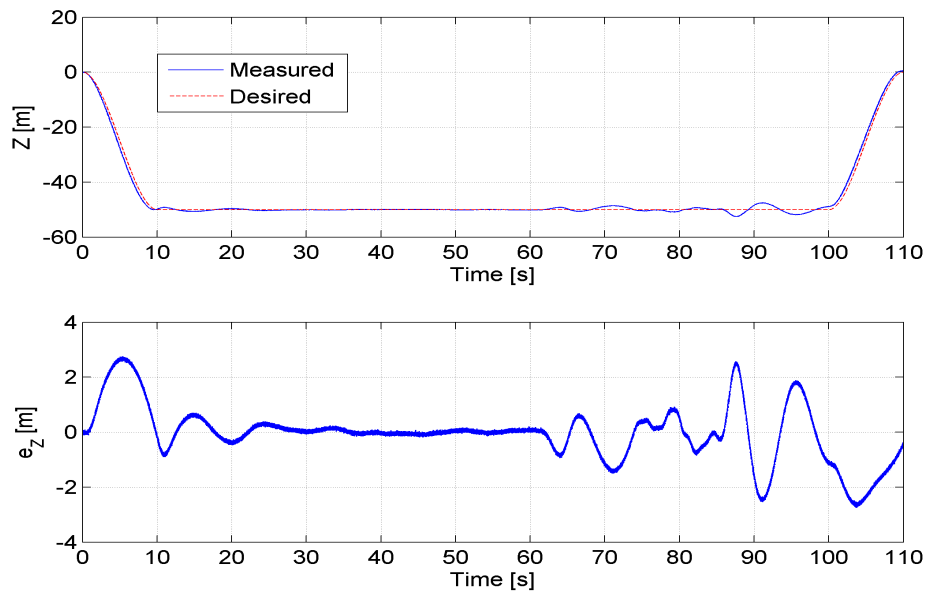


Figure 5.56: Z tracking (top), tracking error (bottom).

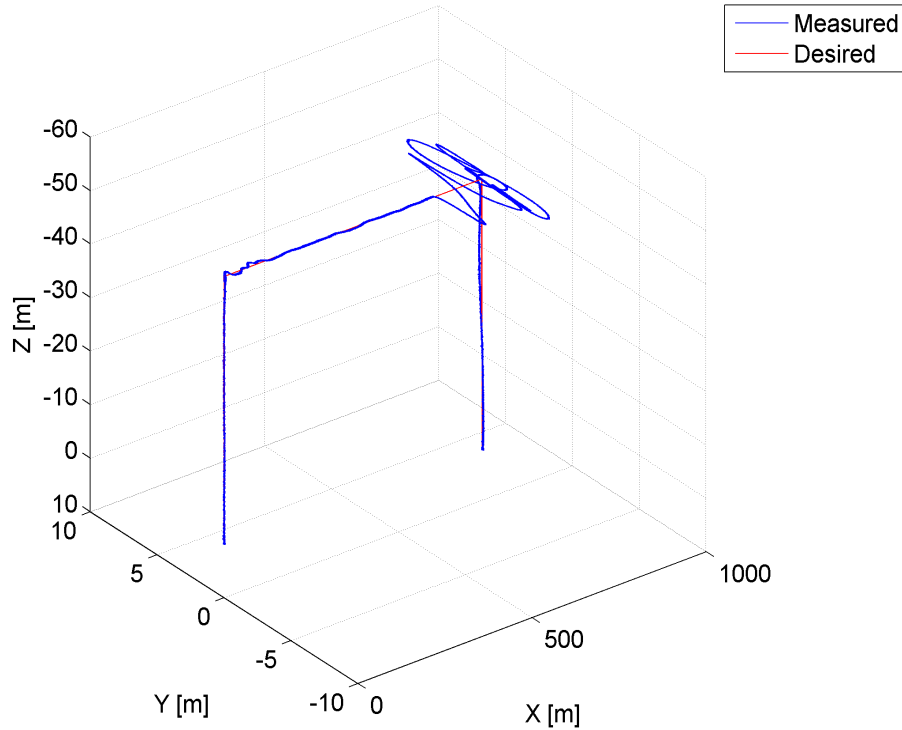


Figure 5.57: Trajectory tracking of the UAV.

the desired pitch angle ( $\theta$ ) relatively well with respect to desired roll ( $\phi$ ) and yaw ( $\psi$ ) angles. However, after the failure UAV's tracking performance decreases. For instance,  $\psi$  tracking error reaches  $80^\circ$  after the failure, whose maximum value is  $40^\circ$  in the wind added failure scenario.

Control inputs of the fixed controller are shown in Figure 5.61. Fixed controller produces noisy control inputs due to the uncertainties, especially in the linear segment of the X trajectory which corresponds to  $t = 30 - 60$ s (see Fig. 5.61). At this segment of the trajectory UAV reaches approximately 50 km/h forward velocity.

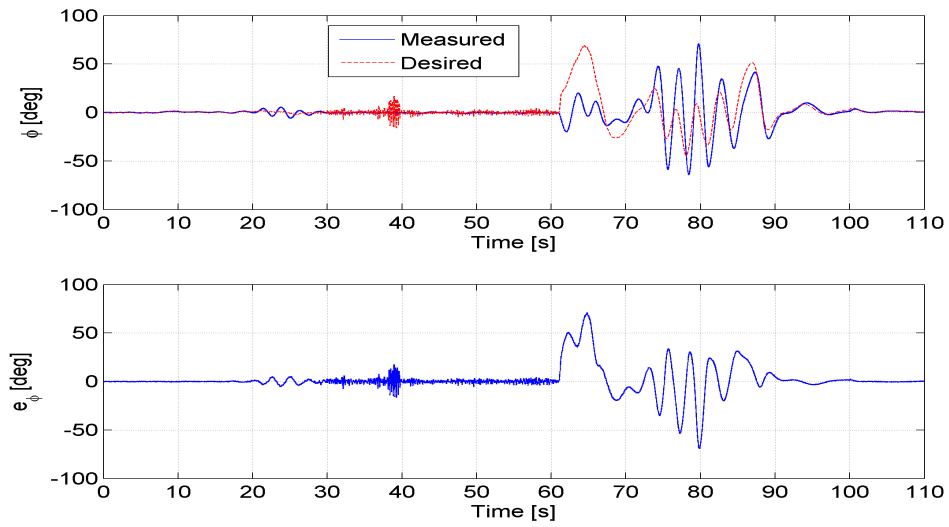


Figure 5.58:  $\phi$  tracking (top), tracking error (bottom).

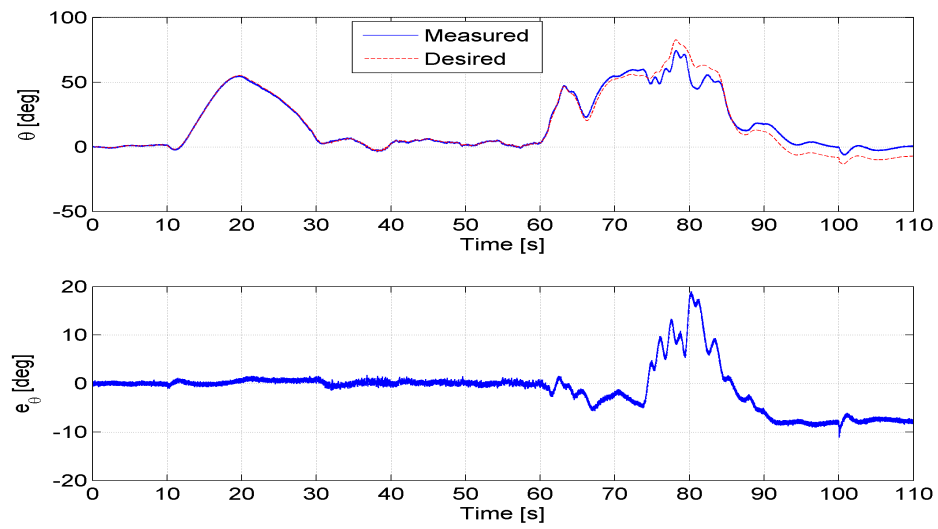


Figure 5.59:  $\theta$  tracking (top), tracking error (bottom).

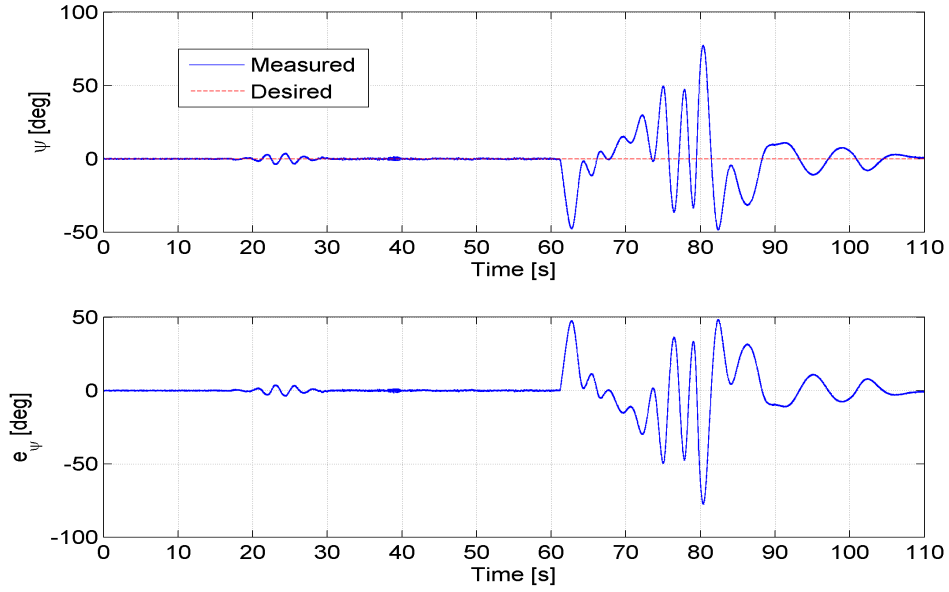


Figure 5.60:  $\psi$  tracking (top), tracking error (bottom).

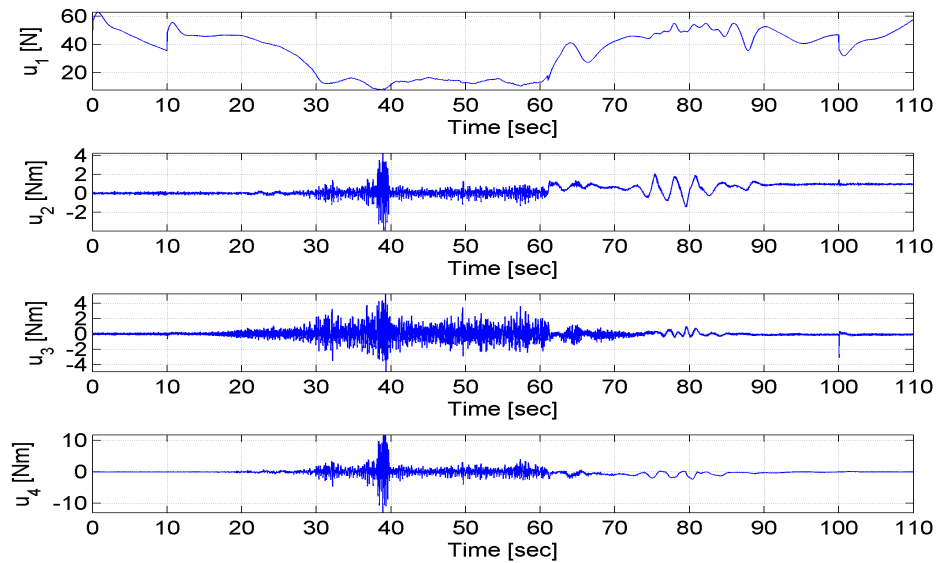


Figure 5.61: Control inputs.

## Adaptive Control Approach

Adaptive controller tracks the desired trajectory with smaller tracking errors with respect to fixed controller, especially after the failure at  $t = 61$ s. Position tracking performance of the proposed controllers are shown in Figure 5.62 - 5.64. Measured signals oscillate between  $\pm 0.1$  m which can be seen in Figure 5.63. A small tracking occurs at the failure instant along the  $X$  and  $Z$  axes (Fig. 5.62 and 5.64).

Attitude tracking curves are shown in Figures 5.66 - 5.68. As it can be seen from the figures tracking error of the proposed nonlinear adaptive controller is close to zero. However after the failure tracking errors reach maximum values of  $4^\circ$ ,  $5^\circ$  and  $5^\circ$  around  $\phi$ ,  $\theta$  and  $\psi$ , respectively.

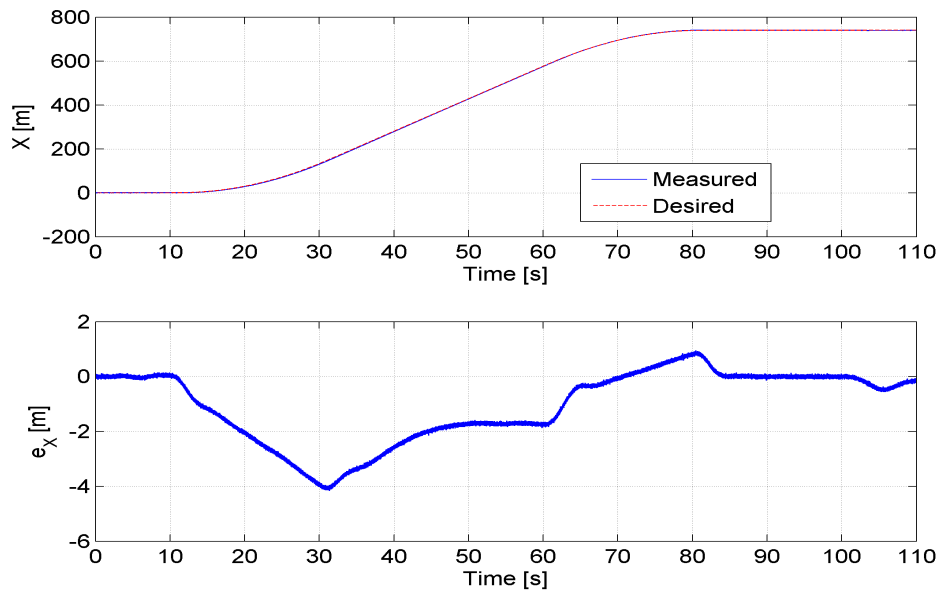


Figure 5.62: X tracking (top), tracking error (bottom).

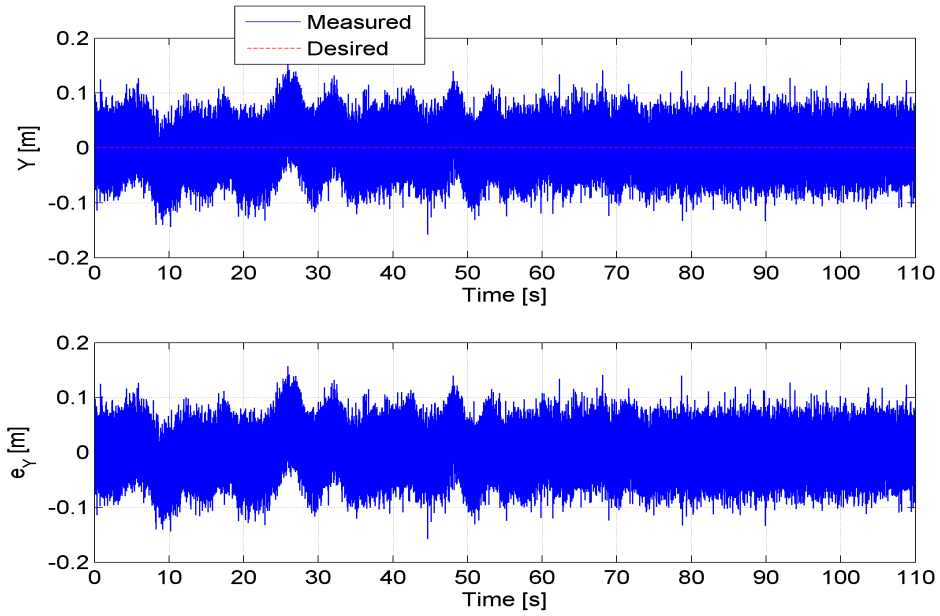


Figure 5.63: Y tracking (top), tracking error (bottom).

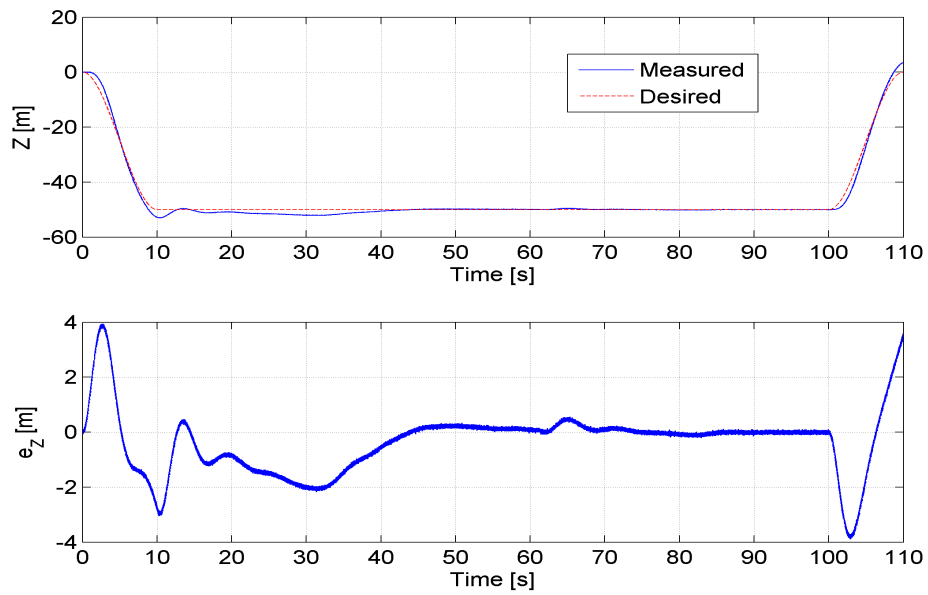


Figure 5.64: Z tracking (top), tracking error (bottom).

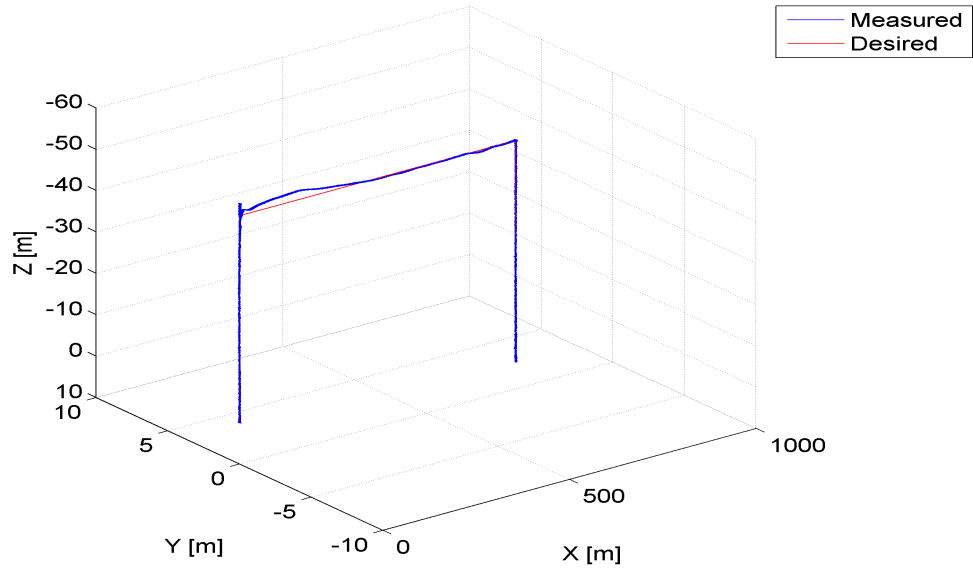


Figure 5.65: Trajectory tracking of the UAV.

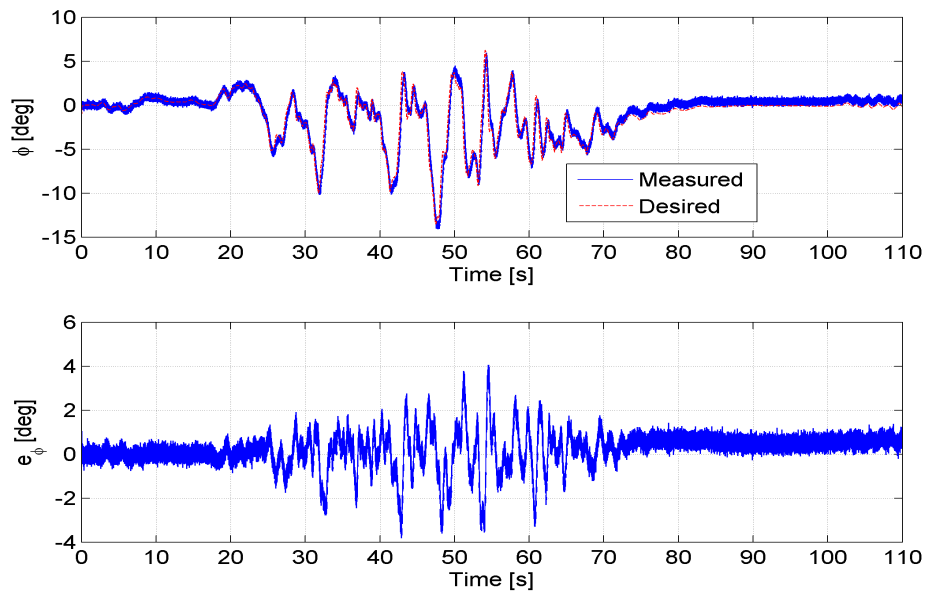


Figure 5.66:  $\phi$  tracking (top), tracking error (bottom).

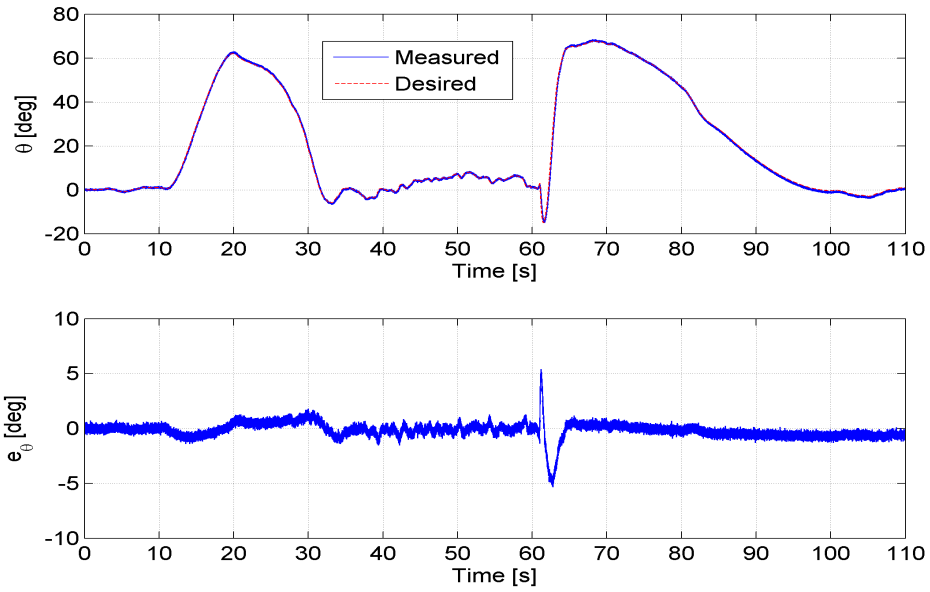


Figure 5.67:  $\theta$  tracking (top), tracking error (bottom).

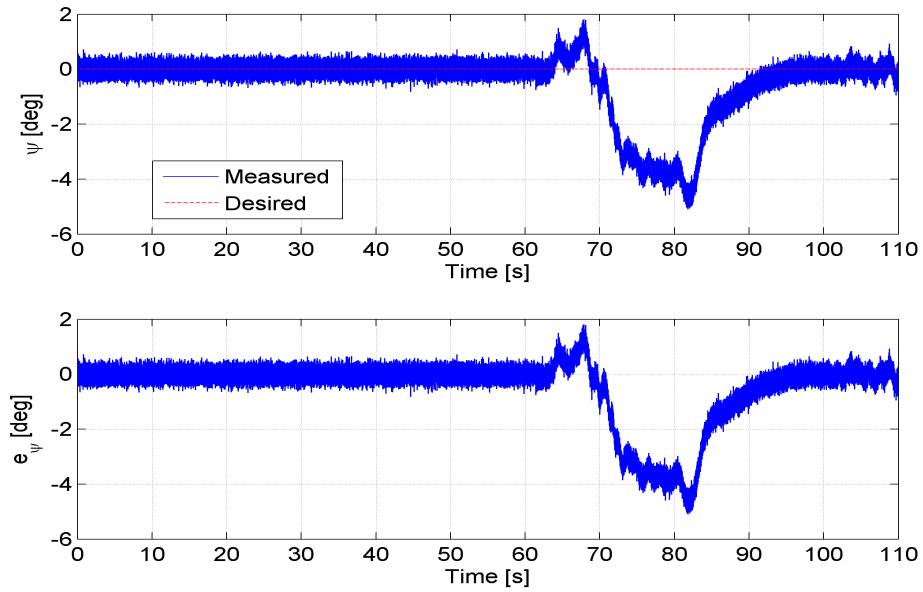


Figure 5.68:  $\psi$  tracking (top), tracking error (bottom).

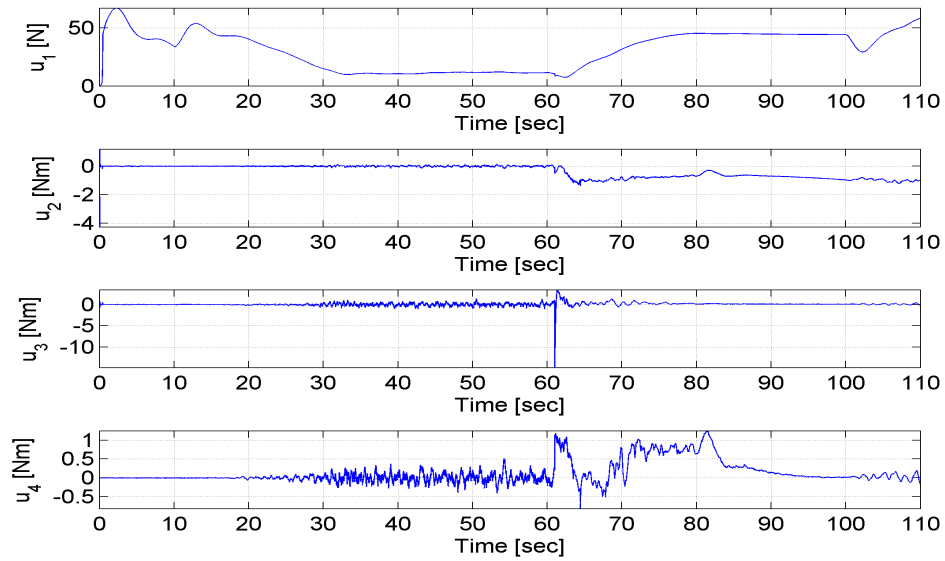


Figure 5.69: Control inputs.

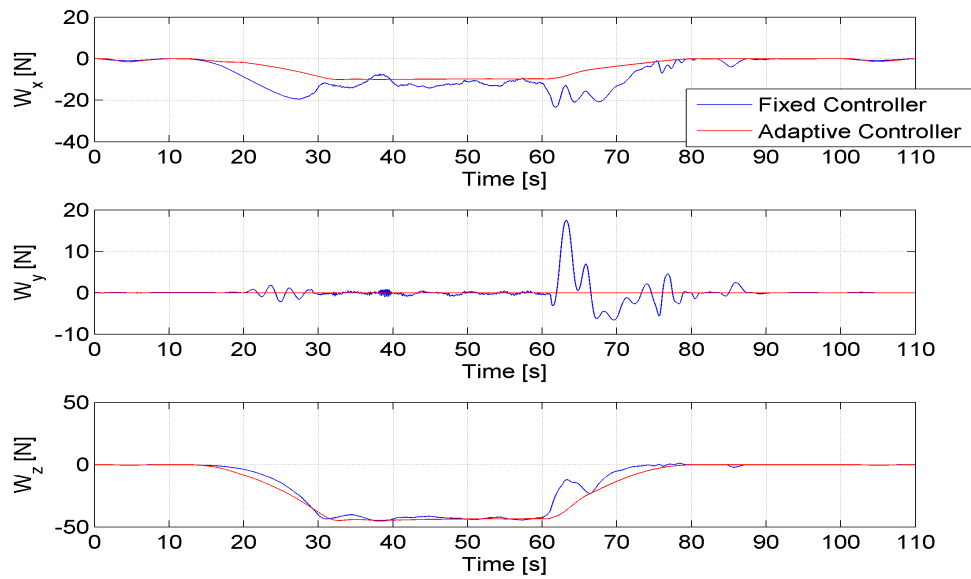


Figure 5.70: Wing Forces.

Control inputs of the UAV are shown in Figure 5.69. When compared with the fixed controller's control inputs (Fig. 5.61), oscillations are much smaller.

Figure 5.70 presents resulting aerodynamic forces acting on the wings. UAV benefits from considerable amount of lift during the long duration flight. To compare the energy gain with respect to a similar quadrotor, it is assumed that wingless quadrotor would need less force in the  $X$  axis due to approximately zero drag and more force in the  $Z$  axis due to the mechanical configuration which results in approximately zero lift. It is calculated that a similar quadrotor spends approximately 1.49 times more energy during the proposed scenario with respect to QTW UAV.

# Chapter V

## 6 Conclusion and Future Works

In this thesis, a hierarchical nonlinear adaptive control framework was developed and applied on a high fidelity quad tilt-wing UAV model. Actuator failures, mass and inertia uncertainties, wind disturbances, measurement noises and center of gravity changes are all included in the model. A suitable LSPB type reference trajectory is designed for the X axis to reduce the power consumption during the flight. Additionally minimum forward velocity, which results in a zero degree pitch angle, was calculated. In order to compensate for the model uncertainties, disturbances and measurement noises a nonlinear hierarchical controller consisting of two levels was developed. A model reference adaptive controller is at the higher level determining necessary forces to make the UAV follow a given trajectory, and a nonlinear adaptive controller is at the lower level making sure that the orientation of the UAV is adjusted properly to produce these forces requested by the upper level controller. The controller development does not need any linearization of the UAV dynamics. Adaptive controller was compared with the fixed controller that was used in earlier flight tests and simulation results show that adaptive controller outperforms the fixed controller.

Regarding the future work, sensors such as inertial measurement unit (IMU), sonar and GPS can be modeled independently to get more realistic results. Moreover, proposed adaptive controller can be implemented on actual SUAVI and a comparison can be made to show the validity of the simulation results.

## References

- [1] E. Guizzo, “How google’s self-driving car works,” *IEEE Spectrum Online*, *October*, vol. 18, 2011.
- [2] M. Raibert, K. Blankespoor, G. Nelson, R. Playter *et al.*, “Bigdog, the rough-terrain quadruped robot,” in *Proceedings of the 17th World Congress*, vol. 17, no. 1, 2008, pp. 10 822–10 825.
- [3] T. Czapla and J. Wrona, “Technology development of military applications of unmanned ground vehicles,” in *Vision Based Systems for UAV Applications*. Springer, 2013, pp. 293–309.
- [4] C. C. Eriksen, T. J. Osse, R. D. Light, T. Wen, T. W. Lehman, P. L. Sabin, J. W. Ballard, and A. M. Chiodi, “Seaglider: A long-range autonomous underwater vehicle for oceanographic research,” *Oceanic Engineering, IEEE Journal of*, vol. 26, no. 4, pp. 424–436, 2001.
- [5] J. Eggers and M. H. Draper, “Multi-uav control for tactical reconnaissance and close air support missions: operator perspectives and design challenges,” in *Proc. NATO RTO Human Factors and Medicine Symp. HFM-135. NATO TRO, Neuilly-sur-Seine, CEDEX, Biarritz, France*, 2006.
- [6] D. W. Murphy and J. Cycon, “Applications for mini vtol uav for law enforcement,” in *Enabling Technologies for Law Enforcement and Security*. International Society for Optics and Photonics, 1999, pp. 35–43.

- [7] Z. Li, Y. Liu, R. Hayward, J. Zhang, and J. Cai, “Knowledge-based power line detection for uav surveillance and inspection systems,” in *Image and Vision Computing New Zealand, 2008. IVCNZ 2008. 23rd International Conference*, Nov 2008, pp. 1–6.
- [8] D. Hausamann, W. Zirrig, G. Schreier, and P. Strobl, “Monitoring of gas pipelines—a civil uav application,” *Aircraft Engineering and Aerospace Technology*, vol. 77, no. 5, pp. 352–360, 2005.
- [9] I. Maza, F. Caballero, J. Capitán, J. Martínez-de Dios, and A. Ollero, “Experimental results in multi-uav coordination for disaster management and civil security applications,” *Journal of intelligent & robotic systems*, vol. 61, no. 1-4, pp. 563–585, 2011.
- [10] T. Tomic, K. Schmid, P. Lutz, A. Domel, M. Kassecker, E. Mair, I. Grixia, F. Ruess, M. Suppa, and D. Burschka, “Toward a fully autonomous uav: Research platform for indoor and outdoor urban search and rescue,” *Robotics Automation Magazine, IEEE*, vol. 19, no. 3, pp. 46–56, Sept 2012.
- [11] C. Zhang, “An uav-based photogrammetric mapping system for road condition assessment,” *Int. Arch. Photogramm. Remote Sens. Spatial Inf. Sci*, vol. 37, pp. 627–632, 2008.
- [12] J. Bendig, A. Bolten, and G. Bareth, “Uav-based imaging for multi-temporal, very high resolution crop surface models to monitor crop growth variability monitoring des pflanzenwachstums mit hilfe multitemporaler und hoch auflösender oberflächenmodelle von getreidebestän-

- den auf basis von bildern aus uav-befliegungen,” *Photogrammetrie-Fernerkundung-Geoinformation*, vol. 2013, no. 6, pp. 551–562, 2013.
- [13] G. Zhou, C. Li, and P. Cheng, “Unmanned aerial vehicle (uav) real-time video registration for forest fire monitoring,” in *Geoscience and Remote Sensing Symposium, 2005. IGARSS '05. Proceedings. 2005 IEEE International*, vol. 3, July 2005, pp. 1803–1806.
- [14] A. Lin, A. Novo, S. Har-Noy, N. Ricklin, and K. Stamatiou, “Combining geoeye-1 satellite remote sensing, uav aerial imaging, and geophysical surveys in anomaly detection applied to archaeology,” *Selected Topics in Applied Earth Observations and Remote Sensing, IEEE Journal of*, vol. 4, no. 4, pp. 870–876, Dec 2011.
- [15] E. Pereira, R. Bencatel, J. Correia, L. Félix, G. Gonçalves, J. Morgado, and J. Sousa, “Unmanned air vehicles for coastal and environmental research,” *Journal of Coastal Research*, pp. 1557–1561, 2009.
- [16] C. Sabo and K. Cohen, “Smart heuristic for pickup and delivery problem (pdp) with cooperative uavs,” in *AIAA Infotech@ Aerospace Conference, St. Louis, MO*, 2011, pp. 2011–1464.
- [17] K. Nonami, F. Kendoul, S. Suzuki, W. Wang, and D. Nakazawa, *Autonomous Flying Robots: Unmanned Aerial Vehicles and Micro Aerial Vehicles*. Springer Science & Business Media, 2010.
- [18] A. Dorobantu, A. Murch, B. Mettler, and G. Balas, “Frequency domain system identification for a small, low-cost, fixed-wing uav,” in *Proceedings of the 2011 AIAA Guidance, Navigation, and Control Conference*, 2011.

- [19] N. Michael, D. Mellinger, Q. Lindsey, and V. Kumar, “The grasp multiple micro-uav testbed,” *Robotics & Automation Magazine, IEEE*, vol. 17, no. 3, pp. 56–65, 2010.
- [20] R. Wood, “The first takeoff of a biologically inspired at-scale robotic insect,” *Robotics, IEEE Transactions on*, vol. 24, no. 2, pp. 341–347, April 2008.
- [21] P. van Blyenburgh, “Uav systems: global review,” in *Conference, Amsterdam, The Netherlands*, 2006.
- [22] E. Cetinsoy, S. Dikyar, C. Hancer, K. Oner, E. Sirimoglu, M. Unel, and M. Aksit, “Design and construction of a novel quad tilt-wing {UAV},” *Mechatronics*, vol. 22, no. 6, pp. 723 – 745, 2012.
- [23] D. Snyder, “The quad tiltrotor: its beginning and evolution,” in *Proceedings of the 56th Annual Forum, American Helicopter Society, Virginia Beach, Virginia*, 2000.
- [24] F. Kendoul, I. Fantoni, and R. Lozano, “Modeling and control of a small autonomous aircraft having two tilting rotors,” in *Decision and Control, 2005 and 2005 European Control Conference. CDC-ECC’05. 44th IEEE Conference on*. IEEE, 2005, pp. 8144–8149.
- [25] Y.-S. Kang, B.-J. Park, C.-S. Yoo, and S. Koo, “Control law modification according to flight test of small scaled tilt rotor uav,” in *AIAA GNC Conference*, 2008, pp. 18–21.
- [26] J. Dickeson, D. Miles, O. Cifdaloz, V. Wells, and A. Rodriguez, “Robust lpv h x221e; gain-scheduled hover-to-cruise conversion for a tilt-wing

- rotorcraft in the presence of cg variations,” in *Decision and Control, 2007 46th IEEE Conference on*, Dec 2007, pp. 2773–2778.
- [27] P. M. Rothhaar, P. C. Murphy, J. Bacon Barton, I. M. Gregory, J. A. Grauer, R. C. Busan, and M. A. Croom, “Nasa langley distributed propulsion vtol tilt-wing aircraft testing, modeling, simulation, control, and flight test development,” in *14th AIAA Aviation Technology, Integration, and Operations Conference, Atlanta, GA*, 2014.
- [28] K. Muraoka, N. Okada, and D. Kubo, “Quad tilt wing vtol uav: aerodynamic characteristics and prototype flight test,” in *AIAA Infotech@ Aerospace Conference*, 2009, pp. 2009–1834.
- [29] K. Muraoka, N. Okada, D. Kubo, and M. Sato, “Transition flight of quad tilt wing vtol uav,” in *28th Congress of the International Council of the Aeronautical Sciences*, 2012, pp. 2012–11.
- [30] S. Suzuki, R. Zhijia, Y. Horita, K. Nonami, G. Kimura, T. Bando, D. Hirabayashi, M. Furuya, and K. Yasuda, “Attitude control of quad rotors qtw-uav with tilt wing mechanism,” *Journal of System Design and Dynamics*, vol. 4, no. 3, pp. 416–428, 2010.
- [31] S. Dikyar, E. Çetinsoy, and M. Ünel, “Flight controller design for vertical, transition and horizontal modes of a tilt-wing quadrotor,” 2011.
- [32] C. Hancer, K. Oner, E. Sirimoglu, E. Cetinsoy, and M. Unel, “Robust position control of a tilt-wing quadrotor,” in *Decision and Control (CDC), 2010 49th IEEE Conference on*, Dec 2010, pp. 4908–4913.

- [33] ———, “Robust hovering control of a quad tilt-wing uav,” in *IECON 2010 - 36th Annual Conference on IEEE Industrial Electronics Society*, Nov 2010, pp. 1615–1620.
- [34] K. T. Öner, E. Çetinsoy, E. Sırımoğlu, C. Hancer, T. Ayken, and M. Ünel, “Lqr and smc stabilization of a new unmanned aerial vehicle,” 2009.
- [35] K. T. Öner, E. Çetinsoy, M. Ünel, M. F. Akşit, I. Kandemir, and K. Gülez, “Dynamic model and control of a new quadrotor unmanned aerial vehicle with tilt-wing mechanism,” 2008.
- [36] Z. Dydek, A. Annaswamy, and E. Lavretsky, “Adaptive control of quadrotor uavs: A design trade study with flight evaluations,” *Control Systems Technology, IEEE Transactions on*, vol. 21, no. 4, pp. 1400–1406, July 2013.
- [37] F. Kendoul, “Survey of advances in guidance, navigation, and control of unmanned rotorcraft systems,” *Journal of Field Robotics*, vol. 29, no. 2, pp. 315–378, 2012.
- [38] S. Bouabdallah, A. Noth, and R. Siegwart, “Pid vs lq control techniques applied to an indoor micro quadrotor,” in *Intelligent Robots and Systems, 2004. (IROS 2004). Proceedings. 2004 IEEE/RSJ International Conference on*, vol. 3, Sept 2004, pp. 2451–2456 vol.3.
- [39] P. Pounds, D. Bersak, and A. Dollar, “Stability of small-scale uav helicopters and quadrotors with added payload mass under pid control,” *Autonomous Robots*, vol. 33, no. 1-2, pp. 129–142, 2012. [Online]. Available: <http://dx.doi.org/10.1007/s10514-012-9280-5>

- [40] S. Bouabdallah, P. Murrieri, and R. Siegwart, "Towards autonomous indoor micro vtol," *Autonomous Robots*, vol. 18, no. 2, pp. 171–183, 2005. [Online]. Available: <http://dx.doi.org/10.1007/s10514-005-0724-z>
- [41] G. M. Hoffmann, H. Huang, S. L. Waslander, and C. J. Tomlin, "Quadrotor helicopter flight dynamics and control: Theory and experiment," in *Proc. of the AIAA Guidance, Navigation, and Control Conference*, vol. 2, 2007.
- [42] A. Tayebi and S. McGilvray, "Attitude stabilization of a four-rotor aerial robot," in *Decision and Control, 2004. CDC. 43rd IEEE Conference on*, vol. 2, Dec 2004, pp. 1216–1221 Vol.2.
- [43] I. D. Cowling, O. A. Yakimenko, J. F. Whidborne, and A. K. Cooke, "A prototype of an autonomous controller for a quadrotor uav," in *European Control Conference, 2007*, pp. 1–8.
- [44] J. How, B. Bethke, A. Frank, D. Dale, and J. Vian, "Real-time indoor autonomous vehicle test environment," *Control Systems, IEEE*, vol. 28, no. 2, pp. 51–64, April 2008.
- [45] M. Bergerman, O. Amidi, J. Miller, N. Vallidis, and T. Dudek, "Cascaded position and heading control of a robotic helicopter," in *Intelligent Robots and Systems, 2007. IROS 2007. IEEE/RSJ International Conference on*, Oct 2007, pp. 135–140.
- [46] M. La Civita, G. Papageorgiou, W. Messner, and T. Kanade, "Design and flight testing of a gain-scheduled h<sub>∞</sub>; loop shaping controller for wide-envelope flight of a robotic helicopter," in *American Control*

- Conference, 2003. Proceedings of the 2003*, vol. 5, June 2003, pp. 4195–4200 vol.5.
- [47] D. Schafroth, C. Bermes, S. Bouabdallah, and R. Siegwart, “Modeling, system identification and robust control of a coaxial micro helicopter,” *Control Engineering Practice*, vol. 18, no. 7, pp. 700 – 711, 2010, special Issue on Aerial Robotics. [Online]. Available: <http://www.sciencedirect.com/science/article/pii/S0967066110000390>
- [48] J. Gadewadikar, F. Lewis, K. Subbarao, K. Peng, and B. Chen, “H-infinity static output-feedback control for rotorcraft,” *Journal of Intelligent and Robotic Systems*, vol. 54, no. 4, pp. 629–646, 2009. [Online]. Available: <http://dx.doi.org/10.1007/s10846-008-9279-5>
- [49] I. Sadeghzadeh, A. Mehta, and Y. Zhang, “Fault/damage tolerant control of a quadrotor helicopter uav using model reference adaptive control and gain-scheduled pid,” in *AIAA Guidance, Navigation, and Control Conference*, 2011, pp. 08–11.
- [50] J. H. Gillula, G. M. Hoffmann, H. Huang, M. P. Vitus, and C. Tomlin, “Applications of hybrid reachability analysis to robotic aerial vehicles,” *The International Journal of Robotics Research*, 2011.
- [51] T. Koo and S. Sastry, “Output tracking control design of a helicopter model based on approximate linearization,” in *Decision and Control, 1998. Proceedings of the 37th IEEE Conference on*, vol. 4, Dec 1998, pp. 3635–3640 vol.4.

- [52] H. Voos, “Nonlinear control of a quadrotor micro-uav using feedback-linearization,” in *Mechatronics, 2009. ICM 2009. IEEE International Conference on*, April 2009, pp. 1–6.
- [53] K. Peng, G. Cai, B. M. Chen, M. Dong, K. Y. Lum, and T. H. Lee, “Design and implementation of an autonomous flight control law for a uav helicopter,” *Automatica*, vol. 45, no. 10, pp. 2333–2338, 2009.
- [54] I. D. Landau, R. Lozano, M. M’Saad, and A. Karimi, *Adaptive control: algorithms, analysis and applications*. Springer Science & Business Media, 2011.
- [55] S. Singh, P. Chandler, C. Schumacher, S. Banda, and M. Pachter, “Adaptive feedback linearizing nonlinear close formation control of uavs,” in *American Control Conference, 2000. Proceedings of the 2000*, vol. 2, 2000, pp. 854–858 vol.2.
- [56] A. Fradkov and B. Andrievsky, “Combined adaptive controller for uav guidance,” *European journal of control*, vol. 11, no. 1, pp. 71–79, 2005.
- [57] D. Lee, H. J. Kim, and S. Sastry, “Feedback linearization vs. adaptive sliding mode control for a quadrotor helicopter,” *International Journal of control, Automation and systems*, vol. 7, no. 3, pp. 419–428, 2009.
- [58] C. Nicol, C. Macnab, and A. Ramirez-Serrano, “Robust adaptive control of a quadrotor helicopter,” *Mechatronics*, vol. 21, no. 6, pp. 927–938, 2011.
- [59] I. Palunko and R. Fierro, “Adaptive control of a quadrotor with dynamic changes in the center of gravity,” in *Proceedings 18th IFAC World Congress*, vol. 18, no. 1, 2011, pp. 2626–2631.

- [60] H. J. Kim and D. H. Shim, “A flight control system for aerial robots: algorithms and experiments,” *Control engineering practice*, vol. 11, no. 12, pp. 1389–1400, 2003.
- [61] D. H. Shim, H. J. Kim, and S. Sastry, “Decentralized nonlinear model predictive control of multiple flying robots,” in *Decision and control, 2003. Proceedings. 42nd IEEE conference on*, vol. 4. IEEE, 2003, pp. 3621–3626.
- [62] Y. Kang and J. Hedrick, “Linear tracking for a fixed-wing uav using nonlinear model predictive control,” *Control Systems Technology, IEEE Transactions on*, vol. 17, no. 5, pp. 1202–1210, Sept 2009.
- [63] J. Zhou and C. Wen, *Adaptive backstepping control of uncertain systems: Nonsmooth nonlinearities, interactions or time-variations*. Springer Science & Business Media, 2008, vol. 372.
- [64] J. Azinheira and A. Moutinho, “Hover control of an uav with backstepping design including input saturations,” *Control Systems Technology, IEEE Transactions on*, vol. 16, no. 3, pp. 517–526, May 2008.
- [65] B. Ahmed, H. R. Pota, and M. Garratt, “Flight control of a rotary wing uav using backstepping,” *International Journal of Robust and Nonlinear Control*, vol. 20, no. 6, pp. 639–658, 2010.
- [66] D. Lee, C. Ha, and Z. Zuo, “Backstepping control of quadrotor-type uavs and its application to teleoperation over the internet,” in *Intelligent Autonomous Systems 12*, ser. Advances in Intelligent Systems and Computing, S. Lee, H. Cho, K.-J. Yoon, and J. Lee, Eds. Springer

- Berlin Heidelberg, 2013, vol. 194, pp. 217–225. [Online]. Available: [http://dx.doi.org/10.1007/978-3-642-33932-5\\_21](http://dx.doi.org/10.1007/978-3-642-33932-5_21)
- [67] M. Sugeno, M. Griffin, and A. Bastian, “Fuzzy hierarchical control of an unmaned helicopter,” *Korea International Conference on Intelligent Systems Proceedings*, vol. 1, pp. 179–182, 1993.
- [68] C. Phillips, C. L. Karr, and G. Walker, “Helicopter flight control with fuzzy logic and genetic algorithms,” *Engineering Applications of Artificial Intelligence*, vol. 9, no. 2, pp. 175–184, 1996.
- [69] M. Santos, V. Lopez, and F. Morata, “Intelligent fuzzy controller of a quadrotor,” in *Intelligent Systems and Knowledge Engineering (ISKE), 2010 International Conference on*. IEEE, 2010, pp. 141–146.
- [70] B. S. Kim and A. J. Calise, “Nonlinear flight control using neural networks,” *Journal of Guidance, Control, and Dynamics*, vol. 20, no. 1, pp. 26–33, 1997.
- [71] G. Buskey, G. Wyeth, and J. Roberts, “Autonomous helicopter hover using an artificial neural network,” in *Robotics and Automation, 2001. Proceedings 2001 ICRA. IEEE International Conference on*, vol. 2, 2001, pp. 1635–1640 vol.2.
- [72] M. Ö. Efe, “Neural network assisted computationally simple pi d control of a quadrotor uav,” *Industrial Informatics, IEEE Transactions on*, vol. 7, no. 2, pp. 354–361, 2011.
- [73] V. Gavrillets, E. Frazzoli, B. Mettler, M. Piedmonte, and E. Feron, “Aggressive maneuvering of small autonomous helicopters: A human-

- centered approach,” *The International Journal of Robotics Research*, vol. 20, no. 10, pp. 795–807, 2001.
- [74] V. Gavrillets, B. Mettler, and E. Feron, “Human-inspired control logic for automated maneuvering of miniature helicopter,” *Journal of Guidance, Control, and Dynamics*, vol. 27, no. 5, pp. 752–759, 2004.
- [75] S. Dikyar, “Nonlinear Control of a Quad Tilt-Wing UAV,” Master’s thesis, Sabanci University, 2011.
- [76] E. Cetinsoy, “Design, Construction and Flight Control of a Quad Tilt-Wing Unmanned Aerial Vehicle,” Ph.D. dissertation, Sabanci University, 2010.
- [77] M. W. Spong, S. Hutchinson, and M. Vidyasagar, *Robot modeling and control*. Wiley New York, 2006, vol. 3.
- [78] K. S. Narendra and A. M. Annaswamy, *Stable adaptive systems*. Courier Corporation, 2012.
- [79] J. Slotine and W. Li, *Applied Nonlinear Control*. Prentice Hall, 1991. [Online]. Available: <http://books.google.com.tr/books?id=cwpRAAAAMAAJ>
- [80] E. Lavretsky, “Adaptive control: Introduction, overview, and applications,” in *Lecture notes from IEEE Robust and Adaptive Control Workshop*, 2008.
- [81] J.-J. Slotine and W. Li, “Adaptive robot control: A new perspective,” in *Decision and Control, 1987. 26th IEEE Conference on*, vol. 26. IEEE, 1987, pp. 192–198.

- [82] J. D. McMinn, "Extension of a kolmogorov atmospheric turbulence model for time-based simulation implementation," in *AIAA Guidance Navigation and Control Conference, AIAA-97-3532, New Orleans, LA, Aug, 1997*, pp. 11–13.
- [83] D. Moorhouse and R. Woodcock, "Us military specification mil-f-8785c," Technical report. US Department of Defense, Tech. Rep., 1980.

## 7 Appendix

### Principal Moment of Inertia Calculations

Wing Angle [deg]	Wing Angle [rad]	$I_{xx_b}$ [kg m <sup>2</sup> ]	$I_{yy_b}$ [kg m <sup>2</sup> ]	$I_{zz_b}$ [kg m <sup>2</sup> ]
0	0	0.239547	0.450669	0.684241
5	0.09	0.239583	0.450651	0.684187
10	0.17	0.239749	0.450649	0.684018
15	0.26	0.24004	0.450661	0.68374
20	0.35	0.240447	0.450689	0.683361
25	0.44	0.240958	0.450732	0.682893
30	0.52	0.241556	0.45079	0.682352
35	0.61	0.242225	0.450862	0.681756
40	0.70	0.242942	0.450948	0.681124
45	0.79	0.243687	0.451046	0.680478
50	0.87	0.244435	0.451157	0.679841
55	0.96	0.245165	0.45128	0.679234
60	1.05	0.245852	0.451413	0.67868
65	1.13	0.246475	0.451556	0.678199
70	1.22	0.247015	0.451707	0.677811
75	1.31	0.247453	0.451865	0.677531
80	1.4	0.247776	0.45203	0.677373
85	1.48	0.247973	0.452199	0.677345
90	1.57	0.248038	0.452372	0.677453

Table 7.1: Evolution of principal moments of inertia from horizontal to vertical mode, before the failure.

Wing Angle [deg]	Wing Angle [rad]	$I_{xx_a}$ [kg m <sup>2</sup> ]	$I_{yy_a}$ [kg m <sup>2</sup> ]	$I_{zz_a}$ [kg m <sup>2</sup> ]
0	0	0.208271	0.417171	0.619631
5	0.09	0.208306	0.417157	0.619583
10	0.17	0.20846	0.417153	0.619428
15	0.26	0.20873	0.417161	0.61917
20	0.35	0.209106	0.417179	0.618819
25	0.44	0.209577	0.417207	0.618383
30	0.52	0.210129	0.417247	0.617879
35	0.61	0.210746	0.417297	0.617322
40	0.70	0.211407	0.417357	0.61673
45	0.79	0.212094	0.417428	0.616122
50	0.87	0.212784	0.417508	0.61552
55	0.96	0.213456	0.417598	0.614944
60	1.05	0.21409	0.417696	0.614414
65	1.13	0.214664	0.417803	0.613949
70	1.22	0.215161	0.417918	0.613566
75	1.31	0.215564	0.418039	0.613282
80	1.40	0.21586	0.418167	0.613107
85	1.48	0.21604	0.4183	0.61305
90	1.57	0.216098	0.418437	0.613117

Table 7.2: Evolution of principal moments of inertia from horizontal to vertical mode. after the failure.